Characterizing co-infection of primary B cells with Kaposi's sarcoma-associated herpesvirus and Epstein-Barr virus: establishing an *in vitro* model of the development of Primary Effusion Lymphoma

By

Aurélia Faure

A dissertation submitted in partial fulfillment of the requirements for the degree of

Doctor of Philosophy
(Physiology Graduate Training Program)

at the
UNIVERSITY OF WISCONSIN-MADISON
2019

Date of final oral examination: 05/16/2019

The dissertation is approved by the following members of the Final Oral Committee:
Paul Ahlquist, Professor, Oncology and Molecular Virology, Plant Pathology
Norman Drinkwater, Professor, Oncology
Eric Johannsen, Associate Professor, Medicine and Oncology
Paul Lambert, Professor, Oncology
Bill Sugden, Professor, Oncology

Abstract

Characterizing co-infection of primary B cells with Kaposi's sarcoma-associated herpesvirus and Epstein-Barr virus: establishing an *in vitro* model of the development of Primary Effusion Lymphoma

Aurélia Faure

Under the supervision of Professor Bill Sugden

at the University of Wisconsin-Madison

Primary Effusion Lymphoma (PEL) is a highly aggressive form of non-Hodgkin's lymphoma found primarily in HIV-infected patients. PELs are causally associated with Kaposi's sarcoma-associated herpesvirus (KSHV) and 90% of PELs are co-infected with Epstein-Barr virus (EBV). KSHV is thought to be the genetic driver of PEL: KSHV is maintained in 100% of PEL cells *in vivo* and *in vitro* and several KSHV genes were found to be essential for the survival or proliferation of these cells. However, understanding how PELs develop has been impaired by the difficulty of infecting B cells with KSHV *in vitro*, and the inability of KSHV to transform them. The role of EBV in PEL has been unclear. We reasoned that because EBV is also found in the majority of examined PELs, it would be providing these cells one or more selective advantages.

In this dissertation, I established a protocol to produce KSHV virus efficiently and reproducibly. I then describe extensive, quantitative experiments in which I define a role for EBV in supporting co-infection of primary B cells by KSHV. I show that optimal infection

of peripheral B cells by KSHV requires co-infection by EBV within 24 hours. I found that EBV plays a dual role in KSHV infection: early events of EBV infection promote infection by KSHV while later events inhibit this co-infection. My experiments also underline the role of B cell activation in infection by KSHV and suggest that EBV promotes infection of peripheral B cells by KSHV in part by providing activation of these cells.

I then demonstrate for the first time that dually infected B cells are stably transformed *in vitro* and maintain both viruses for months in culture. These cells are clonal and express lambda light chain mRNA similar to PEL cells. I show that dually infected cells vary in their proliferative capacities and exhibit distinct, transformed properties. Transformed cells that grow to predominate in a culture express increased levels of most KSHV genes, including those encoded by the latency locus, and differentially express a subset of cellular genes as do *bona fide* PEL cells. These dually infected peripheral B cells are thus both stably transformed and allow a mechanistic analysis of the viral and cellular genes that mediate early events in the progression towards PEL.

Acknowledgements

To my mentor, Bill Sugden: Thank you for teaching me how to be a thoughtful scientist, and for pushing me to make my own decisions in science. I have learned a lot during my years in graduate school and became a much stronger person, thanks to you.

To Donata Oertel: Thank you for your kindness and for welcoming me into the Physiology Graduate Training Program. I really enjoyed our discussions together and they have helped me in many aspects of my life.

To my committee members, Paul Ahlquist, Norman Drinkwater, Eric Johannsen, and Paul Lambert: I really enjoyed sharing my work with you and appreciated all your comments and suggestions; they made my work better. Thank you for your willingness to help me in my career.

To my labmates, Adityarup Chakravorty, Ya-Fang Chiu, Mitch Hayes, Rebecca Hutcheson, Ngan Lam, Thejaswi Nagaraju, Asuka Nanbo, Quincy Rosemarie, Prabha Shrestha, Danielle Westhoff Smith and Ya-Chun Yang: I really enjoyed working with all of you. I will miss our discussions in the lab and the fun we had outside of the lab. I feel lucky I got to know you and hope our paths will cross again in the future.

To my parents and brothers: Thank you for your continued support and for giving me the freedom to make my own life choices, even if we sometimes have to make sacrifices as a family.

To my fiancé, Julien: Thank you for believing in me and for your incredible support these past several years. I am looking forward to our new life together.

Table of Contents

List of Figures

List of Tables

List of Abbreviations

Abbreviation	Full Name
BAC	Bacmid
BALF5	Bam HI-A leftward reading frame 5
BART	Bam HI-A region rightward transcript
BCR	B-cell receptor
bp	Base pair
BSA	Bovine serum albumin
BZLF1	Bam HI Z Leftward reading Frame 1
°C	Degrees centigrade
CCL20	C-C Motif Chemokine Ligand 20
CD19	Cluster of differentiation 19
CD20	Cluster of differentiation 20
CD40L	Cluster of differentiation factor 40 ligand
CDR3	Complementarity-determining region 3
CRISPR/Cas9	Clustered Regularly Interspaced Short Palindromic Repeats/CRISPR-associated protein 9
Cy3	Cyanine 3
DAPI	Diamidino-2-phenylindole
DMEM	Dulbecco’s Modified Eagle’s Medium
DNA	Deoxyribonucleic
Dox	Doxycycline

DR1	Direct repeats 1
DR2	Direct repeats 2
dUTP	Deoxyuridine triphosphate
EBERs	Epstein-Barr virus encoded small RNAs
EBNA1	Epstein-Barr nuclear antigen 1
EBV	Epstein-Barr virus
EDTA	Ethylenediaminetetraacetic acid
EF1α	Elongation factor 1-*alpha*
FACS	Fluorescence-activated cell sorting
FBS	Fetal Bovine Serum
FDR	False discovery rate
FISH	Fluorescence *in situ* hybridization
FITC	Fluorescein isothiocyanate
FMO	Fluorescence Minus One
g	Relative centrifugal force
GDC	Genomic Data Commons
GFP	Green fluorescent protein
gRNA	Guide RNA
GSEA	Gene Set Enrichment Analysis
GTF	Gene transfer format
HDAC	Histone deacetylase
HEPES	4-(2-hydroxyethyl)-1-piperazineethanesulfonic acid
HF	Human fibroblast

HHV	Human Herpesvirus
HIV	Human immunodeficiency virus
HLA-DR	Human Leukocyte Antigen – DR isotype
HUVECs	Human umbilical vein endothelial cells
HygR	Hygromycin resistance gene
IgG	Immunoglobulin G
IGH	Immunoglobulin heavy chain
IGK	Immunoglobulin light chain kappa
IGL	Immunoglobulin light chain lambda
IgM	Immunoglobulin M
IKK	IκB kinase
IL-4	Interleukin 4
IRES	Internal ribosomal entry site
IU	Infectious Unit
kb	Kilobase pairs
KCl	Potassium chloride
KS	Kaposi's sarcoma
KSHV	Kaposi's sarcoma-associated herpesvirus
LANA1	Latency-associated nuclear antigen 1
LANA2	Latency-associated nuclear antigen 2
LCL	Lymphoblastoid cell line
LIR	Long interspersed repeats
LMP2A	Latent membrane protein 2A

M	Molar
MCD	Multicentric Castleman's Disease
µg	Microgram
µL	Microliter
µm	Micrometer
µM	Micromolar
min	Minute
miRNA	Micro-ribonucleic acid
mL	Milliliter
mM	Millimolar
MOI	Multiplicity of infection
mRNA	Messenger ribonucleic acid
MSigDB	Molecular Signatures Database
mut	Mutant
NaBut	Sodium butyrate
NCBI	National Center for Biotechnology Information
NCI	National Cancer Institute
NES	Normalized Enrichment Score
NF-κB	Nuclear factor kappa B
ng	Nanogram
nm	Nanometer
nM	Nanomolar
N.S.	Non-Significant

NSG	NOD scid gamma
ORF	Open reading frame
OriP	Origin of latent plasmid replication of EBV
p	p-value
PBMCs	Peripheral blood mononuclear cells
PBS	Phosphate-buffered saline
PCA	Principal Component Analysis
PCR	Polymerase chain reaction
PEL	Primary Effusion Lymphoma
qPCR	Quantitative or real-time polymerase chain reaction
RNA	Ribonucleic acid
RNA-Seq	RNA-Sequencing
RPMI	Roswell Park Memorial Institute formulation
RTA	Replication and transcription activator
RT-PCR	Reverse transcription polymerase chain reaction
RT-qPCR	Quantitative reverse transcription PCR
SD	Standard Deviation
shRNA	Short hairpin ribonucleic acid
siRNA	Small interfering ribonucleic acid
SRA	Sequence Read Archive
SSC	Standard saline citrate
STAR	Spliced Transcripts Alignment to a Reference
TE	Tris-EDTA

TPA	12-O-tetradecanoylphorbol-13-acetate
TWEAKR	Tumor necrosis factor-like weak inducer of apoptosis receptor
UCDS	Unique coding sequence
v-FLIP	Viral FLICE (FADD-like interleukin-1-β-converting enzyme) inhibitory protein
V_H	Heavy chain variable region
vIL-6	Viral interleukin-6
vIRF3	Viral interferon regulatory factor 3
VPA	Valproic acid
wt	Wild-type

CHAPTER I.

Background and Introduction

Primary Effusion Lymphoma (PEL) is a highly aggressive form of non-Hodgkin's lymphoma found primarily in HIV-infected patients (1). PEL presents as lymphomatous effusions that grow mainly in the body cavities. The prognosis for patients is poor, with a median survival of about 6 months post-diagnosis (1, 2). PELs often exhibit clonal immunoglobulin gene rearrangements and therefore are thought to be a clonal expansion of B cells (1, 3–5). PELs have been distinguished from other body-cavity based lymphomas by their association with Kaposi's sarcoma-associated herpesvirus (KSHV) and the lack of c-*myc* gene rearrangements (1). PEL cells express CD45 and activation-associated antigens such as CD30 and CD38, but often lack B cell-associated antigens such as CD19, CD20 and the B-cell receptor (BCR) (1, 3, 6). The molecular characteristics of different cases of PEL are summarized in Table I.1.

B cells express the heavy and light chain immunoglobulin at their surface to form the B-cell receptor (BCR). The BCR mediates a basal signaling that is required for survival of B cells (7, 8). Why the expression of immunoglobulins can often not be detected at the surface of PEL cells is not clear. Most PEL cells have rearranged heavy and light chain immunoglobulin (1, 3–5). One study suggested that lambda light chain genes are often productively rearranged in PEL (4). In addition, PELs were found to express heavy chain genes at the RNA level and studies suggested that the expressed heavy chain is functional (3). Furthermore, PELs are thought to arise at a late stage of B cell maturation (1, 3, 4). They express antigens associated with the late stages of B cell differentiation or activation (1). In a study of seven different PELs (3), most of them were of germinal or postgerminal center origin as evidenced by highly mutated immunoglobulin heavy chain variable region (V_H) genes suggesting that they were selected by antigen and are mature B cells. Only one PEL was of pregerminal center origin. The six PELs with highly mutated

V_H genes were also infected with Epstein-Barr virus (EBV) (see below) and the only unmutated PEL was EBV-negative. Another study found evidence of antigen selection in five out of seven cases of PELs (4).

Most PELs are dually infected with EBV and KSHV (see below). Although not highly expressed in latent PEL, several viral proteins could modulate the expression of the BCR at the cell surface of PEL cells such as EBV's latent membrane protein 2A (LMP2A) and the proteins K1 and K15 of KSHV. K1 and K15 are weakly expressed during latency in PEL but their expression increases during lytic viral replication (9, 10). These three proteins were shown to both downregulate and replace the function of the BCR. The protein K1 of KSHV downregulates expression of the BCR by blocking its intracellular transport to the cell surface (11). LMP2A and the protein K15 share similarities in protein structure and both were shown to inhibit BCR signaling (10, 12–14). LMP2A and the proteins K1 and K15, when inserted into the EBV genome, can act as a functional analog of the BCR and mediate survival of immunoglobulin-negative B cells (15–17).

PELs are dually infected with two human tumor viruses.

PELs are causally associated with Kaposi's sarcoma-associated herpesvirus (KSHV), and 90% of them are also co-infected with Epstein-Barr virus (EBV) (1, 2, 5, 6, 18, 19). EBV and KSHV (also known as human herpesviruses 4 and 8 (HHV-4 and HHV-8)) are two related oncogenic human ɣ-herpesviruses. EBV infects greater than 90% of the world's population whereas KSHV's pattern of infection is variable with the highest seroprevalence found in Sub-Saharan Africa (Figure I.1). Primary infection with EBV is usually asymptomatic but can cause mononucleosis (20). Primary infection with KSHV is

not well characterized in part due to its lower rate of infection. In some cases, infection by either virus contributes to the development of cancers. EBV causes multiple cancers including Burkitt's lymphomas, Hodgkin's lymphomas and gastric and nasopharyngeal carcinomas (21). KSHV has been causally associated with Kaposi's sarcoma (KS) (22) and Multicentric Castleman's Disease (MCD), a non-malignant lymphoproliferative disorder (23). Both viruses can persist latently in host cells, expressing a limited set of viral genes while maintaining their genomes as extrachromosomal plasmids. The maintenance of KSHV and EBV genomes as plasmids in PELs indicates that both viruses contribute to tumor phenotypes: these viral genomes are lost from proliferating cells if they do not provide their host cells some selective advantages (24–26). PEL, therefore, is a unique tumor: it is the only human tumor to be known to depend on two oncogenic viruses.

KSHV is thought to be the genetic driver for PEL.

The KSHV genome is retained as a plasmid both in PEL cells *in vivo* and upon explantation *in vitro*. In addition, several KSHV genes have been shown to be essential for the survival or proliferation of these cells (27–29). KSHV has a double-stranded DNA genome of approximately 170 kb. These genomes are found in PEL at a high but variable copy number (between 40 to 200 genomes per cell). Most of the viral genes expressed in latency are localized in a 10 kb region of the genome called the latency locus. This locus encodes six protein products: LANA1, v-FLIP, v-cyclin, Kaposin A, B and C and a cluster of miRNAs (30–33) (Figure I.2). The latency-associated nuclear antigen 1 or LANA1 is encoded by ORF73 (34) and allows partitioning and maintenance of KSHV

genomes in latently infected cells (35–37). V-cyclin (ORF72) and the viral FLICE (FADD-like interleukin-1-β-converting enzyme) inhibitory protein or v-FLIP (ORF71) are expressed from a bicistronic transcript, the latter by way of an internal ribosome entry site (IRES) overlapping the v-cyclin coding region (32, 38). The transcripts encompassing ORF K12 and the direct repeats DR1 and DR2 encode three different proteins synthesized by different translational initiation named Kaposin A, B and C (31). These transcripts have been found to be the most abundantly expressed in latency. The same genomic region also encodes 12 pre-miRNAs which are processed into 18 mature miRNAs expressed in latently infected cells (33, 39–42). Outside of the latency locus, one gene is expressed during KSHV latent cycle specifically in PEL, the latent-nuclear antigen 2 (LANA2, ORF K10.5) also called viral interferon regulatory factor 3 (vIRF3) (43, 44). Finally, the viral homologue of IL-6 (vIL-6, ORF K2) is also expressed in latent PEL and its expression is further increased during lytic replication (45–47). KSHV vIL-6 is released by PEL cells and acts in an autocrine loop to drive proliferation of these cells (48, 49). PEL cells are thought to depend on this viral cytokine for proliferation and survival (48, 49).

Several latent KSHV genes were found to directly inhibit apoptosis in PEL cells. Among them, v-FLIP and LANA2 were found to inhibit apoptosis and to be required for survival of PEL cells. V-FLIP inhibits death receptor-mediated apoptosis by inhibiting caspase activation (50, 51). V-FLIP also activates NF-kB and depletion of v-FLIP with siRNA induces apoptosis of PEL cells (27). Interestingly, v-FLIP function is dependent on v-cyclin and vice versa. V-FLIP induced-NF-kB hyperactivation triggers G1 arrest and senescence which is inhibited by v-cyclin (52). V-cyclin is a homolog of cellular-D type

cyclins that promotes cell cycle progression (53), activates a DNA-damage-response and promotes autophagy and senescence (54, 55). Remarkably, v-FLIP blocks v-cyclin-induced autophagy and senescence during latency (55). The interdependence of v-FLIP and v-cyclin functions might explain why they are expressed from the same transcript. LANA2 is another known KSHV anti-apoptotic gene expressed in latency. LANA2 interacts with p53 and inhibits p53-mediated apoptosis (44, 56). Furthermore, partial knock-down of LANA2 expression with siRNA reduces proliferation of PEL cells and is associated with an increase in caspase-3/7 activity (28).

LANA1 and KSHV miR-K10a have also been shown to inhibit apoptosis (57–59). However, whether LANA1's antiapoptotic role is contributing directly to PEL is uncertain. Inhibition of LANA1 expression with shRNA in PEL cells leads to a gradual decrease of KSHV genomes, growth inhibition or apoptosis depending on PEL cell lines (29). It is possible that the latter observation resulted from the loss of other viral genes due to the loss of KSHV genomes. Similarly, there is no evidence that KSHV miRNAs are essential for PEL survival.

The known KSHV viral genes expressed in latently infected PELs and their potential role in inhibition of PEL cell death is summarized in Table I.2.

The role of EBV in PEL is unclear.

Like KSHV, EBV has a double-stranded DNA genome of approximately 170 kb. EBV is present in 90% of PELs at a variable copy number (between 2 and 10 genomes per cell). Between 6% and 45% of the cells lose EBV *in vitro* depending on the PEL cell lines. EBV expresses few viral genes in PEL and at lower levels than in lymphoblastoid

cell lines (LCL) and Burkitt's lymphoma cell lines (60, 61). EBV-positive PELs only express the Epstein-Barr nuclear antigen 1 (EBNA1), EBV's BART miRNAs and the Epstein-Barr virus encoded small RNAs (EBERs) (62). EBV's BART miRNAs were shown to inhibit apoptosis in Burkitt's lymphoma cell lines by inhibiting expression of caspase 3 (63). However, there is no evidence that EBV's miRNAs are required for PEL survival. Similar to KSHV's LANA1, EBNA1 allows partitioning and maintenance of EBV genomes and regulates cellular and viral gene expression ((64) and Westhoff Smith D. et al., unpublished). The expression level of EBNA1 was found to be atypically low in PEL compared to Burkitt's lymphoma cell lines (60). This low level may be due to KSHV's LANA1 negatively regulating EBNA1 expression (65). Forcing the loss of EBV genomes from PEL cells by inhibiting EBNA1 with its dominant negative derivative inhibits PEL cell growth at limiting dilution (60). It should be noted that inhibiting EBNA1 with its dominant negative derivative or using a small molecule, Netropsin, to inhibit EBNA1's binding to AT-rich DNA does not impair cell growth in bulk culture (66, 67). A recent study found that forcing the loss of EBV genomes from PEL cells by targeting EBNA1 with CRISPR/Cas9 gRNAs inhibits the maintenance of their KSHV genomes (68).

Therefore, because EBV is found as a plasmid in most PELs, EBV provides selective advantages to PEL cells, but what these advantages are is not well understood. KSHV encodes both anti-apoptotic and growth promoting genes that are sufficient for tumor survival in other malignancies associated with this virus. In addition, KSHV is maintained in 100% of PEL cells *in vivo* and *in vitro* and studies have demonstrated the dependence of these cells on KSHV to survive and proliferate (27–29). EBV's role in PEL is not as clear. EBV seems to play a role in supporting proliferation of PEL cells based on

the findings that forcing its loss from PEL cells inhibits their proliferation at limiting dilution and the maintenance of their KSHV genomes (60, 68). It should be noted that PEL cells could have evolved both *in vivo* and in cell culture to be less dependent on EBV. Different EBV-induced lymphomas, such as Burkitt's lymphoma and posttransplant lymphoproliferative disorder, have been found to differ in their dependence on EBV, and it has been proposed that these tumors evolve to be less dependent on the virus (24, 25).

KSHV does not transform B cells *in vitro*: we lack a model to understand the development of PEL.

We formerly lacked a model which allows complete characterization *in vitro* of the early steps of development of PEL: B cells have been notoriously difficult to infect with KSHV *in vitro* and when they can be infected, KSHV has not been found to transform them. The difficulty to infect B cells with KSHV *in vitro* was unexpected given its detection in B-cell fractions *in vivo*. Even though KSHV causes Kaposi's Sarcoma (KS) where it infects endothelial cells (22, 69–71), KSHV viral DNA has been detected in populations of circulating B cells *in vivo* in both healthy individuals and KS patients (72–74). In addition to PEL, KSHV has also been associated with Multicentric Castleman's Disease (MCD), a non-malignant lymphoproliferative disorder (23). While cells of endothelial and fibroblast origin can be efficiently infected with KSHV *in vitro*, attempts to infect lymphoblastic cell lines including B and T cell lines have been unsuccessful (75–78). In these studies, neither EBV-negative nor EBV-positive B cell lines could be infected. Several studies have found that primary CD19+ B cells isolated from peripheral blood and umbilical cord blood mononuclear cells are susceptible to KSHV infection (76, 78, 79). However, KSHV

did not lead to transformation of these cells and infection could only be detected by DNA PCR or RT-PCR shortly after infection. Recently, several groups have reported more robust infection of primary B cells isolated from tonsils with 0.5% to 10% of tonsillar B cells being infected with KSHV (80–84). In this instance, KSHV infection could only be studied in these cells for short periods of time because of KSHV's apparent inability to transform them (81, 83, 84).

Searching for a role of EBV in PEL: establishing an *in vitro* model of the development of PEL.

Therefore, the conditions necessary for KSHV to infect B cells that lead to PEL remain unclear. We reasoned that because EBV is also found as a plasmid in the majority of examined PELs, it would be providing these cells one or more selective advantages. Contrary to KSHV, EBV can infect and transform peripheral B cells *in vitro* and induce their long-term proliferation (85, 86). One study has reported detection of KSHV DNA by PCR in newly-transformed B cells following exposure to both viruses, suggesting that cells can be dually infected *in vitro* (78). In addition, a recent study found that KSHV was detected more often in the spleen and blood of NSG mice reconstituted with human CD34-positive cells when these mice were infected with KSHV and EBV compared to KSHV alone (87). In this dissertation, I describe extensive, quantitative experiments in which I define a role for EBV in supporting co-infection by KSHV. We show that EBV promotes infection of peripheral B cells with KSHV, and that this efficiency of infection is optimal within 24 hours of EBV infection. We characterized the dually infected, proliferating B cells: they were transformed, maintaining both KSHV and EBV for months

in culture. The dually infected cells were clonal and expressed lambda light chain mRNA similar to PEL cells. Some transformed cells grew more slowly than cells infected only with EBV and were often overgrown whereas others grew to dominate the culture. These latter cells showed increased expression of most KSHV genes, including those encoded by the latency locus and KSHV vIL-6 gene, regulated the expression of some cellular genes as do PEL cells, and thus shared multiple properties with PEL cells. This *in vitro* transformation of peripheral B cells by KSHV and EBV, for the first time, allows a mechanistic analysis of the viral and cellular genes that mediate early events in the progression towards PEL.

Table I.1: Immunophenotypic analysis of 22 cases of PEL.

The molecular characteristics of 22 cases of PEL are summarized. The data are derived from analysis of 26 lymphomatous effusions comprising 22 cases of PEL and 4 cases of other malignant lymphomas occurring in the body cavities (1, 3). When the exact number of PEL cases could not be determined, the number is preceded by ≤.

Table I.1

Antigens	Expressed	Not expressed	ND*
CD45	21	1	0
B cell-associated antigens			
CD19	0	≤ 20	≤ 6
CD20	≤ 1	≤ 21	0
CD22	≤ 2	≤ 18	≤ 6
Surface Immunoglobulin	≤ 4	≤ 16	≤ 6
T cell-associated antigens			
CD3	0	≤ 22	≤ 3
CD5	0	≤ 20	≤ 6
Activation-associated antigens			
HLA-DR	≤ 11	≤ 7	≤ 8
Epithelial membrane antigen	≤ 7	≤ 6	≤ 13
CD30	≤ 12	≤ 7	≤ 7
CD38	≤ 9	≤ 1	≤ 16
CD71	≤ 8	0	≤ 18

* ND: Not determined.

Figure I.1: Seroprevalence of KSHV.

Map showing KSHV seroprevalence rates (adapted from (88)). Data were summarized in (89) and were obtained from healthy, HIV-negative individuals (usually blood donors).

Figure I.1

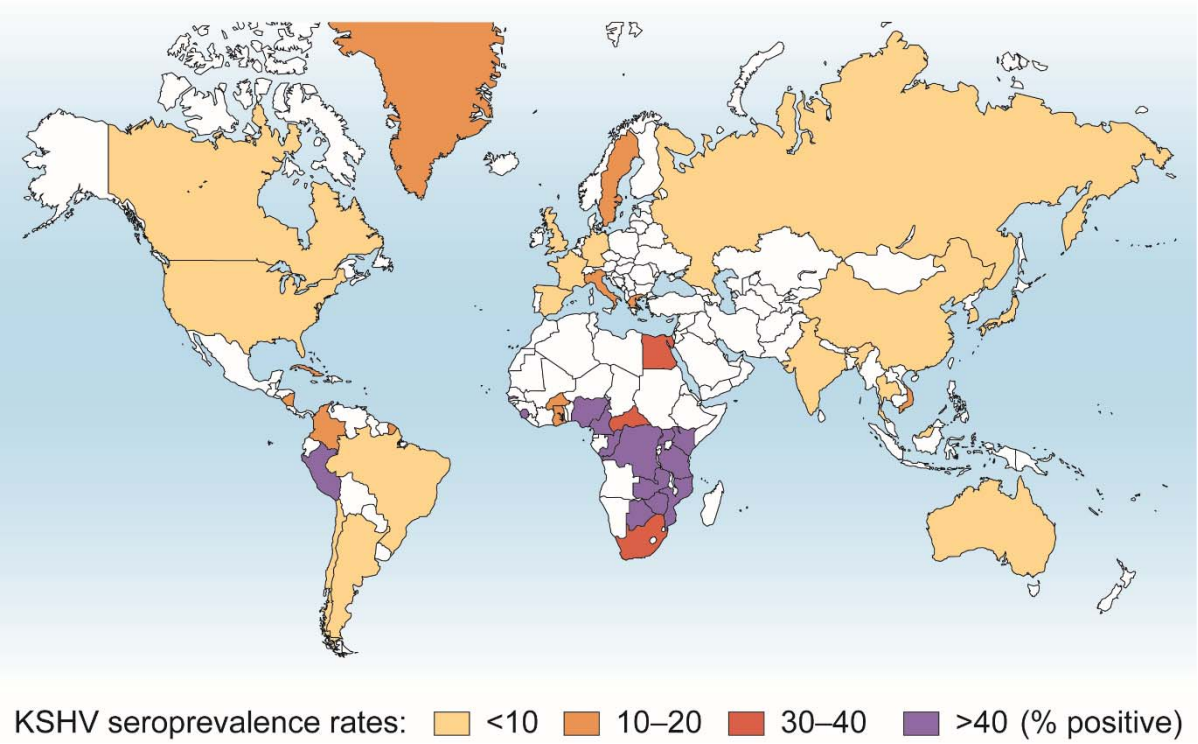

Figure I.2: Structure of the KSHV latency locus.

Organization of the known open reading frames (ORFs), pre-miRNAs and mRNA transcripts within the latency locus of KSHV. ORFs are shown in brown and repeat regions in pink. The positions of KSHV pre-miRNAs are shown by black arrowheads (33, 39, 41, 42). Promoters active in latently infected cells (LTd and LTc) are indicated by black arrows. Several KSHV mRNAs known to be expressed in latency from the LTd and LTc promoters are indicated (30–32, 90–92). This figure was adapter from (40, 93). DR1 and DR2: direct repeats 1 and 2; LIR: long interspersed repeats.

Figure I.2

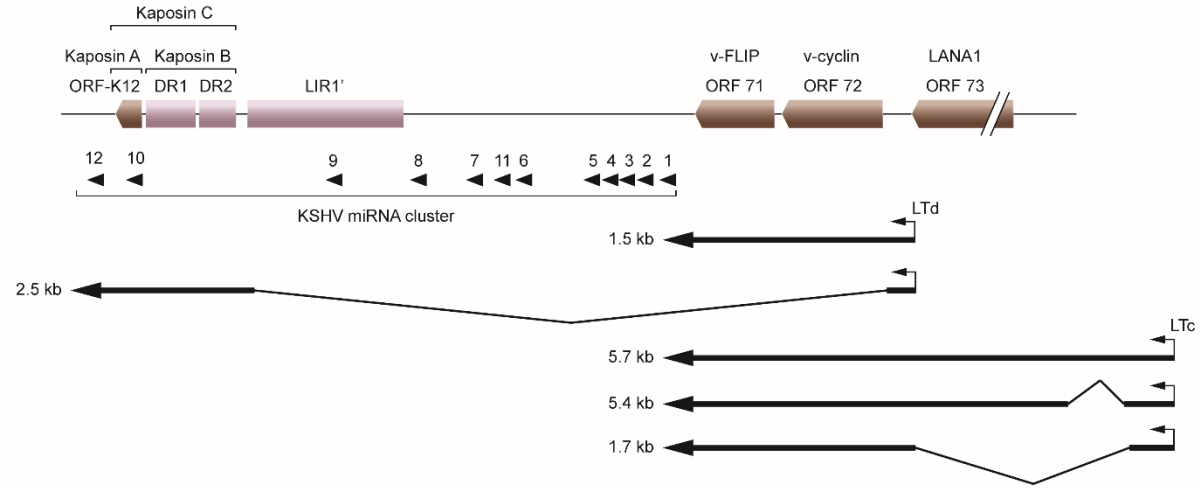
Kaposin C
Kaposin A
Kaposin B
ORF-K12
DR1
DR2
LIR1'
v-FLIP
ORF 71
v-cyclin
ORF 72
LANA1
ORF 73
12
10
9
8
7
11
6
5
4
3
2
1
KSHV miRNA cluster
LTd
1.5 kb
2.5 kb
LTc
5.7 kb
5.4 kb
1.7 kb

Table I.2: KSHV anti-apoptotic genes expressed in latently infected PEL cells.

Summary of KSHV known anti-apoptotic genes expressed in latently infected PEL cells and their potential role in inhibiting cell death by the activation (↑) or inhibition (↓) of cellular targets.

Table I.2

Gene		Putative Targets	Functional consequences	References
v-FLIP	↓	Procaspase 8	Inhibits death receptor-mediated apoptosis	(50, 51)
	↑	IKK/NF-κB	Induces expression of cellular NF-κB-dependent anti-apoptotic genes	(27)
			Induces G1 arrest and senescence in absence of v-cyclin	(52)
LANA2 (vIRF3)	↓	p53	Inhibits p53-mediated apoptosis	(44, 56)
LANA1	↓	p73	Inhibits p73-mediated apoptosis	(57)
	↓	p53	Inhibits p53-mediated apoptosis	(58)
miR-K10a	↓	Tumor necrosis factor-like weak inducer of apoptosis receptor (TWEAKR)	Decreases TWEAK-induced caspase activation	(59)

CHAPTER II.

Materials and Methods

Isolation of peripheral B cells.

Peripheral blood B lymphocytes were purified from whole blood collected from healthy donors and buffy coats obtained from Interstate Blood Bank Inc. (Memphis, TN). Study protocols were approved by the University of Wisconsin-Madison Health Sciences Minimal Risk Institutional Review Board. Informed consent was obtained from all donors. Peripheral blood mononuclear cells (PBMCs) were isolated from EDTA-treated blood by Ficoll-Paque (GE Healthcare Life Sciences) density gradient separation. Ten different donors were used and each condition for which $n \geq 3$ was tested in 3 to 4 different donors. Peripheral CD19+ B cells were purified from PBMCs by negative selection according to the instructions of the manufacturer (B Cell Isolation Kit II, Human, Miltenyi Biotec). The isolation yielded > 90% CD19-positive B cells as determined by staining with anti-CD19 monoclonal antibody and flow cytometry analysis.

Cell culture.

293 (94) and Daudi (95) cell lines were used for titration of KSHV and the recombinant 2089 strain of EBV respectively. LL8 CD40 ligand feeder cells (96, 97) were used for *in vitro* activation of peripheral B cells. 293 cells and LL8 CD40 ligand feeder cells were grown in DMEM supplemented with 10% Fetal Bovine Serum (FBS). Daudi cells, peripheral B cells and the BC-1 PEL cell line (6) were cultured in RPMI supplemented with 10% FBS. Antibiotics (200 U/ml penicillin and 200 µg/ml streptomycin) were added to all cell lines and primary cultures. All cells were incubated in 5% CO_2 at 37°C. All cells used in this dissertation were routinely tested for mycoplasma contamination using the primers described by van Kuppeveld et al. (98).

Antibodies.

Anti-CD19 antibody clone LT19 conjugated to APC or VioBlue was purchased from Miltenyi Biotec. Two anti-DC-SIGN antibodies and their respective isotype controls were used: anti-human DC-SIGN/CD209 clone 120507 and mouse IgG2B isotype control conjugated to APC (R&D Systems) and anti-human DC-SIGN/CD209 clone DCN46 and mouse IgG2b, κ isotype control conjugated to V450 (BD Biosciences). The anti-gpK8.1A 4A4 antibody (hybridoma culture supernatant) was a kind gift from Dr. Bala Chandran.

KSHV and EBV virus stocks preparation.

iSLK cells (75) carrying the recombinant wild-type KSHV BAC16 (99) or the mutant KSHV BAC16RTAStop (100) (iSLKBAC16 and iSLKBAC16RTAstop cells were kindly provided by Dr. Jae U. Jung) were grown in DMEM supplemented with 10% FBS, 250 µg/ml G418, 1 µg/ml puromycin and 1,200 µg/ml hygromycin. One clone of iSLKBAC16 cells (clone 5) was isolated (see CHAPTER III) and used in CHAPTER IV and CHAPTER V to produce KSHV BAC16 virus. iSLKBAC16 clone 5 and iSLKBAC16RTAstop cells were induced with 1 µg/ml doxycycline and 1 mM valproic acid in the absence of G418, puromycin, and hygromycin. The supernatant was harvested at day 4 and 8 and cleared of cells and debris by multiple rounds of centrifugation (500 g for 10 mins followed by 3,000 g for 10 mins). B95-8 cells (101) were grown in RPMI supplemented with 10% FBS and were induced when they reached 7x10^5 cells/ml with 20 ng/ml TPA and 3.5 mM sodium butyrate. The supernatant was collected at day 5 and cells and debris were removed by centrifugation at 500 g for 10 mins and filtration with a 0.8 µm low-protein

binding filter. 293 cells carrying the recombinant EBV genome 2089 (102) were grown in DMEM supplemented with 10% FBS. To induce viral production, cells were transfected in 15 cm plates when they were ~50-60% confluent with vectors expressing BZLF1 and BARF4 (10 µg of each vector) using Lipofectamine 2000 (Invitrogen). Following transfection, the medium was changed to DMEM with 10% FBS and the supernatant was harvested 5 days later. Alternatively, 293 cells carrying 2089 and expressing BZLF1 fused to the estrogen receptor ligand-binding domain were cultured in DMEM supplemented with 10% FBS, 1 µg/ml puromycin and 200 µg/ml hygromycin. Virus production was induced with 200 nM tamoxifen, the medium was removed 24 hours later and changed to DMEM with 10% FBS. The supernatant was collected 2 and 4 days later. Supernatants containing 2089 virus were cleared of cells and debris by multiple rounds of centrifugation (500 g for 10 mins followed by 3,000 g for 10 mins). All viruses were maintained at a pH of 7.2 by addition of HEPES when necessary. KSHV and EBV viral supernatants were concentrated 100-fold by centrifugation at 48,000 g for 2 hours and viral pellets were resuspended at 4°C overnight in RPMI supplemented with 10% FBS and 50 mM HEPES. Separate aliquots were kept at -80°C and thawed immediately before use; another round of centrifugation at 950 g for 10 mins was performed before use for KSHV and 2089 viral preparations to remove any remaining debris.

Titration of virus stocks by real-time PCR and infectivity assays.

The number of KSHV and EBV physical particles in viral stocks was measured by real-time PCR. Viral stocks were treated with DNAse I (Roche) and proteinase K (Roche) before viral DNA extraction by Phenol/Chloroform. An aliquot of 4 µl of isolated viral DNA

was analyzed by real-time PCR as previously described (25). Briefly, reactions were performed in a 384-well plate in a final volume of 20 µl with 0.5 µM of both the forward and reverse primer, 0.2 µM of the probe, Rox reference dye (Invitrogen), and AmpliTaq Gold 360 Master Mix (Applied Biosystems). Primers and probes used to measure the number of molecules of BALF5 (EBV) and LANA1 (KSHV) are listed in Table II.1. The reactions were incubated at 50°C for 2 minutes, then at 95°C for 10 minutes followed by 40 cycles of 95°C for 15 seconds and 60°C for 1 minute. Data were collected on a 7900HT real-time instrument (Applied Biosystems) and analyzed using SDS Version 2.4 software. The number of viral particles was determined by creating a standard curve using linearized plasmids containing the DNA sequence of either BALF5 or LANA1.

For KSHV and 2089 viral stocks, the number of infectious particles was determined on 293 and Daudi cells respectively (for more details on the titration of KSHV viral stocks, see CHAPTER III). Briefly, 293 or Daudi cells were incubated with serially diluted virus for 1 hour at 4°C. Following incubation, additional medium (DMEM or RPMI with 10% FBS and 50 mM HEPES) was added and cells and virus were incubated for an additional 72 hours at 37°C. The number of GFP-positive cells was determined by fluorescence microscopy. The number of infectious viral particles was calculated by multiplying the percentage of GFP-positive cells by the total number of cells at the time of infection. For B95-8 viral stocks, a multiplicity of infection (MOI) of 1 was determined by the amount of virus needed for ~60% of peripheral B cells to become blasts in 72 hours. For all viral stocks used in CHAPTER IV and CHAPTER V, approximately one in 100 to one in 200 physical particles was infectious.

PCR to identify wild-type and mutant KSHV BAC16 strains.

DNA was isolated from mutant and wild-type KSHV BAC16 viral particles as described above. A fragment of 476 bp spanning the mutation in ORF50 was amplified by PCR with the GoTaq Flexi DNA Polymerase at the following conditions: denaturation at 95ºC for 1 minute, annealing at 60ºC for 1 minute and extension at 72ºC for 1 minute for 35 cycles using the primers listed in Table II.1. The PCR product was purified using the QIAquick PCR Purification Kit (Qiagen) and digested with the NheI restriction enzyme for 2 hours at 37ºC.

Infection and *in vitro* activation of peripheral B cells.

In each experiment, 1.5x10^5 to 2x10^6 B cells were used per condition. In all experiments, a fraction of the cells was left uninfected as a negative control and no cell growth or GFP expression was observed. During incubation with viruses, 50 mM HEPES was added to the culture medium of peripheral B cells. For exposure to KSHV, the recombinant wild-type or mutant KSHV BAC16 virus was added to B cells at MOI 2 to 3 and cells and virus were centrifugated at 950 g for 90 mins at room temperature (103). Following spinoculation, cells were washed to remove unbound viruses and resuspended in their culture medium. For experiments in which a neutralizing antibody was used, B cells were exposed to KSHV BAC16 at MOI 2 as previously described. Cells were washed to remove excess, unbound virus and treated 24 hours later with anti-gpK8.1A 4A4 for two hours at 37°C. Cells were then washed and infected with EBV. For exposure to EBV, B cells were exposed to B95-8 virus at MOI 1 to 2 or 2089 at MOI 3 for 1 hour at 4°C, washed and resuspended in their culture medium. Infection with 2089 virus was only used

as a positive control for flow cytometry analysis. For experiments of *in vitro* activation of B cells, B cells were plated on top of irradiated or mitomycin C-treated LL8 CD40 ligand feeder cells and grown in RPMI supplemented with 10% FBS, 100 nM sodium selenite and 2 ng/ml IL-4 (R&D Systems, Recombinant Human IL-4). For mitomycin C treatment, feeder cells were treated with 4 µg/ml mitomycin C for 2 hours at 37°C.

Flow cytometry.

Peripheral B cells were stained with the Ghost Dye Red 780 viability dye and anti-CD19 monoclonal antibody conjugated to APC according to the manufacturers' protocols (TONBO Biosciences and Miltenyi Biotec respectively). For measuring DC-SIGN expression, cells were stained with the Ghost Dye Red 780 viability dye, anti-CD19 monoclonal antibody conjugated to APC or VioBlue and anti-DC-SIGN monoclonal antibody clone DCN46 conjugated to V450 or clone 120507 conjugated to APC and their respective isotype controls. For all staining procedures, the buffer used contained 1X PBS pH 7.2, 0.5% bovine serum albumin (BSA) and 2 mM EDTA. While staining with antibodies, 100 µg/ml mouse IgG (Jackson ImmunoResearch) was added to block non-specific binding. Appropriate compensation and Fluorescence Minus One (FMO) controls were used. Infection with KSHV was determined by GFP expression. For gating of GFP-positive cells, peripheral B cells were infected with the B95-8 strain of EBV as a negative control and the recombinant 2089 strain of EBV as a positive control. At least 10,000 cells were analyzed per condition on a BD LSR Fortessa cytometer and data analysis was performed using FLowJo software. For sorting of GFP-positive cells, cells were sorted on a BD FACSAria II BSL-2 cell sorter.

Cell cycle analysis.

EBV- and/or KSHV-infected peripheral B cells were fixed in 95% ethanol on ice and treated with 100 µg/mL RNAse A (Roche) in PBS. Cells were then stained with 60 µg/mL propidium iodide in PBS overnight at 4°C. At least 10,000 cells were analyzed per condition on a BD FACSCalibur cytometer equipped with 488-nm and 633-nm lasers. Data analysis was performed using ModFit LT, Version 5.0.

Growth curves and quantification of the number of GFP-positive cells in populations of infected B cells by fluorescence microscopy.

Peripheral B cells were stained with trypan blue and the number of live cells was measured with a hematocytometer at different time points following infection or sorting. Cells were passaged as needed and the dilution factor was monitored to calculate the number of doublings. When the number of GFP-positive cells was quantified, GFP-positive cells were counted at the same time points using fluorescence microscopy.

Quantification of the number of EBV and KSHV genomes per cell in infected B cells by real-time PCR.

Infected peripheral B cells were harvested in Trizol or Trizol LS (Invitrogen). DNA was isolated from lysed cells following the protocol from Invitrogen. Briefly, chloroform was added to the samples and following centrifugation, the aqueous phase was discarded. A back extraction buffer containing 4 M guanidine thiocyanate, 50 mM sodium citrate and 1 M Tris (free base) was added to the interphase-organic phase mixture. After

homogenization and centrifugation, the aqueous phase was isolated, 10 µg of acrylamide carrier was added, and the DNA was precipitated by adding isopropanol. The DNA pellet was washed with 70% ethanol and resuspended in TE. For each sample, approximately 100 ng of purified total DNA was analyzed by real-time PCR as described above. The number of viral DNA copies per cell was estimated by measuring the number of molecules of BALF5 (EBV), LANA1 (KSHV) and rhodopsin in each sample using the primers listed in Table II.1. Standard curves were created using linearized plasmids containing the DNA sequence of either BALF5, LANA1 or rhodopsin.

Fluorescence *in situ* hybridization.

Cells were fixed and hybridized with probes as previously described (26, 104). In brief, cells were treated with 0.075 M KCl for 20 min at 37°C, fixed in methanol:acetic acid at a 3:1 ratio for 30 min at room temperature, and spread on cold slides. Slides were dried and prehybridized in a buffer with 2 x SSC and 0.5% (vol/vol) Nonidet P-40 (Sigma-Aldrich) for 30 min at 37°C, dehydrated in a cold ethanol series (70%, 80%, and 95%) for 2 min each, air-dried at 50°C, denatured in a buffer with 70% formamide and 2 x SSC, pH 5.3, for 2 min at 72°C followed by dehydration with a cold ethanol series, and air-dried. The KSHV cosmid Z8 (105) was labeled with biotin-16-dUTP (Roche), and EBV p135.16 was labeled with digoxigenin-11-2′-deoxy-uridine-5′-triphosphate (Roche) by nick translation as hybridization probes for detection of KSHV and EBV genomes in cells, respectively. 200 ng of the labeled probe was precipitated along with 6 µg Salmon Sperm DNA (Invitrogen) and 4 µg Human Cot-1 DNA (Invitrogen) and resuspended in CEP hybridization buffer (55% formamide, 1 x SSC, pH 7.0, and 10% dextran sulfate) followed

by denaturation at 70°C for 10 min. 45 ng of the probe was then hybridized with each sample at 37°C overnight in a moist chamber. The slides were washed twice in 2 x SSC containing 50% formamide for 30 min at 50°C and twice in 2 x SSC for 30 min at 50°C. The hybridized probe was detected by incubation with 10 µl of a detection solution containing a mouse monoclonal anti-digoxin–FITC conjugate (Sigma-Aldrich) and a streptavidin-Cy3 conjugate (Sigma-Aldrich) for 20 min at 37°C. The slides were washed twice in 4 x SSC containing 0.05% Triton X-100 for 5 min at room temperature and mounted in Vectashield mounting medium with DAPI (Vector Laboratories) for staining chromosomes. The percentage of KSHV-positive and EBV-positive cells as well as the number of plasmids per cell were determined by counting the number of signals in at least 45 cells for each sample. FISH slides were imaged on an Axiovert 200M microscope and AxioVision software (Zeiss) was used for acquisition of the images. Images were digitally processed for presentation with Adobe Photoshop.

RNA isolation for RNA-Sequencing.

Dually infected B cells were harvested in Trizol or Trizol LS (Invitrogen). RNA was isolated using the Direct-zol RNA MiniPrep Kit (Zymo Research) and RNA quality was assessed using an Agilent 2100 Bioanalyzer.

Library Preparation and High-Throughput Sequencing.

Library preparation and sequencing was performed by the Oklahoma Medical Research Foundation Clinical Genomics Center (Oklahoma City, OK). The concentration of RNA was ascertained via fluorometric analysis on a Thermo Fisher Qubit fluorometer.

The overall quality of RNA was verified using an Agilent TapeStation instrument. Following initial quality control steps, sequencing libraries were generated using the Illumina Truseq Stranded mRNA library preparation kit according to the manufacturer's protocol. The final libraries for each sample were assayed on the Agilent TapeStation for appropriate size and quantity. These libraries were then pooled in equimolar amounts based on Qubit estimates. Final pools were quantified using qPCR on a Roche LightCycler 480 instrument with Kapa Biosystems Illumina Library Quantification reagents. Sequencing was performed on an Illumina NovaSeq 6000 instrument using XP clustering chemistry with paired-end 150 bp reads. RNA-Seq data were deposited in SRA (PRJNA544266).

RNA-Seq analysis.

Reads were mapped to the NCI Genomic Data Commons (GDC) reference genome with STAR_2.5.1b (106). Parameters for first and second pass mapping were selected from the GDC Harmonized mRNA Analysis Pipeline. First pass mapping used the GDC.h38.d1.vd1 STAR2 index. Second pass mapping was performed with an intermediate genome generated with the junctions of all samples. Reads mapping to cellular and viral genes were quantified with featureCounts v1.6.2 (107). The reverse strand mode was used consistent with the library preparation. For cellular genes, the GENCODE v22 GTF annotation was used. Viral gene counts were determined using a modification of the approach by Bruce et al. (108). Briefly, reads mapping to the unique coding sequence (UCDS) region of each KSHV gene were summed (UCDS regions were obtained from Bruce et al. (108)). For nested transcripts, an estimated count of the

overlapping portion of the larger transcript B was subtracted from the raw count of the UCDS region of the smaller transcript A using the formula: Counts($UCDS_A$) = RawCounts($UCDS_A$) - [RawCounts($UCDS_B$) x (Length($UCDS_A$) / Length($UCDS_B$))]. A similar approach was applied to EBV. UCDS regions were demarcated using the NCBI reference NC_007605.1 and regions identified by Dr. Eric Johannsen (Table II.2). Where possible, non-overlapping regions were identified and separated by at least 152 bp. When transcript structure prohibited this approach, nested transcripts were identified and quantified as described above (Figure II.1). Following this approach, only 0.7% to 3.1% of viral reads were unassigned to a specific transcript by featureCounts. For differential expression analysis, data normalization, model fitting, and fold-change calculations were performed in R (3.5.1) with DESeq2 version 1.22.1 (109). Genes with fewer than 10 reads across all samples were omitted from the analysis. Fold-change shrinkage was applied using the apeglm method (110). In heatmaps, the coloring is the columnwise z-scores of the variance-stabilizing transformation. The normalized expression in the coverage plots of RNA-seq reads was plotted using deepTools factoring in the total number of mapped reads (in millions) for each group of samples (7 samples of KSHV+/EBV+ fast cells and 5 samples of KSHV+/EBV+ slow cells). Gene Set Enrichment Analysis (GSEA) was performed with GSEA v3.0 (111, 112) with gene sets obtained from Klein et al. (genes downregulated or upregulated in PEL) (113) and MSigDB hallmark gene sets (database v6.2) (114). Gene expression from the DESeq2 comparison of the KSHV+/EBV+ fast cells vs the KSHV+/EBV+ slow cells was ranked with ranking metric -log(p-value)*sign(Log Fold Change) using GSEA PreRanked. Immunoglobulin clonotypes were determined using MiXCR v2.1.11 (115) with built-in V/D/J/C library: repseqio.v1.5. The recommended

pipeline for RNA-seq input was used. Clonotypes were determined using the IGH VDJ (CDR3) calls from MiXCR. The percentage of each immunoglobulin heavy and light chain in the different populations of cells was obtained from the MiXCR IGH and IGK/IGL results respectively. Publicly available datasets for KSHV-positive primary effusion lymphomas were obtained from SRA (PRJEB18662, PRJNA352335, PRJNA362820).

Complementation assay.

Each EBNA1-OriP plasmid, p3828, p174 or p3829, was electroporated into the BC-1 PEL cell line. BC-1 cells were then cultured in RPMI supplemented with 10% FBS and 1,200 µg/ml hygromycin. Total DNA was isolated after 9 months of culture using the DNeasy Blood and Tissue Kit (Qiagen). For each sample, 100 ng of purified total DNA was analyzed by real-time PCR as described above. The number of EBV genomes and plasmids copies per cell was estimated by measuring the number of molecules of BALF5, hygromycin and rhodopsin in each sample. Standard curves were created using linearized plasmids containing the DNA sequence of either BALF5, hygromycin or rhodopsin. The sequences of the primers used are listed in Table II.1.

Statistics.

The program Mstat, Version 6.3 or 6.4, was used for statistical analyses (N. Drinkwater, McArdle Laboratory for Cancer Research, School of Medicine and Public Health, University of Wisconsin) and is available for downloading (http://www.mcardle.wisc.edu/mstat). For analysis of flow cytometry data, at least three biological replicates were used for statistical analyses.

Table II.1: List of primers and probes used for real-time PCR and PCR.

The sequences of the primers and probes used for real-time PCR for detection of EBV, KSHV, rhodopsin and hygromycin are indicated. The primers used for amplification of the fragment in KSHV ORF50 (RTA) by PCR are also listed.

Table II.1

	Gene	Host	Primer	Sequence
Real-time PCR	BALF5	EBV	Forward	5'-CGGAAGCCCTCTGGACTTC-3'
			Reverse	5'-CCCTGTTTATCCGATGGAATG-3'
			Probe	5'-6-FAM/TGTACACGCACGAGAAATGCGCC/TAMRA-3'
	LANA1	KSHV	Forward	5'-AACAAATTGCCAGTAGCCCACCAG-3'
			Reverse	5'-TAACTGGAACGCGCCTCATACGAA-3'
			Probe	5'-6-FAM/ATACACCAG/ZEN/ACGATGACCCACAACCT/IABkFQ-3'
	Rhodopsin	Cellular	Forward	5'-ATCAGGAACCATTGCCACGTCCTA-3'
			Reverse	5'-AGGCCAAAGATGGACACACAGAGT-3'
			Probe	5'-6-FAM/AGCCTCTAG/ZEN/TTTCCAGAAGCTGCACA/IABkFQ-3'
	Hygromycin	Cellular	Forward	5'-GATGCAATAGGTCAGGCTCTCG-3'
			Reverse	5'-ATGTCCTGCGGGTAAATAGCTG-3'
			Probe	5'-6-FAM/AATTCCCCAATGTCAAGCACTTCCG/TAMRA-3'
PCR	ORF50 (RTA)	KSHV	Forward	5'-ACGTGGCAGTCTGGATTGAG-3'
			Reverse	5'-AATGCCTTGGGATGCCTCTG-3'

Table II.2: EBV unique coding sequences (UCDS).

The unique coding sequence (UCDS) of each EBV gene is indicated. UCDS were derived from the EBV reference sequence NC_007605.1 and were designed to limit overlap between adjacent transcripts. UCDS were spaced at least 152 bp apart to limit overlap of a 150 bp read. To determine EBV gene counts, reads mapping to the UCDS region of each EBV gene were summed. For nested transcripts, an estimated count of the overlapping portion of the larger transcript B was subtracted from the raw count of the UCDS region of the smaller transcript A using the formula: $Counts(UCDS_A) = RawCounts(UCDS_A) - [RawCounts(UCDS_B) \times (Length(UCDS_A) / Length(UCDS_B))]$.

Table II.2

UCDS	Start (bp)	End (bp)	Size (bp)	Strand	Subtract UCDS
BNRF1	1834	5256	3423	+	
EBERS	6629	7128	500	+	
BCRF1	9675	10184	510	+	
EBNA2	36216;36529	36377;37488	1122	+	
BHLF1	39829	40269	441	-	
BHRF1	42088	42660	573	+	
BFLF2	43694	44632	939	-	BFLF1
BFLF1	44784	46237	1454	-	
BFRF0.5	46236	46602	367	+	
BFRF1	46754	47519	766	+	BFRF0.5
BFRF2	47671	49004	1334	+	BFRF1
BFRF3	49293	49746	454	+	BFRF2
BPLF1	49793	59079	9287	-	
BOLF1	59880	62951	3072	-	
BORF1	62950	63753	804	+	
BORF2	64119	66520	2402	+	BORF1
BaRF1	66676	67517	842	+	
BMRF1	67669	68440	772	+	BaRF1
BMRF2	68898	69900	1003	+	BMRF1
SM/BMLF1	70458	71771	1314	-	BSLF1
BSLF1	72039	74593	2555	-	
BSRF1	74636	75289	654	+	
BLLF3	75353	76186	834	-	
BLRF1	76259	76524	266	+	
BLRF2	76677	77122	446	+	BLRF1
BLLF2	77282	77725	444	-	BLLF1
BLLF1	78365	79865	1501	-	
EBNA3A	79955;80382	80293;82874	2832	+	
EBNA3B	83065;83500	83421;85943	2801	+	
EBNA3C	86096;86517	86442;89132	2963	+	EBNA3B
BZLF2	89160	89828	669	-	
BZLF1	90367	90867	501	-	BRLF1
BRLF1	91081	92637	1557	-	
BRRF1	92894	93823	930	+	
BRRF2	94014	95563	1550	+	
EBNA1	95715;96637	95928;97586	1164	+	
BKRF2	97738	97989	252	+	
BKRF3	98141	98761	621	+	BKRF2
BKRF4	98914	99496	583	+	BKRF3
BBLF4	99545	101971	2427	-	

UCDS	Start (bp)	End (bp)	Size (bp)	Strand	Subtract UCDS
BBRF1	101916	103584	1669	+	
BBRF2	103736	104493	758	+	BBRF1
BBLF2/3	104496;105227	105098;106750	2127	-	
BBRF3	106849	108063	1215	+	
BBLF1	108472	108643	172	-	BGLF5
BGLF5	108838	109964	1127	-	BGLF4
BGLF4	110116	111056	941	-	BGLF3.5
BGLF3.5	111328	111666	339	-	BGLF3
BGLF3	111818	112651	834	-	
BGDRF1	112650;116927	113585;118060	2070	+	
BGLF2	113578	114540	963	-	BGLF-1
BGLF1	114692	116010	1319	-	BDLF4
BDLF4	116195	116648	454	-	BDLF3.5
BDLF3.5	116800	116945	146	-	
BDLF3	118077	118734	658	-	BDLF2
BDLF2	118886	120087	1202	-	BDLF1
BDLF1	120239	120943	705	-	
BcLF1	121095	125178	4084	-	
BcRF1	125177	127264	2088	+	
BTRF1	127430	128630	1201	+	BcRF1
BXLF2	128992	130673	1682	-	BXLF1
BXLF1	130826	132572	1747	-	
BXRF1	132571	132962	392	+	
BVRF1	133127	134836	1710	+	BXRF1
BVLF1	134812	135627	816	-	
BVRF2	135638	136342	705	+	
BdRF1	136494	137452	959	+	BVRF2
BILF2	137493	138236	744	-	
BILF1	151706	152641	936	-	
BALF5	153244	156215	2972	-	
BALF4	156367	158783	2417	-	
BALF3	158935	160474	1540	-	
BALF2	161002	164281	3280	-	
BALF1	164434	164945	512	-	
BARF1	165046	165708	663	+	
LMP2A	166103	166458	356	+	
BNLF2b	166543	166766	224	-	BNLF2a
BNLF2a	166919	167028	110	-	LMP1
LMP1	167705	168478	774	-	
LMP2B	169294	169448	155	+	

Figure II.1: Schematic representation of the approach used to determine EBV and KSHV viral gene counts.

The unique coding sequences (UCDS) were designed to limit overlap between adjacent transcripts. For EBV, UCDS were spaced at least 152 bp apart to limit overlap of a 150 bp read.

(A) To determine viral gene counts, reads mapping to the UCDS region of each viral gene were summed.

(B) For nested transcripts, an estimated count of the overlapping portion of the larger transcript was subtracted from the raw count of the UCDS region of the smaller transcript.

The formulas used to determine viral gene counts in both (A) and (B) are indicated. The black boxes with arrowheads represent the open reading frames (ORFs) of each transcript and the direction of transcription.

Figure II.1

A

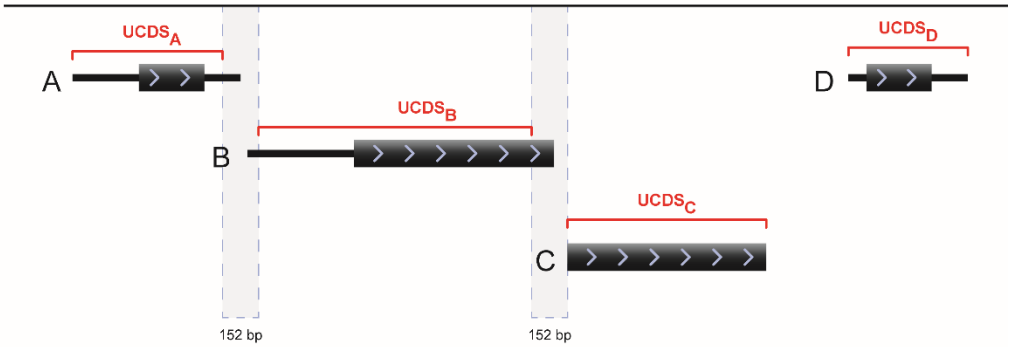

$$Counts(UCDS_A) = RawCounts(UCDS_A) \qquad Counts(UCDS_C) = RawCounts(UCDS_C)$$

$$Counts(UCDS_B) = RawCounts(UCDS_B) \qquad Counts(UCDS_D) = RawCounts(UCDS_D)$$

B

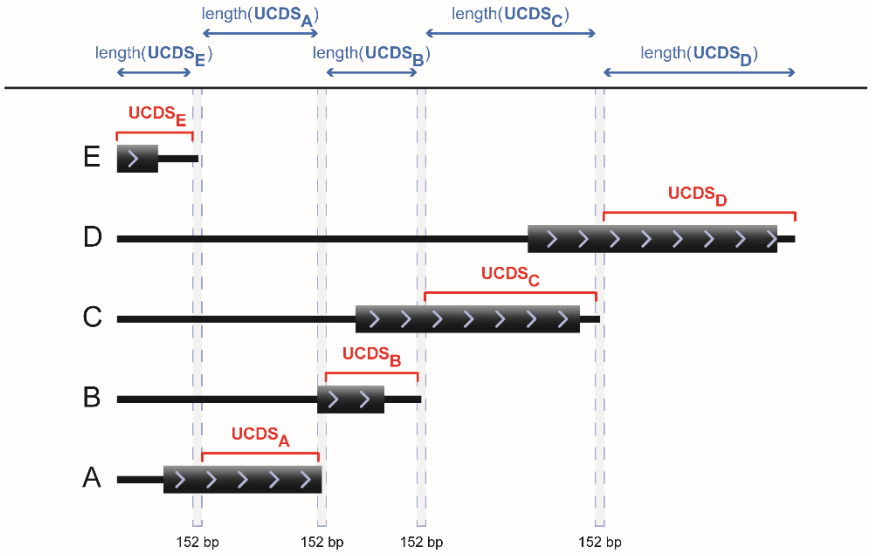

$$Counts(UCDS_E) = RawCounts(UCDS_E) - RawCounts(UCDS_A) \times \frac{Length(UCDS_E)}{Length(UCDS_A)}$$

$$Counts(UCDS_A) = RawCounts(UCDS_A) - RawCounts(UCDS_B) \times \frac{Length(UCDS_A)}{Length(UCDS_B)}$$

$$Counts(UCDS_B) = RawCounts(UCDS_B) - RawCounts(UCDS_C) \times \frac{Length(UCDS_B)}{Length(UCDS_C)}$$

$$Counts(UCDS_C) = RawCounts(UCDS_C) - RawCounts(UCDS_D) \times \frac{Length(UCDS_C)}{Length(UCDS_D)}$$

$$Counts(UCDS_D) = RawCounts(UCDS_D)$$

CHAPTER III.

Optimizing KSHV mass production and infection

A note on the contributions to this chapter:

Some of the KSHV viral stocks in this chapter were produced by an undergraduate student, Manjistha Ahooja, under my mentorship. Bill Sugden also helped produce some of the viral stocks and generated the clones of iSLKBAC16 cells.

INTRODUCTION

In order to study the efficiency of infection of peripheral B cells with KSHV (see CHAPTER IV and CHAPTER V), we needed to establish a protocol to produce and titer KSHV virus efficiently and reproducibly. In this chapter, we tested and compared different protocols for the mass production and titer of KSHV virus. iSLKBAC16 cells (75, 99) were used to produce KSHV virus because these cells are carrying the recombinant wild-type KSHV BAC16 (99) that does not contain the duplication found in KSHV BAC36 (116). KSHV BAC16 is derived from the rKSHV.219 virus, isolated from the JSC-1 PEL cell line (99). We measured the number of KSHV physical particles obtained upon induction of iSLKBAC16 cells by real-time PCR and optimized the protocol described by Brulois et al. (99). We found that KSHV genome integrates with some frequency in iSLKBAC16 cells which led to a significant reduction in the production of KSHV virions when these cells were maintained in culture for prolonged periods of time. We show that cloning the iSLKBAC16 cells can prevent the decrease in the production of KSHV virus over time.

The recombinant KSHV BAC16 virus contains a GFP reporter driven by the constitutively active promoter EF1α. We thus used GFP expression to monitor successful infection of cells with KSHV. 293 cells, which have been reported to be susceptible to KSHV infection (76, 77), were used to titer KSHV virus. We found that the filtration of KSHV viral stocks affects both the number of physical particles obtained and their infectivity. Furthermore, we found that KSHV does not bind efficiently to cells and that washing cells following exposure to the virus decreases the efficiency of infection. Centrifugation, also called spinoculation, has been shown to enhance the infection of human umbilical vein endothelial cells (HUVECs) by KSHV but its mechanism is not

understood (103). We show that spinoculation increases the binding of KSHV to cells, which led to a two-fold increase in the efficiency of infection of 293 cells by KSHV.

RESULTS

I. Optimizing KSHV mass production

KSHV genome integrates with some frequency in iSLKBAC16 cells.

iSLKBAC16 cells were grown in DMEM supplemented with 10% FBS, 250 µg/ml G418, 1 µg/ml puromycin and 1,200 µg/ml hygromycin. We first induced these cells following the protocol described by Brulois et al. (99) with 1 µg/ml doxycycline and 1 mM sodium butyrate in the absence of G418, puromycin, and hygromycin. The supernatant was harvested at day 4 and 5 and cleared of cells and debris by centrifugation at 500 g for 10 mins and filtration with a 0.8 µm filter. For concentrated virus stocks, the supernatant was concentrated 100-fold by centrifugation at 48,000 g for 2 hours. We compared the number of physical particles per ml in the supernatant of iSLKBAC16 cells maintained in culture for a short period of time (early passage) and cells maintained in culture for more than one year (late passage). We found that cells from an early passage produced on average 8 to 15-fold more KSHV viral particles than cells maintained in culture for a long period of time (Figure III.1). Using fluorescence *in situ* hybridization (FISH), we found that cells from a late passage had one KSHV copy genome per cell, indicating that KSHV was integrated in these cells. To prevent cells with an integrated KSHV genome to be selected in culture over time, we generated clones from early passage iSLKBAC16 cells. We then studied the production of KSHV virus from two different clones (clone 2 and clone 5) and early passage iSLKBAC16 cells only.

Valproic acid and sodium butyrate activate KSHV virus production with similar efficiencies.

Valproic acid (VPA) was found to be one of the most efficient histone deacetylase (HDAC) inhibitors in inducing KSHV reactivation (117). We therefore tested whether induction of iSLKBAC16 cells with VPA instead of sodium butyrate would increase the production of KSHV virus. We measured the number of KSHV physical particles per ml in the supernatant and concentrated viral stocks of cells induced with sodium butyrate or VPA by real-time PCR. The protocol for induction with VPA was similar to that of sodium butyrate: cells were induced with 1 μg/ml doxycycline and 1 mM VPA in the absence of selection. The supernatant was harvested at day 4 to 8 and cleared of cells and debris by centrifugation and filtration. For both sodium butyrate and VPA, viral production was induced from early passage iSLKBAC16 cells or iSLKBAC16 clones 2 and 5. We found no difference in the number of KSHV physical particles in the supernatant of cells induced with sodium butyrate or VPA (Figure III.2).

Filtration of viral supernatants decreases the number of KSHV physical particles by 4-fold.

As described above, cells and debris were removed from viral supernatants by centrifugation at 500 g for 10 mins and filtration with a 0.8 μm filter. We asked whether filtering the viral supernatants affects the number of KSHV physical particles obtained. Cells were induced with VPA following the protocol described above and the supernatants were either filtered or not filtered prior to concentration. The number of KSHV physical particles per ml was measured by real-time PCR in the supernatants of clone 2 and clone 5 iSLKBAC16 cells. Following concentration of the viral supernatants, we found that clone 5 produced up to 9-fold more KSHV physical particles than clone 2 (Figure III.3). In

addition, we found that the number of KSHV physical particles per ml in the concentrated virus stocks obtained from clone 5 iSLKBAC16 cells were on average 4-fold higher when they were not filtered compared to those that were filtered (Figure III.3). Although not statistically significant, possibly because we need more replicates, these data suggest that clone 5 can be more efficiently induced than clone 2 and that filtration decreases the number of physical particles in the viral supernatants.

II. Optimizing KSHV infection

KSHV titer is not affected by the number of cells plated for infection.

293 cells were used to titer KSHV virus stocks because they are one of the cell lines found to be the most susceptible to KSHV infection (76, 77). The recombinant KSHV BAC16 virus contains a GFP reporter that allowed us to monitor successful infection of 293 cells with KSHV. 293 cells were grown in DMEM supplemented with 10% FBS. 293 cells were plated in 24-well plates at different concentrations and were exposed to KSHV supernatants or concentrated viral stocks by incubation at 4°C for 1 hour in their culture medium supplemented with 50 mM HEPES. Following incubation, 293 cells were washed to remove excess, unbound virus and were resuspended in their culture medium. The number of GFP-positive cells was determined by fluorescence microscopy 3 or 4 days post-exposure to KSHV. The number of infectious viral particles was calculated by multiplying the percentage of GFP-positive cells by the total number of cells at the time of infection.

We compared the number of infectious particles per physical particles obtained when the virus was titered on different concentrations of cells. The number of 293 cells

per well was counted on the day of infection. We asked whether there is a difference in infectivity if we expose less than 1E+05 cells (between 2.8E+04 and 5.6E+04 cells) or approximately 1E+05 cells (between 1.08E+05 and 1.12E+05 cells) to KSHV. In this experiment, the KSHV viral supernatants or concentrated stocks titered were not filtered. Cells and debris were removed by centrifugation prior to infection or concentration. We found no difference in the titer depending on the number of cells exposed to the virus (Figure III.4). On average 1 in 700 to 1,000 KSHV viral particles was infectious on 293 cells.

Washing cells following exposure to KSHV significantly decreases the titer.

Because the infectivity with KSHV was low (for EBV, 1 in 100 or 1 in 200 physical particles is usually found to be infectious), we asked whether incubating the cells with the virus for a longer period of time would improve the infection. 293 cells and KSHV virus were incubated for 1 hour at 4°C as previously described. Following incubation, cells were washed or additional medium (DMEM with 10% FBS and 50 mM HEPES) was added and cells and virus were incubated for an additional 72 hours at 37°C. As above, the number of GFP-positive cells was counted using fluorescence microscopy and the number of infectious viral particles was determined. The number of physical particles for one infectious unit was compared when the titer was measured with or without washing the cells following exposure to the virus. If the infectivity decreases, this ratio will increase. For both filtered and non-filtered virus stocks, we found that washing the cells following exposure to the virus significantly decreases the titer by 3 to 9-fold (Figure III.5). When

cells were not washed, we found on average between 1 in 300 and 1 in 600 viral particles to be infectious on 293 cells.

The filtering of KSHV viral stocks significantly decreases their infectivity.

When we compared the titer measured with viral stocks that were or were not filtered, we found that KSHV viral stocks that were not filtered were more infectious (Figure III.6). When cells were washed following exposure to KSHV, the non-filtered viral stocks were significantly more infectious, with a 7-fold difference in the number of infectious units per physical particles. There was a lower difference when cells were not washed following infection, with the non-filtered viral stocks being only two times more infectious. This result could be explained by the longer period of incubation of cells with the virus which would result in more cells being infected over time. When the titer was performed without washing the cells following infection, on average 1 in 300 viral particles was infectious in non-filtered viral stocks.

Spinoculation significantly increases KSHV titer.

Centrifugation, also called spinoculation, has been shown to enhance the infection of human umbilical vein endothelial cells (HUVECs) by KSHV (103). The mechanism by which spinoculation enhances KSHV infection of HUVECs is not understood (103). We asked whether spinoculation also increases the efficiency of infection of 293 cells by KSHV. 293 cells were exposed to non-filtered KSHV viral stocks by incubation at 4°C for 1 hour or cells and virus were centrifugated at 950 g for 90 mins at room temperature (spinoculation). Cells were either washed following exposure to the virus, or additional

medium was added and cells and virus were incubated for an additional 72 hours at 37°C. When cells were washed, we found that spinoculation significantly increases the efficiency of infection of 293 cells by KSHV by 2-fold (Figure III.7). Contrary to incubation at 4°C, washing the cells following exposure to the virus did not significantly decrease the titer. The titer measured when cells were washed following spinoculation was similar to the titer obtained when cells were infected at 4°C and the cells and virus were incubated for an additional 3 days at 37°C. By titering KSHV virus stocks using spinoculation, we found on average between 1 in 150 and 1 in 300 viral particles to be infectious.

Spinoculation increases the binding of KSHV to cells.

In order to understand how spinoculation enhances KSHV infection, we used a neutralizing antibody against KSHV glycoprotein gpK8.1A (anti-gpK8.1A 4A4). Virion envelope-associated gpK8.1A is thought to mediate KSHV binding to target cells via interaction with heparan sulfate moieties (118). Studies have indicated that the gpK8.1A glycoprotein is involved in KSHV binding to target cells but is not required for viral entry (119, 120). 293 cells were exposed to non-filtered KSHV viral stocks in the presence or absence of anti-gpK8.1A 4A4 by incubation at 4°C for 1 hour or by spinoculation. For exposure with spinoculation, cells and virus were centrifugated at 950 g for 90 mins at room temperature. Following exposure to KSHV, additional medium was added and cells and virus were incubated for an additional 3 or 7 days at 37°C. The percentage of GFP-positive 293 cells was then measured by fluorescence microscopy.

When cells were exposed to KSHV by incubation at 4°C and cells and virus were subsequently incubated at 37°C, the number of cells infected increased over time, from

25-50% at 3 days to 70% at 7 days. We found that the anti-gpK8.1A 4A4 antibody inhibited infection by KSHV by 40% to 70% in 293 cells at 3 days post-infection (Table III.1). The inhibition of KSHV infection was transient: the percentage of cells infected was similar in the presence or absence of the antibody at 7 days post-infection. These results are consistent with the anti-gpK8.1A 4A4 antibody inhibiting KSHV binding to cells but not viral entry. Interestingly, we found that when cells were exposed to KSHV by spinoculation and cells and virus were subsequently incubated at 37°C, the number of cells infected was the same, approximately 70%, at 3 and 7 days post-infection. The anti-gpK8.1A 4A4 antibody inhibited infection by KSHV by only 8% at 3 days post-infection and we did not see an inhibition of infection at 7 days post-infection. These results indicate that spinoculation increases the efficiency by which KSHV binds to cells.

III. Protocol established for production and titration of KSHV viral stocks.

Based on these experiments, we established a protocol for production and titration of KSHV viral stocks on 293 cells. The KSHV viral stocks used in CHAPTER IV and CHAPTER V were produced and titered according to this protocol.

For production of KSHV virus, we used iSLKBAC16 clone 5 cells. Cloning of iSLKBAC16 cells prevented the selection in culture of cells with an integrated KSHV genome. We also found clone 5 to be the more efficiently induced than clone 2. iSLKBAC16 clone 5 cells were induced with 1 µg/ml doxycycline and 1 mM valproic acid in the absence of selection. Because we found filtration to decrease both the number of physical particles and their infectivity, the viral supernatant was not filtered but was cleared of cells and debris by multiple rounds of centrifugation (500 g for 10 mins followed

by 3,000 g for 10 mins). The viral supernatants were then concentrated by centrifugation at 48,000 g for 2 hours and separate viral aliquots were kept at -80°C. Concentrated viral stocks were thawed immediately before use and another round of centrifugation at 950 g for 10 mins was performed to remove any remaining debris.

For titration of KSHV viral stocks, we found that the number of 293 cells plated did not affect the titer. 293 cells were counted on the day of infection and approximately 1E+05 cells were exposed to KSHV by incubation at 4°C for 1 hour. Each virus stock was titered by serial dilution. We found that washing cells following exposure to the virus underestimates the titer. Therefore, following incubation, cells were not washed but additional medium was added and cells and virus were incubated for an additional 72 hours at 37°C. The number of GFP-positive cells was determined by fluorescence microscopy and the number of infectious viral particles was calculated by multiplying the percentage of GFP-positive cells by the total number of cells at the time of infection. For all viral stocks used in CHAPTER IV and CHAPTER V, approximately one in 100 to one in 200 physical particles was infectious.

Figure III.1: KSHV genome integrates with some frequency in iSLKBAC16 cells.

The number of physical particles per ml in the supernatant (A) or concentrated virus stock (B) obtained after induction of iSLKBAC16 cells maintained in culture for a short period of time (early passage) or for more than one year (late passage) was measured by real-time PCR. The number of biological replicates is indicated for each condition. * $p < 0.05$ by Wilcoxon rank sum test. Error bars show the 95% confidence interval.

Figure III.1

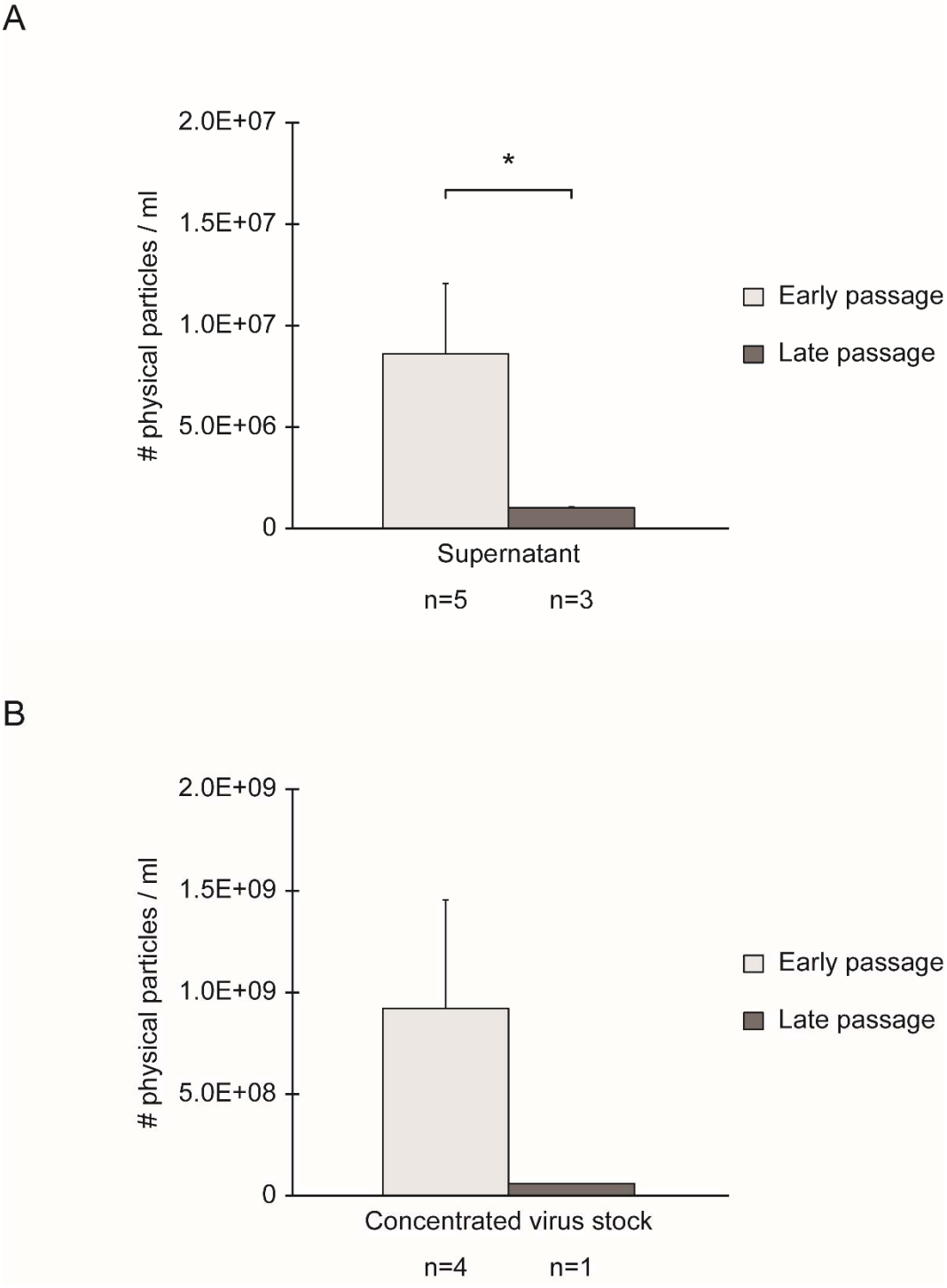
A
2.0E+07
1.5E+07
1.0E+07
5.0E+06
0
physical particles / ml
*
Early passage
Late passage
Supernatant
n=5
n=3
B
2.0E+09
1.5E+09
1.0E+09
5.0E+08
0
physical particles / ml
Early passage
Late passage
Concentrated virus stock
n=4
n=1

Figure III.2: Valproic acid and sodium butyrate activate KSHV virus production with similar efficiencies.

The number of KSHV physical particles per ml in the supernatant (A) and concentrated viral stocks (B) of cells induced with sodium butyrate (NaBut) or valproic acid (VPA) was measured by real-time PCR. Viral production was induced from early passage iSLKBAC16 cells or iSLKBAC16 clones 2 and 5. The number of biological replicates is indicated for each condition. N.S. $p > 0.05$ by Wilcoxon rank sum test. Error bars show the 95% confidence interval.

Figure III.2

A

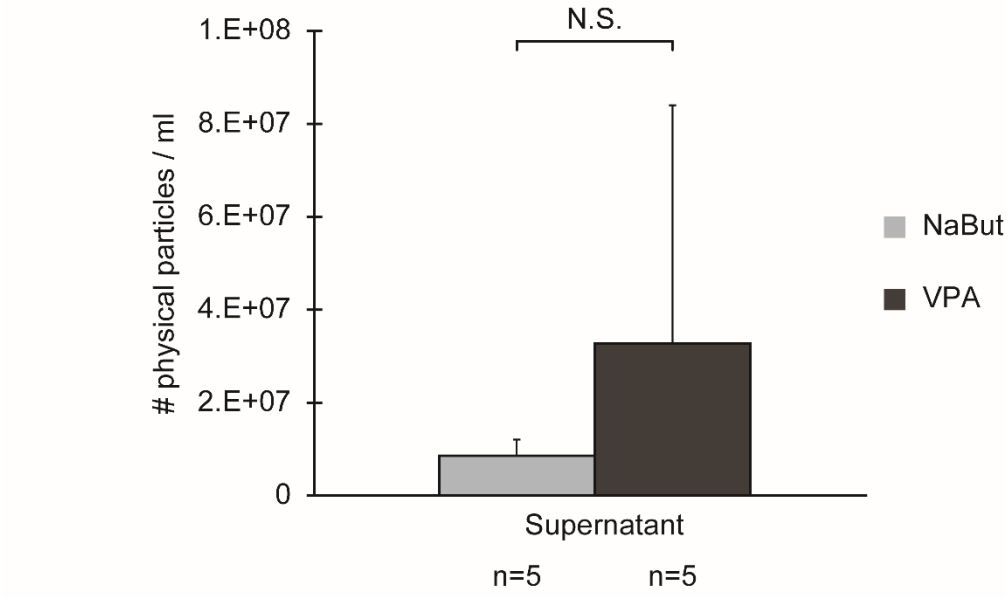

B

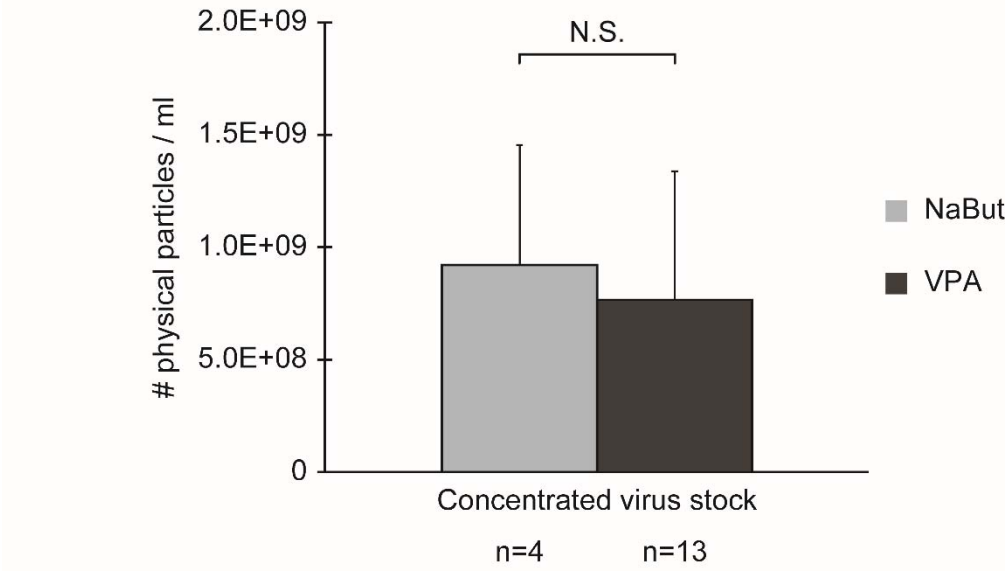

Figure III.3: Filtration of viral supernatants decreases the number of KSHV physical particles by 4-fold.

The number of KSHV physical particles per ml was measured by real-time PCR in supernatants (A) and concentrated viral stocks (B) obtained from clone 2 and clone 5 iSLKBAC16 cells induced with VPA. The supernatants were either filtered or not filtered prior to concentration. The number of biological replicates is indicated for each condition. Error bars show the 95% confidence interval.

Figure III.3

A

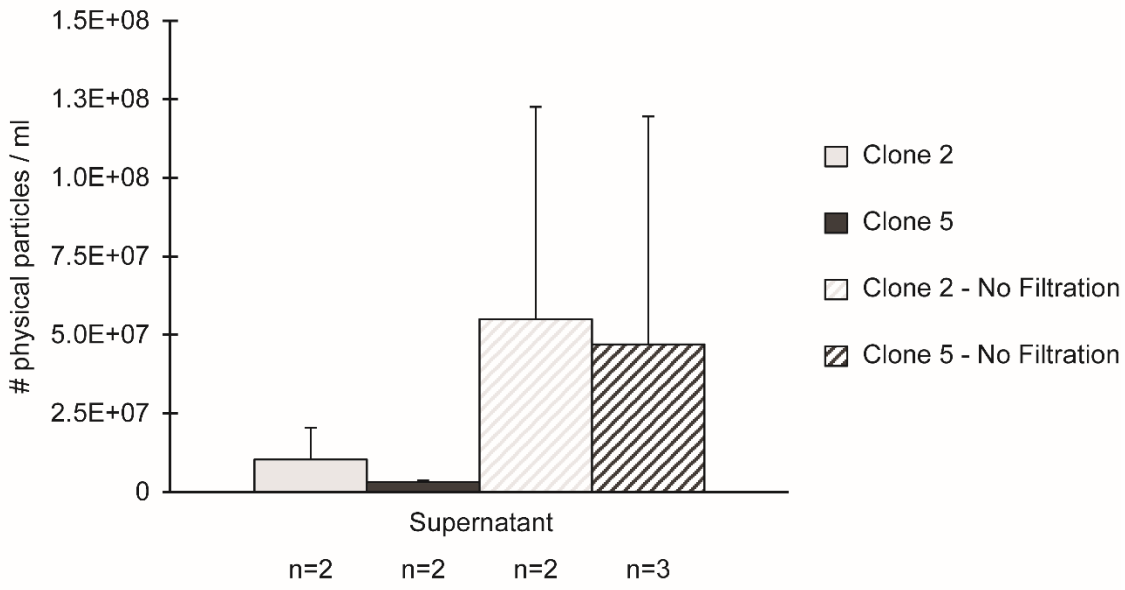

B

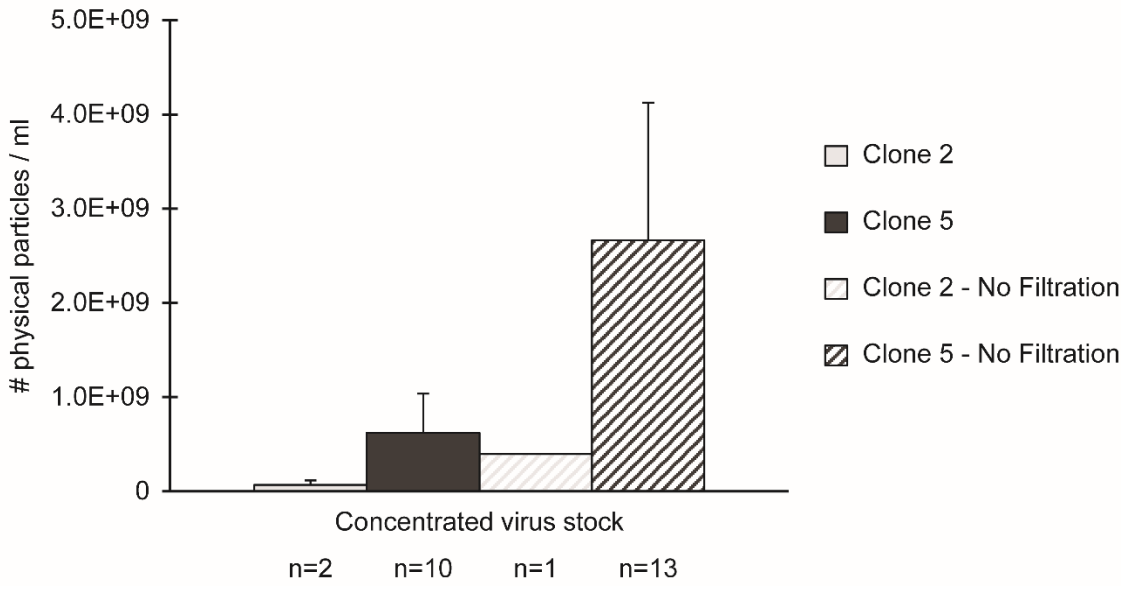

Figure III.4: KSHV titer is not affected by the number of cells plated for infection.

Different concentrations of 293 cells (less than 1E+05 cells or more than 1E+05 cells per well of a 24-well plate) were exposed to KSHV by incubation at 4°C for 1 hour. 293 cells were then washed to remove excess, unbound virus and resuspended in their culture medium. The number of GFP-positive cells was determined by fluorescence microscopy 3 or 4 days post-exposure to KSHV. The number of infectious units (IU) was calculated by multiplying the percentage of GFP-positive cells by the total number of cells at the time of infection. The number of physical particles (previously determined by real-time PCR) for one infectious unit was calculated for each titer. The number of biological replicates is indicated for each condition. N.S. $p > 0.05$ by Wilcoxon rank sum test. Error bars show the 95% confidence interval.

Figure III.4

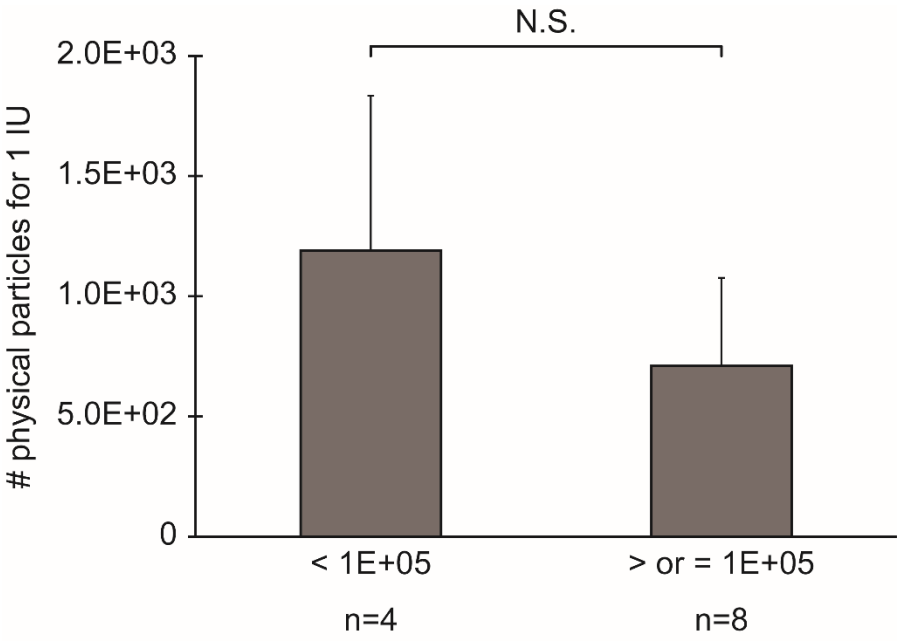
N.S.
2.0E+03
1.5E+03
1.0E+03
5.0E+02
0
physical particles for 1 IU
< 1E+05
n=4
> or = 1E+05
n=8

Figure III.5: Washing cells following exposure to KSHV significantly decreases the titer.

293 cells were exposed to KSHV by incubation at 4°C for 1 hour. Following incubation, 293 cells were either washed to remove excess, unbound virus or additional medium was added to the cells. The number of GFP-positive cells was determined by fluorescence microscopy 3 or 4 days post-exposure to KSHV. The number of physical particles for one infectious unit (IU) was determined as described in Figure III.4 for both filtered (A) and non-filtered (B) virus stocks. The number of biological replicates is indicated for each condition. ** $p < 0.01$ by Wilcoxon rank sum test. Error bars show the 95% confidence interval.

Figure III.5

A

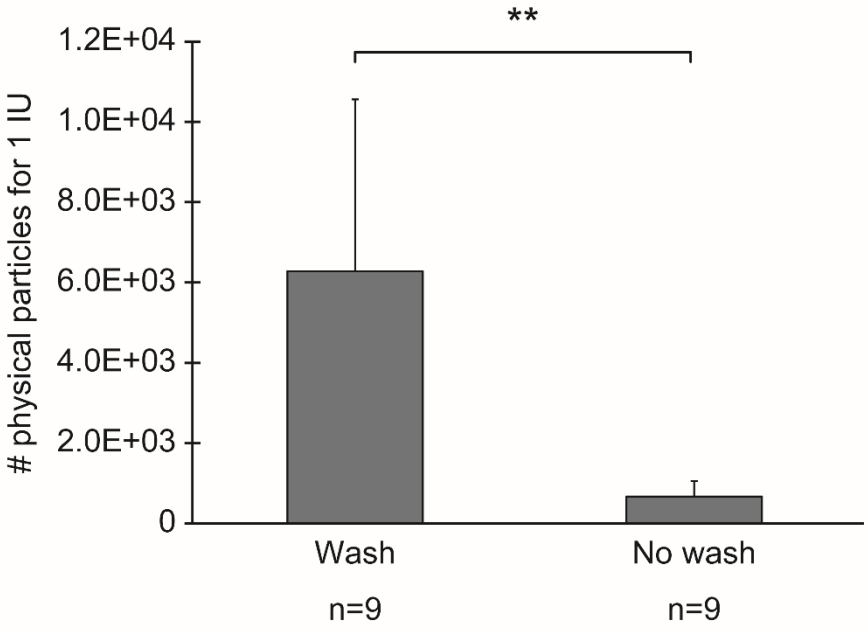

B

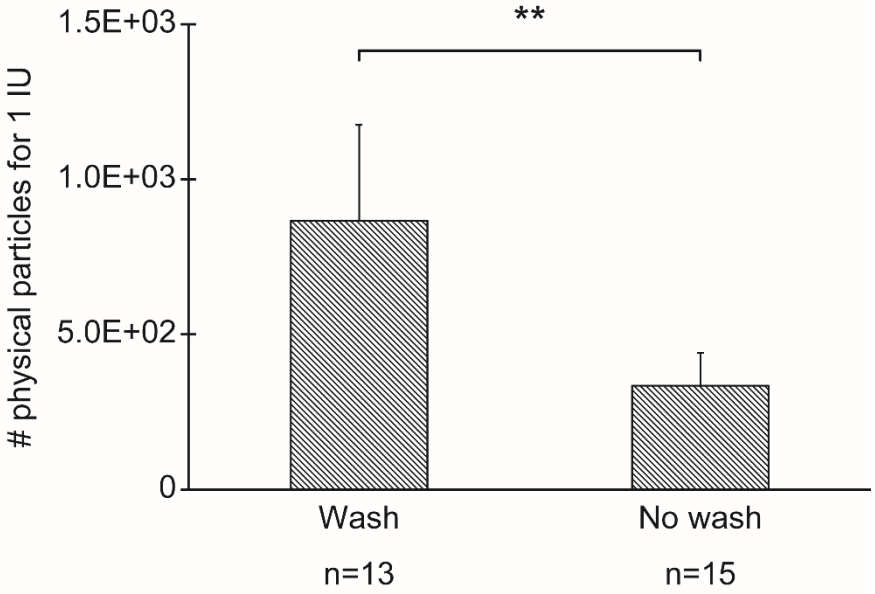

Figure III.6: The filtering of KSHV viral stocks significantly decreases their infectivity.

KSHV virus stocks that were or were not filtered were titered on 293 cells. 293 cells were exposed to KSHV by incubation at 4°C for 1 hour. Following incubation, 293 cells were either washed to remove excess, unbound virus (A) or additional medium was added to the cells (B). The number of GFP-positive cells was determined by fluorescence microscopy 3 or 4 days post-exposure to KSHV. The number of physical particles for one infectious unit (IU) was determined as described in Figure III.4. The number of biological replicates is indicated for each condition. ** $p < 0.01$ by Wilcoxon rank sum test. Error bars show the 95% confidence interval.

Figure III.6

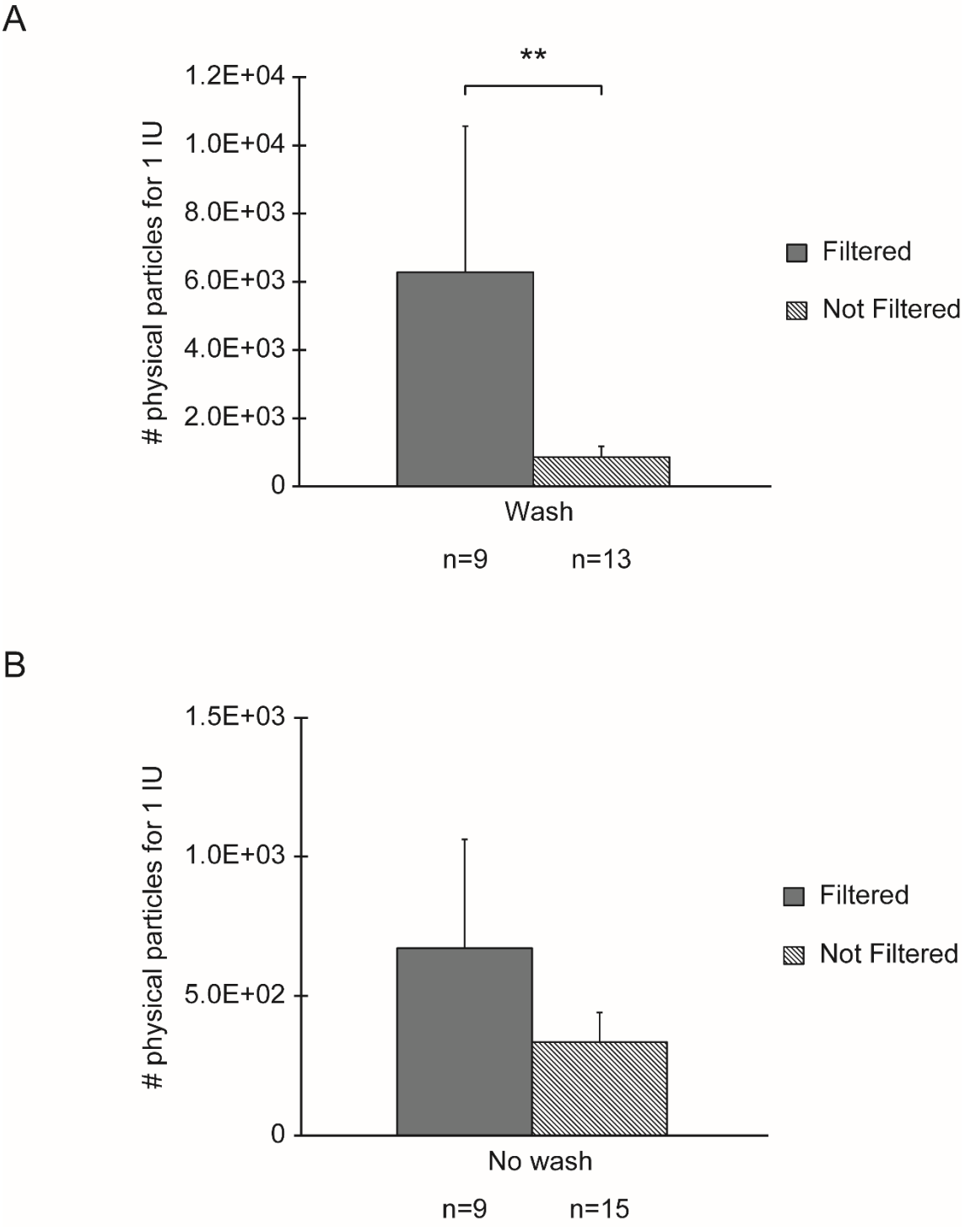
A
**
1.2E+04
1.0E+04
8.0E+03
6.0E+03
4.0E+03
2.0E+03
0
physical particles for 1 IU
Filtered
Not Filtered
Wash
n=9
n=13
B
1.5E+03
1.0E+03
5.0E+02
0
physical particles for 1 IU
Filtered
Not Filtered
No wash
n=9
n=15

Figure III.7: Spinoculation significantly increases KSHV titer.

293 cells were exposed to non-filtered KSHV viral stocks by incubation at 4°C for 1 hour or by spinoculation. For exposure with spinoculation, cells and virus were centrifugated at 950 g for 90 mins at room temperature. Cells were either washed following exposure to the virus, or additional medium was added and cells and virus were incubated for an additional 72 hours at 37°C. The number of physical particles for one infectious unit (IU) was determined as described in Figure III.4. The number of biological replicates is indicated for each condition. * $p < 0.05$; ** $p < 0.01$ by Wilcoxon rank sum test. Error bars show the 95% confidence interval.

Figure III.7

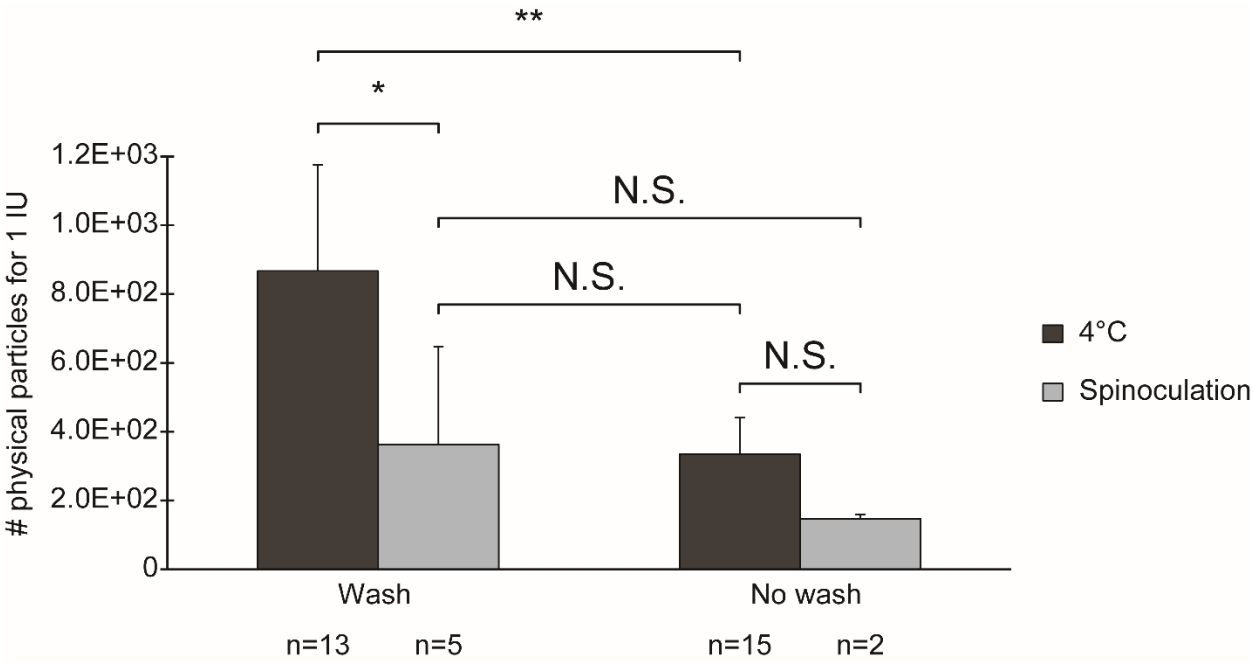
**
*
N.S.
N.S.
N.S.
1.2E+03
1.0E+03
8.0E+02
6.0E+02
4.0E+02
2.0E+02
0
physical particles for 1 IU
Wash
No wash
n=13
n=5
n=15
n=2
4°C
Spinoculation

Table III.1: Spinoculation increases the binding of KSHV to cells.

293 cells were exposed to non-filtered KSHV viral stocks in the presence or absence of anti-gpK8.1A 4A4 by incubation at 4°C for 1 hour or by spinoculation. For exposure with spinoculation, cells and virus were centrifugated at 950 g for 90 mins at room temperature. Following exposure to KSHV, additional medium was added and cells and virus were incubated for an additional 3 or 7 days at 37°C. The percentage of GFP-positive 293 cells measured by fluorescence microscopy is indicated.

Table III.1

Method of titration	Count # GFP+ cells at	Biological replicate #	% of GFP+ cells		% inhibition
			KSHV	KSHV + anti-gpK8.1A 4A4	
Incubation at 4°C	3 days	1	25.0	14.5	42.0
		2	55.5	16.9	69.5
	7 days	1	70.0	70.0	0.0
Spinoculation	3 days	1	76.0	69.6	8.4
	7 days	1	70.0	70.0	0.0

DISCUSSION

In this chapter, we have established a reproducible protocol to produce and titer KSHV virus from iSLKBAC16 cells. We found that the KSHV genome can integrate in iSLKBAC16 cells and that cells with an integrated genome can be selected in culture over time. Therefore, we established a clone, iSLKBAC16 clone 5, that can be maintained in culture and can be efficiently induced to produce KSHV virus. We also found that by filtering the viral supernatant, we both lost viral particles and decreased their infectivity. Cells and debris were therefore removed by multiple rounds of centrifugation prior to concentration of the viral supernatant and immediately before infection. Interestingly, we found that KSHV does not bind efficiently to cells and that washing the cells following exposure to the virus significantly decreased the efficiency of infection. We found that spinoculation increased the binding of KSHV to cells, and that the efficiency of infection measured after washing the cells was similar to that of cells exposed to KSHV for an additional 3 days at 37°C. Therefore, for experiments that required washing the cells following exposure to KSHV, such as the experiments performed on peripheral B cells in the following chapters, cells were exposed to the virus by spinoculation.

CHAPTER IV.

EBV infection supports an optimal infection of peripheral B cells by KSHV

Parts of this chapter have been adapted into a manuscript. The manuscript has been accepted for publication and is referenced below:

Aurélia Faure, Mitch Hayes and Bill Sugden (2019) How Kaposi's sarcoma-associated herpesvirus stably transforms peripheral B cells towards Lymphomagenesis. *Proc Natl Acad Sci*, in press.

INTRODUCTION

KSHV is lost from proliferating cells if it does not provide its host cells selective advantages (26).The maintenance of KSHV genome as plasmid in PEL cells both *in vivo* and *in vitro* indicates that KSHV contributes to their phenotypes. In addition, several KSHV genes have been shown to be essential for the survival or proliferation of these cells (27–29). However, we formerly lacked a model which allows complete characterization *in vitro* of the early steps of development of PEL: B cells have been notoriously difficult to infect with KSHV *in vitro* and when they can be infected, KSHV has not been found to transform them. We first asked whether we could define conditions to infect B cells with KSHV *in vitro*. Previous attempts to infect lymphoblastic cell lines including B and T cell lines have been unsuccessful (75–78). In these studies, neither EBV-negative nor EBV-positive B cell lines could be infected. Several studies have found that primary CD19+ B cells isolated from peripheral blood and umbilical cord blood mononuclear cells are susceptible to KSHV infection (76, 78, 79). However, infection could only be detected by DNA PCR or RT-PCR shortly after infection. Recently, several groups have reported more robust infection of primary B cells isolated from tonsils with 0.5% to 10% of tonsillar B cells being infected with KSHV (80–84).

Therefore, the conditions necessary for KSHV to infect B cells that lead to PEL remain unclear. We reasoned that because EBV is also found as a plasmid in the majority of examined PELs, it would be providing these cells one or more selective advantages. Contrary to KSHV, EBV can infect and transform peripheral B cells *in vitro* and induce their long-term proliferation (85, 86). One study has reported detection of KSHV DNA by PCR in newly-transformed B cells following exposure to both viruses, suggesting that

cells can be dually infected *in vitro* (78). In this chapter, I describe extensive, quantitative experiments in which I define a role for EBV in supporting co-infection by KSHV. We show that EBV promotes infection of peripheral CD19+ B cells with KSHV, likely in part by providing activation of these cells. We found that the efficiency of infection of peripheral B cells with KSHV is optimal within 24 hours of EBV infection: early events of EBV infection promote infection by KSHV while later events inhibit this co-infection.

RESULTS

In vitro activation of peripheral B cells supports detectable but inefficient KSHV infection.

Peripheral blood mononuclear cells (PBMCs) were isolated from blood and CD19+ B cells were purified from them by negative selection to avoid stimulation of cell surface receptors. These CD19+ B cells were exposed to concentrated viral stocks of KSHV BAC16 using a multiplicity of infection (MOI) of 2 to 3 as determined on 293 cells. KSHV BAC16 is derived from the rKSHV.219 virus, isolated from the JSC-1 PEL cell line (99). The recombinant KSHV BAC16 virus contains a GFP reporter driven by the constitutively active promoter EF1α. Previous studies (81) and our own observations showed that, even following extensive washes, KSHV viral particles remain bound to the surface of primary B cells. We found that when B cells were exposed to KSHV and extensively washed before being plated on top of human fibroblasts (HF), the fibroblasts became infected with KSHV. On the contrary, we found that the HF were not infected with KSHV when incubated with the supernatant from the last wash. These results indicate that the fibroblasts were infected with B-cell bound virus. Therefore, GFP expression allowed us to monitor successful KSHV infection, as opposed to nucleic acid detection that does not distinguish viral entry from cell-surface bound particles. In addition, we confirmed that GFP expression indicates the presence of KSHV DNA in cells as measured by fluorescence *in situ* hybridization (FISH) (see CHAPTER V).

We found that peripheral B cells were refractory to infection by KSHV. Peripheral CD19+ B cells were spinoculated with KSHV BAC16 virus, before washing to remove unbound virus and subsequently cultured for 4 to 7 days to allow GFP expression. We

monitored the number of CD19+ B cells expressing GFP by flow cytometry and detected no KSHV-infected (GFP+) CD19+ B cells in 5 independent biological replicates obtained from 3 different blood donors (Figure IV.1). Furthermore, no GFP-positive cells were detected by fluorescence microscopy at day 1, 2, or 3 confirming that no detectable KSHV infection occurred prior to flow cytometric analysis. These results demonstrate that KSHV cannot establish successful infection in resting, peripheral CD19+ B cells.

Because peripheral B cells could not be successfully infected with KSHV while other researchers have reported successful infection of tonsillar B cells which often contain activated B cells, we tested whether B cell activation supports detectable KSHV infection. Isolated CD19+ B cells were exposed to KSHV BAC16 at different time points prior to or following activation with IL-4 and CD40L. We found that *in vitro* activation of peripheral B cells could support, in some cases, detectable but inefficient KSHV infection (Figure IV.1). Infection of peripheral B cells with KSHV was highest when cells were infected with KSHV prior to IL-4 and CD40L activation (0.13 ± 0.14% with a maximum of 0.28% of GFP-positive cells). In comparison, 0.02 ± 0.02%, 0.03 ± 0.01% and 0.06 ± 0.06% of B cells were GFP-positive when cells were exposed to KSHV only or KSHV respectively 1 day and 3 days following B cell activation. In addition, no KSHV infection was detected when cells were exposed to KSHV and activated with IL-4 and CD40L on the same day in a single experiment (Table IV.1). These low efficiencies in presence of IL-4 and CD40L were confirmed as live cells were passaged for approximately 5 doublings and GFP-positive cells could still be detected by flow cytometry.

EBV infection supports an optimal infection of peripheral B cells by KSHV.

We tested whether EBV co-infection supports an optimal infection of peripheral B cells with KSHV. Peripheral CD19+ B cells were infected with the B95-8 strain of EBV at MOI 1 to 2. An average of 70% of the cells were blasts at day 3 or 4 post-infection with EBV (average from 7 independent biological replicates). CD19+ B cells were exposed to KSHV BAC16 at different time points prior to, on the same day as, or following EBV infection. EBV infection promoted optimal infection (up to a 20-fold increase relative to activated B cells) of peripheral B cells with KSHV (up to 2.50 ± 1.13%) (Figure IV.2A and B). The efficiency of infection with KSHV was comparable to that previously reported in tonsillar B cells (80–84). However, EBV played a conflicting role in KSHV infection: early events of EBV infection promoted infection by KSHV but later events inhibited this co-infection. We found that infection of peripheral B cells with KSHV was highest when cells were exposed to KSHV one day prior to EBV infection (2.50 ± 1.13% with a maximum of 3.53% of GFP-positive cells). This efficiency decreased rapidly following infection with EBV, declining to 0.64 ± 0.45% with KSHV infection at day 1 and to 0.10 ± 0.05% at day 3 post-EBV infection. Treating cells with IL-4 and CD40L on the same day as EBV infection and infecting them with KSHV one day later did not increase the efficiency of infection in a single experiment (Table IV.1). These measurements are consistent with reports of EBV-positive B cell lines being resistant to KSHV infection (76–78). When cells were exposed to the two viruses on the same day the efficiency of infection with KSHV was 1.11 ± 0.33%. Therefore, optimal infection of peripheral B cells with KSHV is achieved when cells are exposed to KSHV within 24 hours of EBV infection.

We examined what EBV contributes to foster KSHV infection. First, we tested whether any potential KSHV entry receptor is absent on non-activated peripheral B cells

and subsequently expressed on activated or EBV-infected B cells. DC-SIGN, also called CD209, was reported to be a receptor for KSHV entry in peripheral CD19+ B cells (121) and is the only potential receptor for KSHV that was previously considered to be present on B lymphocytes (122, 123). We used two different anti-DC-SIGN antibodies that we validated on the human monocytic THP-1 cell line as a positive control. Both antibodies bind 3 to 5% of THP-1 cells consistent with findings from previous studies (124, 125) (Figure IV.3A). No expression of DC-SIGN on either uninfected B cells or EBV-infected B cells at 1 day post-infection was detectable with anti-DC-SIGN antibody clone 120507 (Figure IV.3B). Similar results were obtained with anti-DC-SIGN antibody clone DCN46 on uninfected B cells or EBV-infected B cells at 4 days post-infection: the same percentage of cells was bound by the antibody and its respective isotype control indicating non-specific binding (Figure IV.3C). Low expression of DC-SIGN (0.29%) was detected on B cells activated with IL-4 and CD40L for 1 day but did not correlate with the efficiency of infection with KSHV. These results indicate that DC-SIGN is not required for KSHV entry into B cells.

Second, we tested whether EBV is necessary for KSHV entry into B cells. We determined if KSHV infection could be blocked with a neutralizing antibody against KSHV glycoprotein gpK8.1A (anti-gpK8.1A 4A4) immediately before infection with EBV. Virion envelope-associated gpK8.1A is thought to mediate KSHV binding to target cells via interaction with heparan sulfate moieties (118). Studies have indicated that the gpK8.1A glycoprotein is involved in KSHV binding to target cells but is not required for viral entry (119, 120). The anti-gpK8.1A 4A4 antibody inhibited infection by KSHV by 40% to 70% in 293 cells (see Table III.1 in CHAPTER III). The inhibition by anti-gpK8.1A 4A4 antibody

was transient when cells and virus were incubated for prolonged periods of time. In this experiment, CD19+ B cells were washed following exposure to KSHV to remove excess, unbound virus. CD19+ B cells were treated with anti-gpK8.1A 4A4 24 hours following exposure to KSHV and immediately before infection with EBV. The percentage of CD19+ B cells infected remained the same whether or not these cells were treated with the neutralizing antibody (Figure IV.2C) indicating that KSHV virions became inaccessible to the neutralizing antibody prior to EBV infection either by entry into B cells or irreversible adsorption onto them. Therefore, KSHV either can enter non-activated peripheral B cells or bind them irreversibly but cannot establish infection in the absence of EBV infection or B cell activation which is also provided by EBV. We could not detect GFP expression in non-activated peripheral B cells following exposure to KSHV, indicating that, if KSHV enters non-activated B cells, B cell activation or blast-formation is needed for KSHV gene expression. Importantly, and contrary to infections with EBV, exposure to KSHV alone did not induce proliferation and did not rescue non-activated B cells from cell death. Cells exposed to KSHV alone behaved as uninfected B cells: approximately one week following isolation or exposure to KSHV the number of viable cells was similar in these two populations of B cells and was significantly lower than in cells infected with EBV (Table IV.2).

We found that the survival and the rate of growth of the populations of cells exposed to both EBV and KSHV is affected by the timing of infection. The number of viable cells 4 to 8 days post-infection was significantly lower in cells exposed to KSHV prior to EBV compared to cells exposed to the two viruses in the reverse order (Table IV.2). We monitored the growth of populations of CD19+ B cells exposed to both viruses

or EBV alone for approximately 40 days following infection (Figure IV.4). We found that the population of cells exposed to KSHV prior to EBV grew significantly slower than the population exposed to the two viruses in the reverse order. We know that EBV infection induces proliferation of B cells; we thus tested whether prior exposure to KSHV induces a delay in entry into the cell cycle. Peripheral B cells were exposed to EBV and the percentage of cells in each stage of the cell cycle was monitored in absence or presence of KSHV infection. Cells were fixed and stained with propidium iodide at day 5 to 7 post-infection with EBV and analyzed by flow cytometry (Figure IV.5A). We found that the percentage of cells in G0/G1 was higher when cells were exposed to KSHV prior to EBV indicating that these cells were delayed in their entry into the cell cycle. We also observed an increase in the percentage of cells in sub G1 (58 ± 5%), which is used as a measure of apoptosis, in this population (Figure IV.5B). The percentage of cells in sub G1 was the lowest when cells were exposed to EBV alone (24 ± 11%) and in between when cells were exposed to KSHV following infection with EBV (40 ± 1%). Therefore, our data indicate that cells infected one day later with EBV have a lower number of viable cells, which is consistent with our finding that exposure to KSHV alone does not lead to survival of B cells, and this subset of viable cells is then delayed in its entry into the cell cycle and grow more slowly when infected with EBV. The difference in growth of the two populations of B cells exposed to both viruses thus likely indicates that the timing of EBV infection allows selection of different subsets of CD19+ B cells.

KSHV lytic gene expression is not required for infection of peripheral B cells.

We also tested for any required role for KSHV's lytic cycle in infection of peripheral B cells. Some groups reported latent KSHV infection (81), while others found high rates of spontaneous activation of the lytic cycle (82) during the first 5 days following infection of tonsillar B cells. We used a strain of KSHV, KSHV BAC16RTAstop, that does not express the viral protein RTA (100) which is required for entry into the lytic cycle. Cells infected with this strain of KSHV therefore cannot undergo the lytic cycle. For construction of KSHV BAC16RTAstop, a stop codon was inserted in the second exon of the RTA gene which resulted in a new NheI restriction site (100). We isolated DNA from KSHV BAC16RTAstop viral particles and confirmed that the RTA gene was mutated in this strain of KSHV by enzymatic digestion (Figure IV.6A). Isolated CD19+ B cells were exposed to KSHV BAC16RTAstop at different time points prior to or following EBV infection or activation with IL-4 and CD40L. The mutant strain of KSHV infected peripheral B cells with similar efficiencies as the wild-type KSHV BAC16 strain (Figure IV.6B). Thus, KSHV lytic gene expression is not required for optimal infection of peripheral B cells.

Figure IV.1: IL-4 and CD40L activation of peripheral B cells supports detectable but inefficient KSHV infection.

Isolated CD19+ B cells were exposed to KSHV BAC16 at MOI 2 to 3 by spinoculation at different time points following or prior to activation with IL-4 and CD40L. In all conditions, cells were cultured for 4 to 7 days following exposure to KSHV. Live cells were analyzed for CD19 and GFP expression using a BD LSR Fortessa cytometer, and analysis was performed using FlowJo software. Each dot represents the percentage of GFP-positive cells measured in one biological replicate. The number of biological replicates is indicated for each condition. The mean of data is indicated by the horizontal bar. $p > 0.05$ between each condition by Wilcoxon rank sum test.

Figure IV.1

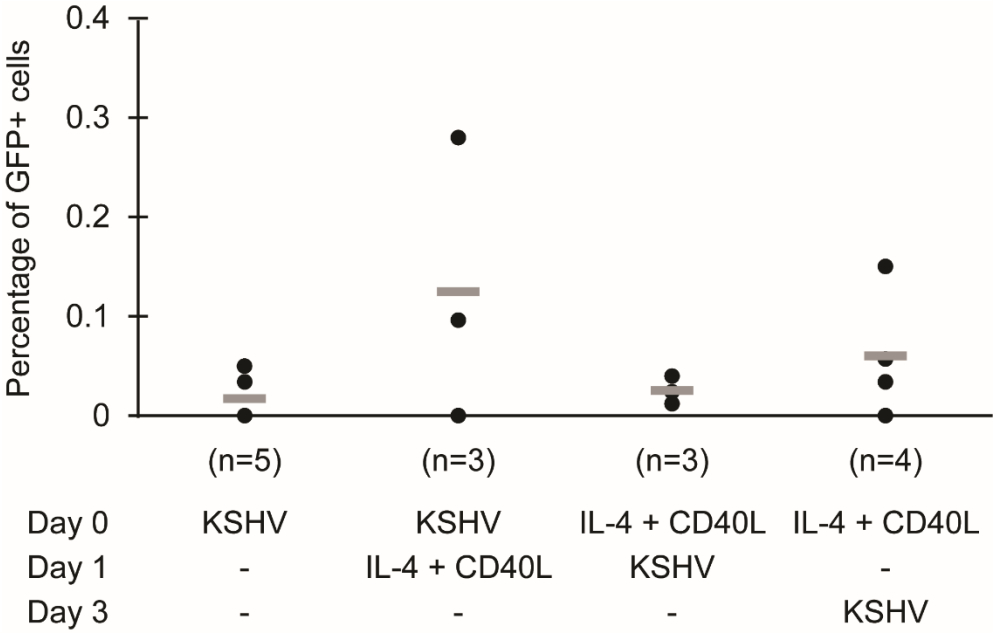
Percentage of GFP+ cells
0.4
0.3
0.2
0.1
0
(n=5)
(n=3)
(n=3)
(n=4)
Day 0
KSHV
KSHV
IL-4 + CD40L
IL-4 + CD40L
Day 1
-
IL-4 + CD40L
KSHV
-
Day 3
-
-
-
KSHV

Figure IV.2: EBV infection supports an optimal infection of peripheral B cells by KSHV.

(A and B) Isolated CD19+ B cells were exposed to KSHV BAC16 at MOI 2 to 3 by spinoculation at different time points following, prior to, or on the same day as EBV infection.

(C) Isolated CD19+ B cells were exposed to KSHV BAC16 at MOI 2 by spinoculation. Cells were washed to remove excess, unbound virus and treated 24 hours later with anti-gpK8.1A 4A4 for two hours at 37°C. Cells were then washed and infected with EBV.

In all conditions, cells were cultured for 4 to 7 days following exposure to KSHV. Live cells were analyzed for CD19 and GFP expression using a BD LSR Fortessa cytometer, and analysis was performed using FlowJo software. (A) One representative experiment is shown out of 3 to 8 independent biological replicates. (B and C) Each dot represents the percentage of GFP-positive cells measured in one biological replicate. The number of biological replicates is indicated for each condition. The mean of data is indicated by the horizontal bar. * $p < 0.05$; ** $p < 0.01$ by Wilcoxon rank sum test.

Figure IV.2

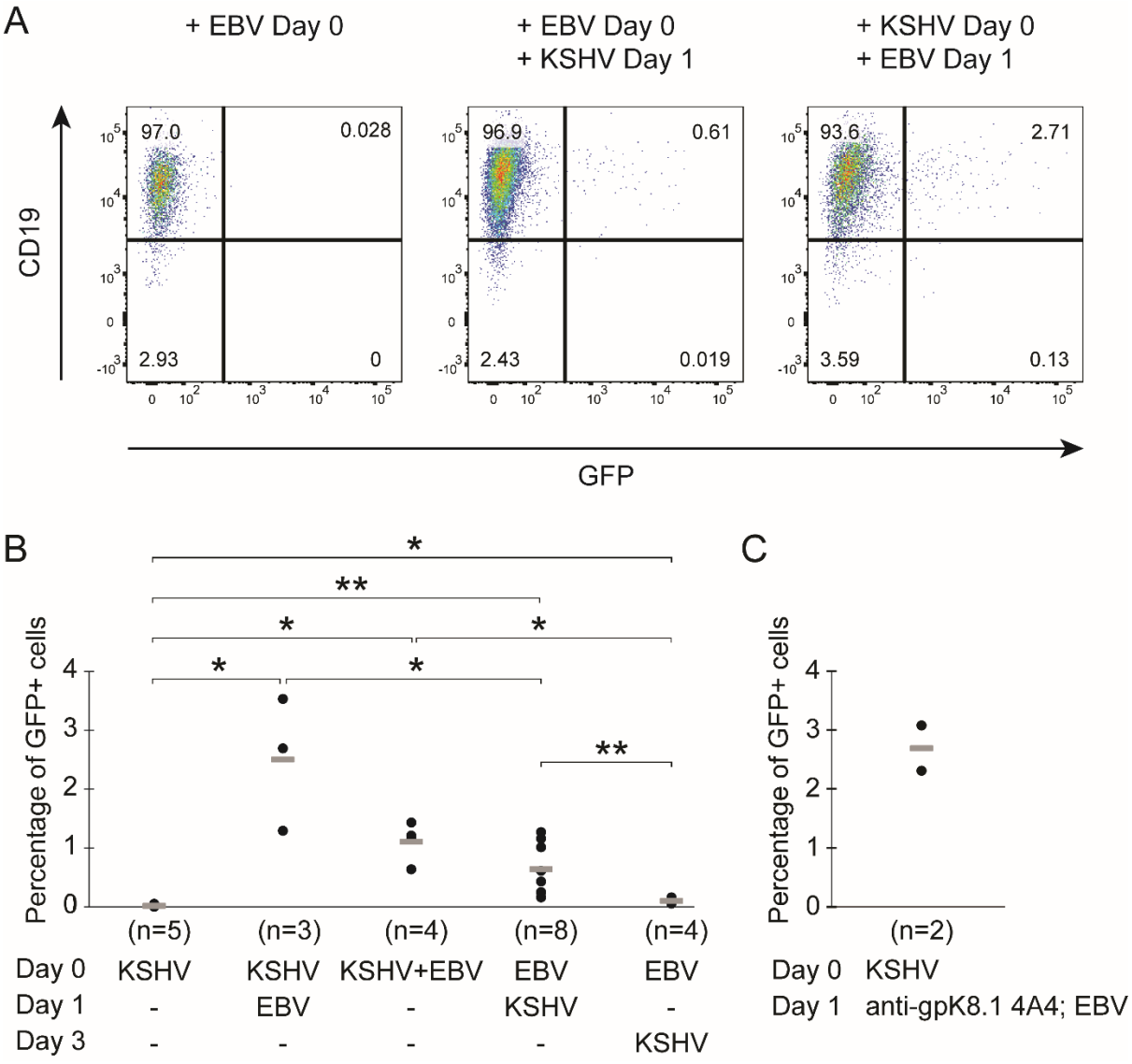
A
+ EBV Day 0
+ EBV Day 0
+ KSHV Day 1
+ KSHV Day 0
+ EBV Day 1
CD19
GFP
97.0
0.028
2.93
0
96.9
0.61
2.43
0.019
93.6
2.71
3.59
0.13
B
Percentage of GFP+ cells
(n=5)
(n=3)
(n=4)
(n=8)
(n=4)
Day 0 KSHV KSHV KSHV+EBV EBV EBV
Day 1 - EBV - KSHV -
Day 3 - - - - KSHV
C
Percentage of GFP+ cells
(n=2)
Day 0 KSHV
Day 1 anti-gpK8.1 4A4; EBV

Table IV.1: Additional conditions tested for the efficiency of infection with KSHV.

Isolated CD19+ B cells were exposed to KSHV BAC16 at MOI 2 to 3 by spinoculation at the same time or following EBV infection or activation with IL-4 and CD40L (day of exposure/treatment shown in parentheses). In all conditions, cells were cultured for 4 to 7 days following exposure to KSHV. Live cells were analyzed for CD19 and GFP expression using a BD LSR Fortessa cytometer, and analysis was performed using FlowJo software. The percentage of GFP-positive cells measured in each condition is indicated.

Table IV.1

	Percentage of GFP+ cells	# biological replicates
IL-4 + CD40L + KSHV (Day 0)	**0.00** %	n=1
EBV + IL-4 + CD40L (Day 0) **+ KSHV** (Day 1)	**0.48** %	n=1

Figure IV.3: DC-SIGN is not required for KSHV entry into B cells.

(A) To confirm sensitivity of two independent antibodies to DC-SIGN, the percentage of THP-1 cells binding anti-DC-SIGN antibody clone 120507 or anti-DC-SIGN antibody clone DCN46 and their respective isotype controls was measured by flow cytometry.

(B) The percentage of GFP-positive cells following exposure to KSHV (hatched) was compared to the percentage of cells binding anti-DC-SIGN antibody clone 120507 (solid black) or its corresponding isotype control (solid grey). The efficiency of infection with KSHV and DC-SIGN expression were measured on non-activated CD19+ B cells, and on B cells 1 day following infection with EBV or treated for 1 day with IL-4 and CD40L.

(C) The percentage of GFP-positive cells following exposure to KSHV (hatched) was compared to the percentage of cells binding anti-DC-SIGN antibody clone DCN46 (solid black) or its corresponding isotype control (solid grey). The efficiency of infection with KSHV and DC-SIGN expression were measured on non-activated CD19+ B cells, and on B cells 4 days following infection with EBV.

(B and C) Live cells were analyzed for CD19, GFP and DC-SIGN expression using a BD LSR Fortessa cytometer, and analysis was performed using FlowJo software. DC-SIGN expression was measured in 1 or 2 independent biological experiments in each condition.

Figure IV.3

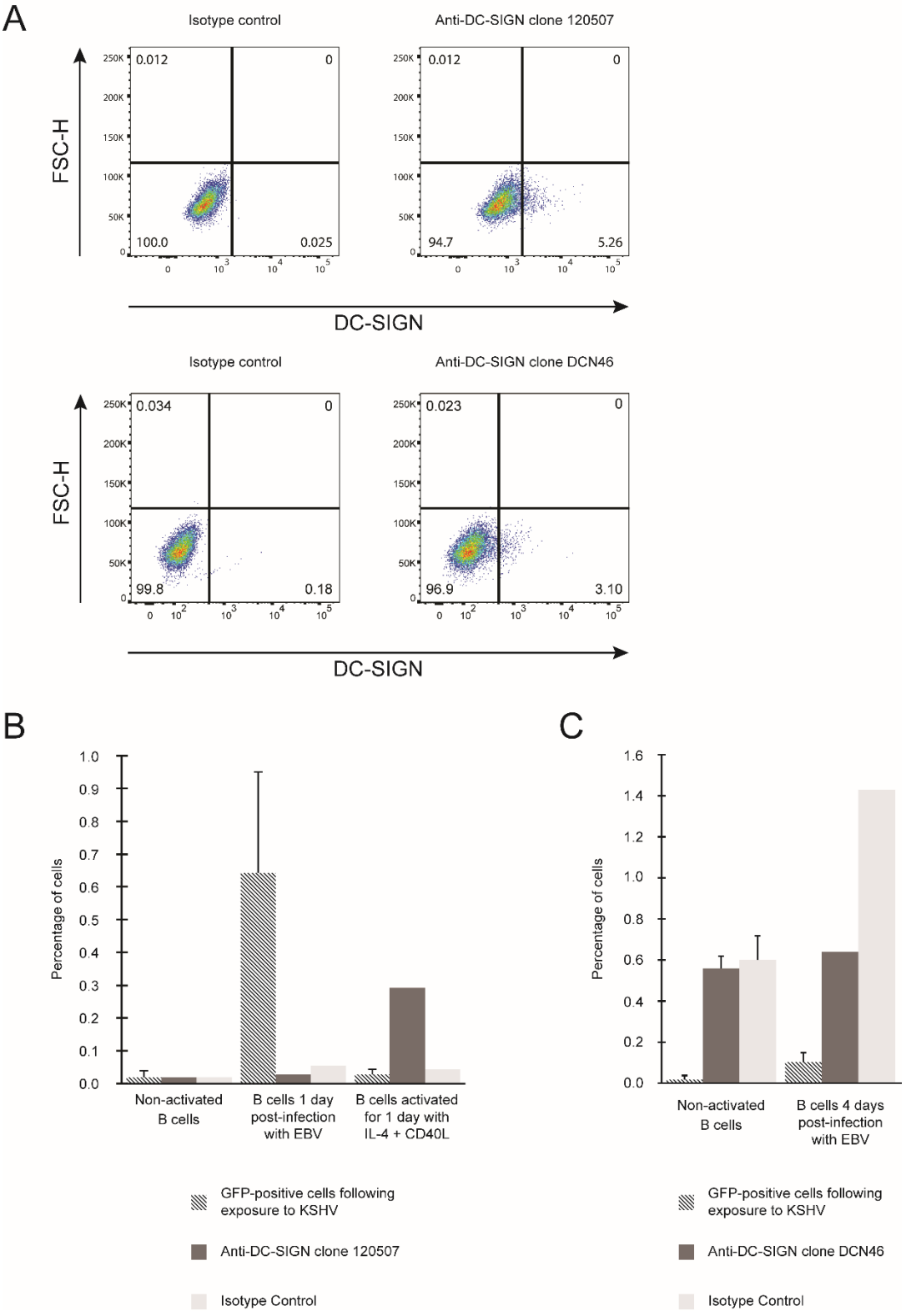
A
Isotype control
Anti-DC-SIGN clone 120507
FSC-H
DC-SIGN
0.012
0
100.0
0.025
94.7
5.26
Isotype control
Anti-DC-SIGN clone DCN46
0.034
0
99.8
0.18
0.023
0
96.9
3.10
B
Percentage of cells
Non-activated B cells
B cells 1 day post-infection with EBV
B cells activated for 1 day with IL-4 + CD40L
GFP-positive cells following exposure to KSHV
Anti-DC-SIGN clone 120507
Isotype Control
C
Percentage of cells
Non-activated B cells
B cells 4 days post-infection with EBV
GFP-positive cells following exposure to KSHV
Anti-DC-SIGN clone DCN46
Isotype Control

Table IV.2: The survival of populations of CD19+ B cells exposed to EBV and/or KSHV depends on the type of virus and the timing of infection.

Peripheral B cells were stained with the Ghost Dye Red 780 viability dye and the percentage of viable cells was measured by flow cytometry at day 4 to 8 following exposure to EBV and/or KSHV (day of exposure shown in parentheses). The percentage of viable cells in uninfected B cells was measured at day 7 and 8 following isolation from peripheral blood.

* $p < 0.05$; ** $p < 0.01$ by Wilcoxon rank sum test (compared to the percentage of viable cells in the condition EBV (Day 0)).

† $p < 0.05$; †† $p < 0.01$ by Wilcoxon rank sum test (compared to the percentage of viable cells in the condition EBV (Day 0) + KSHV (Day 1)).

Table IV.2

	Percentage of viable cells (± SD)	**# biological replicates**
Uninfected B cells	**17.1** ± 0.8%*†	n=2
EBV (Day 0)	**82.4** ± 23.2%	n=11
KSHV (Day 0)	**35.3** ± 20.7%**††	n=5
EBV + KSHV (Day 0)	**88.0** ± 7.7%	n=2
EBV (Day 0) **+ KSHV** (Day 1)	**89.2** ± 8.3%	n=8
EBV (Day 0) **+ KSHV** (Day 3)	**93.5** ± 5.6%	n=4
KSHV (Day 0) **± anti-gpK8.1 4A4** (Day 1) **+ EBV** (Day 1)	**74.2** ± 11.3%†	n=5

Figure IV.4: The rate of growth of populations of CD19+ B cells exposed to both EBV and KSHV is affected by the timing of infection.

The growth of populations of CD19+ B cells exposed to both KSHV and EBV or EBV only was tracked over time. The first time point on the X-axis (Day 0) corresponds to the first day of infection. Data from 2 to 4 independent biological experiments are shown for each population. The R-squared of the trendlines is indicated. * $P < 0.05$ by Sen-Adichie test.

Figure IV.4

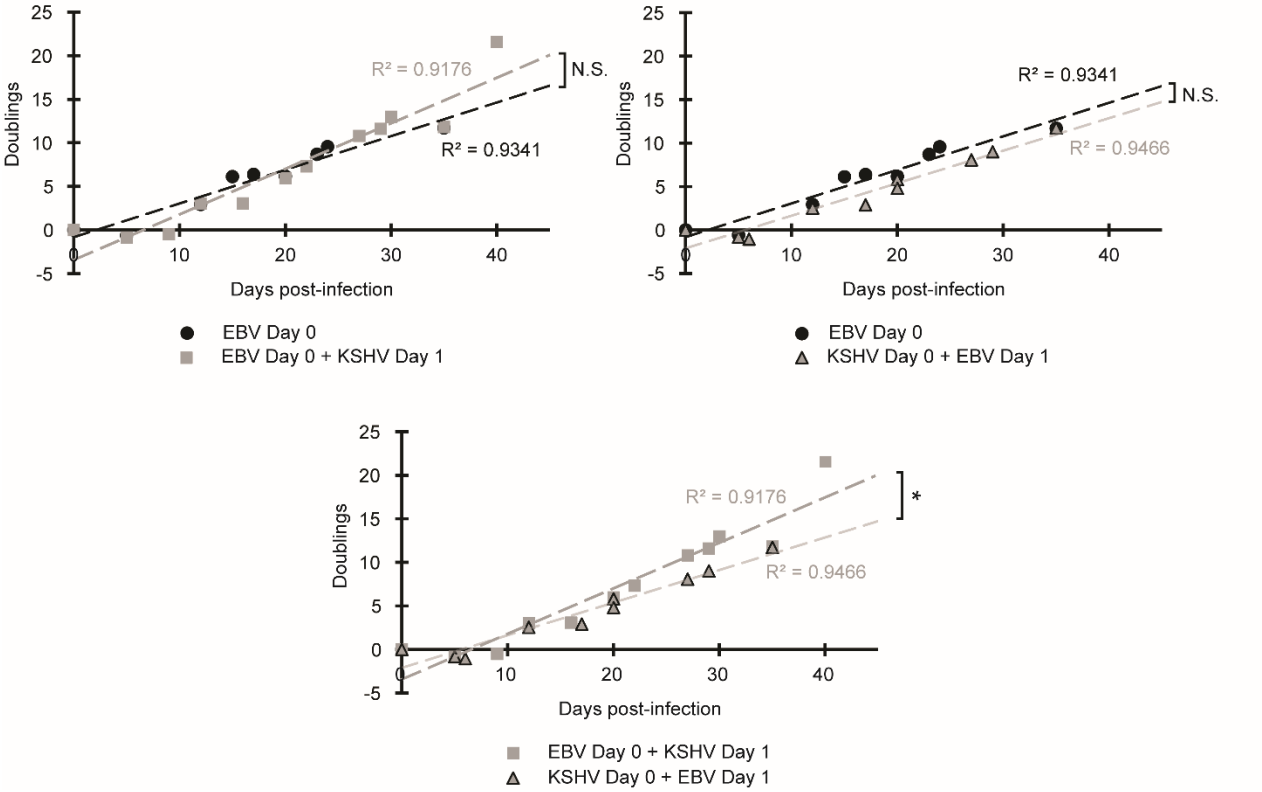
Doublings
Days post-infection
R² = 0.9176
R² = 0.9341
N.S.
EBV Day 0
EBV Day 0 + KSHV Day 1
R² = 0.9341
R² = 0.9466
N.S.
EBV Day 0
KSHV Day 0 + EBV Day 1
R² = 0.9176
R² = 0.9466
*
EBV Day 0 + KSHV Day 1
KSHV Day 0 + EBV Day 1

Figure IV.5: Peripheral CD19+ B cells exposed to KSHV prior to EBV are delayed in their entry into the cell cycle.

(A) Cells exposed at different time points to EBV only or to both EBV and KSHV were fixed at day 5 to 7 post-infection with EBV. The percentage of cells in each stage of the cell cycle was determined by propidium iodide staining and fluorescence-activated cell sorting (FACS) analysis. The average of 2 independent experiments (± SD) is shown.

(B) Cells in (A) were analyzed by FACS to determine the percentage of cells in sub G1 in each population. Data from 2 independent biological experiments are shown for each population.

Figure IV.5

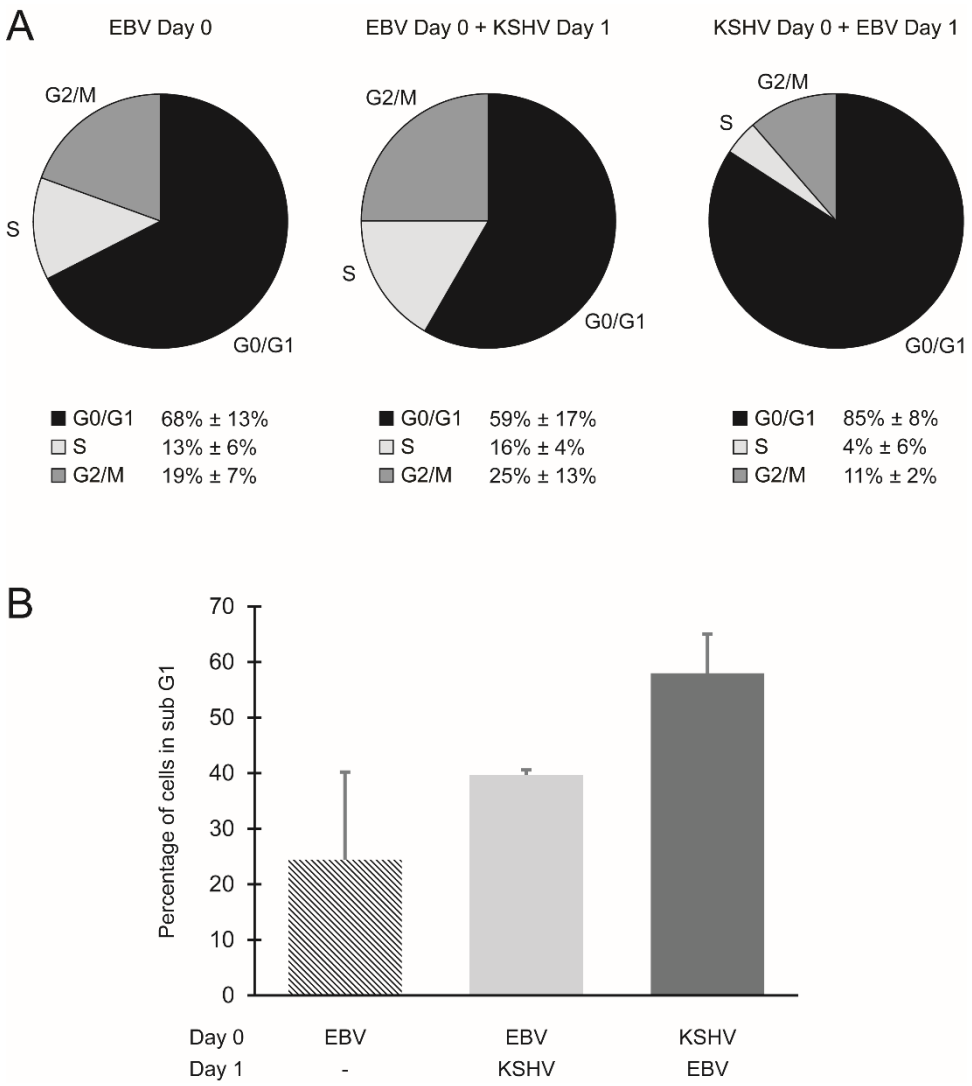
A
EBV Day 0
EBV Day 0 + KSHV Day 1
KSHV Day 0 + EBV Day 1
G2/M
S
G0/G1
G0/G1 68% ± 13%
S 13% ± 6%
G2/M 19% ± 7%
G0/G1 59% ± 17%
S 16% ± 4%
G2/M 25% ± 13%
G0/G1 85% ± 8%
S 4% ± 6%
G2/M 11% ± 2%
B
Percentage of cells in sub G1
70
60
50
40
30
20
10
0
Day 0 EBV EBV KSHV
Day 1 - KSHV EBV

Figure IV.6: KSHV lytic gene expression is not required for infection of peripheral B cells.

(A) DNA was isolated from mutant (mut) and wild-type (wt) KSHV BAC16 viral particles. A fragment of 476 bp spanning the mutation in ORF50 (RTA), which introduces a stop codon resulting in a new NheI restriction site, was amplified by PCR and digested with NheI.

(B) Isolated CD19+ B cells were exposed to KSHV BAC16RTAstop at MOI 2 to 3 by spinoculation at different time points following or prior to EBV infection or activation with IL-4 and CD40L. In all conditions, cells were cultured for 4 to 7 days following exposure to KSHV BAC16RTAstop. Live cells were analyzed for CD19 and GFP expression using a BD LSR Fortessa cytometer, and analysis was performed using FlowJo software.

Figure IV.6

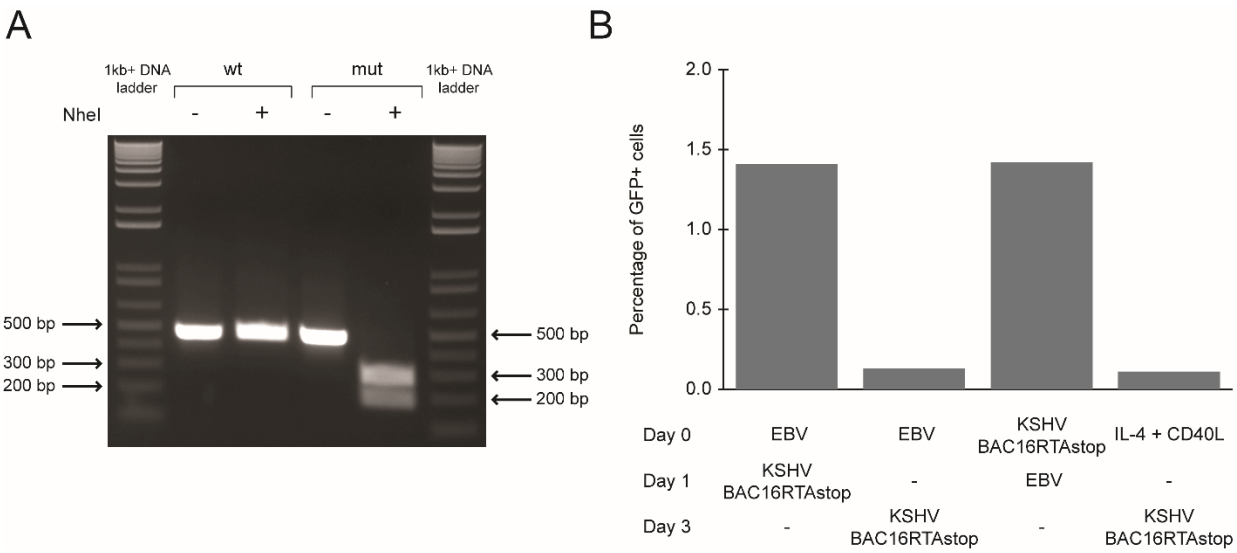
A
1kb+ DNA ladder
wt
mut
1kb+ DNA ladder
NheI
-
+
-
+
500 bp
300 bp
200 bp
500 bp
300 bp
200 bp
B
Percentage of GFP+ cells
2.0
1.5
1.0
0.5
0.0
Day 0
EBV
EBV
KSHV BAC16RTAstop
IL-4 + CD40L
Day 1
KSHV BAC16RTAstop
-
EBV
-
Day 3
-
KSHV BAC16RTAstop
-
KSHV BAC16RTAstop

DISCUSSION

Primary Effusion Lymphomas (PELs) are characterized by their being derived from B cells infected with KSHV and in most cases dually infected with EBV. These lymphomas have not been readily modeled *in vitro* although multiple studies have detected initial infections, particularly of tonsillar B cells, with KSHV. We set out to determine conditions in which peripheral B cells could be infected with KSHV both because these cells are readily available and because they are not prone to be activated as is often the case for portions of tonsillar-derived B cells. We found that an optimal infection of peripheral B cells with KSHV required co-infection by EBV within 24 hours. We found that the infecting EBV partner allowed activation of the B cells and expression of KSHV genes.

Our study highlights the role of B cell activation in infection with KSHV. Infection with KSHV could only be detected in peripheral B cells activated with IL-4 and CD40L or by infection with EBV. An experiment using a neutralizing antibody against KSHV suggests that KSHV can either bind irreversibly or enter non-activated peripheral B cells. We could not detect GFP expression following exposure to KSHV, indicating that, if KSHV enters non-activated B cells, B cell activation or blast-formation is needed for KSHV gene expression. Therefore, our results suggest that tonsillar B cells are more susceptible than peripheral B cells to KSHV infection because they are isolated from patients with highly activated tonsils (83).

We found that co-infection with EBV allowed more efficient infection with KSHV than activation with IL-4 and CD40L. In addition, the order and timing of infection with EBV and KSHV significantly altered the efficiency of infection with KSHV: early events of EBV infection promoted infection by KSHV while later events inhibited this co-infection.

Our finding that KSHV infection of activated B cells is inhibited over time is consistent with reports of EBV-positive B cell lines being resistant to KSHV infection (76–78). It is possible that later events of EBV infection, involving changes in expression of cell surface molecules, inhibit KSHV infection by decreasing KSHV binding to B cells or by downregulating a receptor for entry. The former hypothesis is supported by preliminary results where more human fibroblasts (HF) became infected with KSHV when co-cultivated with B cells exposed to KSHV alone compared to B cells exposed to EBV prior to KSHV, suggesting that less KSHV virions were bound to EBV-infected B cells.

CHAPTER V.

Dually infected B cells are stably transformed *in vitro*

Parts of this chapter have been adapted into a manuscript. The manuscript has been accepted for publication and is referenced below:

Aurélia Faure, Mitch Hayes and Bill Sugden (2019) How Kaposi's sarcoma-associated herpesvirus stably transforms peripheral B cells towards Lymphomagenesis. *Proc Natl Acad Sci*, in press.

A note on the contributions to this chapter:

Mitch Hayes contributed to the sorting of populations of dually infected B cells and the RNA-Sequencing analysis. Bill Sugden helped count the number of KSHV signals per cell in FISH slides in Figure V.4. Bill Sugden and Nora Herzog, an undergraduate student, electroporated the EBNA1-OriP plasmids p3828, p174 and p3829 into the BC-1 PEL cell line.

INTRODUCTION

In CHAPTER IV, we have defined conditions to infect peripheral B cells with KSHV using a dual infection with EBV. Contrary to EBV, KSHV has not previously been found to transform B cells *in vitro*. KSHV did not lead to transformation of peripheral CD19+ B cells and umbilical cord blood mononuclear cells and infection of these cells could only be detected by DNA PCR or RT-PCR shortly after exposure to the virus (76, 78, 79). Similarly, KSHV did not transform tonsillar B cells (81, 83, 84). Because KSHV and EBV are both retained as plasmids in PELs, we asked whether the dually infected cells obtained in CHAPTER IV were transformed by the dual infection. We first isolated dually infected, GFP-positive cells from infected populations of B cells and asked whether KSHV and EBV were maintained in them. We then studied and compared the phenotypes of different dually infected B cells over time. We found that the dually infected cells were transformed, maintaining both KSHV and EBV for months in culture. In addition, these cells were clonal and expressed lambda light chain mRNA similar to PEL cells. We show that some transformed cells grew more slowly than cells infected only with EBV and were often overgrown whereas others grew to dominate the culture. These latter cells showed increased expression of most KSHV genes, including those encoded by the latency locus and the viral interleukin-6 gene. In addition, they also regulated the expression of some cellular genes as do PEL cells, and thus shared multiple properties with these cells. This *in vitro* transformation of peripheral B cells by KSHV and EBV, for the first time, allows a mechanistic analysis of the viral and cellular genes that mediate early events in the progression towards PEL.

RESULTS

Dually infected, proliferating B cells are transformed to maintain both viruses.

B cells have not yet been dually infected *in vitro* and propagated successfully over long times in culture. GFP-positive cells were sorted therefore from populations of cells exposed to both EBV and KSHV 3 to 7 weeks post-infection. FACS-sorting initially yielded 60-90% GFP-positive cells. Subsequently, the fraction of GFP-positive cells in these sorted populations was monitored over time by fluorescence microscopy.

In some populations, the fraction of GFP-positive cells decreased over time (Figure V.1A) and correlated with the fraction of cells positive for KSHV by FISH (Figure V.1B). The fraction of KSHV-infected and EBV-infected cells was monitored over time by FISH in both GFP-negative and GFP-positive populations (Figure V.1C-F). In KSHV-positive cells, the copy number of KSHV genomes ranged from 2 to 28 with an average of 11 genomes per cell indicating that KSHV is extrachromosomal in these cells. In addition, GFP-negative populations were negative for KSHV by FISH, confirming that GFP was not silenced but that loss of GFP indicated either a decrease in the fraction of dually infected cells or a loss of KSHV genomes from dually infected cells in these populations. Most GFP-negative and GFP-positive cells were positive for EBV by FISH demonstrating that KSHV-infected cells were also infected with EBV. EBV-positive cells were maintained in both GFP-negative and GFP-positive cells over time and the number of EBV genomes ranged from 1 to 44 in these cells. The growth of GFP-positive and GFP-negative cells was also monitored over time (Figure V.2A and B). The GFP-positive cells grew at the same or slower rate than the GFP-negative cells. We also continued to see the effect of the timing of infection with EBV and KSHV on the rate of growth (see CHAPTER IV): in

populations of B cells exposed to KSHV prior to EBV, both the GFP-negative and GFP-positive cells grew significantly slower than cells in populations of B cells exposed to the two viruses in the reverse order.

Among the populations of infected B cells that we followed, some GFP-positive, KSHV-positive cells began to predominate. We observed multiple fluctuations in the percentage of GFP-positive cells over time. Some populations, in which the percentage of GFP-positive cells had previously decreased, still maintained a low number of GFP-positive cells for several months. In others, the percentage of GFP-positive cells spontaneously increased in absence of any selection by FACS, and either continued to increase over time or later decreased. We therefore tested whether the dually infected cells in populations of infected B cells were transformed to maintain both KSHV and EBV stably. We followed and repeatedly sorted two different populations of infected cells for GFP, measured the number of EBV and KSHV genomes in them, and analyzed their proliferation and clonal composition based on VDJ recombination in the immunoglobulin heavy chain locus. In the first population (population 1), the GFP-positive cells outgrew the GFP-negative cells to become stably, dually infected (we term these cells "KSHV+/EBV+ fast"). The percentage of GFP-positive cells increased from 1.4% to 90% over 5.5 months and KSHV was still maintained in these cells after 7 months of culture (Figure V.3A). We cultured and sorted portions of population 1 and compared their phenotypes to those of a second population (population 2) that needed FACS selection of the GFP-positive fraction (termed "KSHV+/EBV+ slow") to avoid its being overgrown. Early in the culturing of this second population (before FACS selection), the percentage of dually infected, GFP-positive cells increased to ~10% before the GFP-negative cells

(EBV-only infected cells) began to overgrow them. These two populations were compared longitudinally for three to five months.

Cells from unsorted and sorted populations were collected at different time points and analyzed for the presence of KSHV and EBV by qPCR (Figure V.3B). The average number of KSHV genomes per cell in the population 1 increased over time from ~3 to 31 genomes per cell. Analysis by FISH showed that this increase is due to the percentage of KSHV-positive cells (KSHV+/EBV+ fast cells) increasing over time in the population and reaching almost 100%, while the average number of KSHV genomes remained constant in these cells (Figure V.4). In the population 2, there was on average ~6 KSHV genomes per cell by qPCR which correlated with a low fraction of cells being KSHV-positive (KSHV+/EBV+ slow cells) at the time of analysis. Analysis by FISH indicated that the average number of KSHV genomes per cell in the KSHV+/EBV+ fast and the KSHV+/EBV+ slow cells was similar (between 11 and 16 genomes per cell) and that KSHV was present as a plasmid in these cells (with a range of 1 to 52 and 1 to 27 KSHV signals per cell respectively). Furthermore, analysis by FISH confirmed that the KSHV+/EBV+ fast cells were not overgrown by KSHV-negative cells: close to 100% of the cells remained KSHV-positive following each sort, as opposed to the KSHV+/EBV+ slow cells that were overgrown by the EBV-only infected cells (only ~35% of the cells were KSHV-positive 31 days after sort). The average number of EBV genomes per cell was similar in the population 1 (~11 to 22 genomes per cell) and the population 2 (~10 genomes per cell). In the population 1, analysis by qPCR found a higher copy number of both EBV and KSHV genomes at day 160 after KSHV infection (> 30 genomes per cell). However, analysis by FISH showed that there was on average ~15 KSHV genomes per

cell in the KSHV+/EBV+ fast cells at this time point. The higher number of both EBV and KSHV genomes in this sample can either be explained by a small fraction of the cells supporting KSHV's and EBV's lytic cycle or an artifact of the qPCR.

To look for competitive growth advantages between dually infected and EBV-only infected cells, we analyzed the clonal composition of the populations 1 and 2. RNA was isolated at different time points before and after sorting of GFP-positive cells and analyzed computationally with MiXCR, to determine the percentage of each clone based on VDJ recombination in the immunoglobulin heavy chain locus (Figure V.5). In the first population, the dually infected GFP-positive cells (KSHV+/EBV+ fast cells) represented primarily one clone which overgrew other cells in the population and was also selected by sorting the GFP-positive cells. Analysis with MiXCR indicated that this clone expressed IgM and λ light chain mRNA (Table V.1). Interestingly, in the second population, dually infected KSHV+/EBV+ slow cells were likely also clonal because a clone and its progeny, also expressing IgM and λ light chain mRNA, predominated after each sort of GFP-positive cells. However, contrary to the KSHV+/EBV+ fast cells, these cells were overgrown by other clones. The EBV-only infected clones that overgrew the KSHV+/EBV+ slow cells expressed IgM or IgG and κ light chain mRNA as shown by the increase in IgG and κ light chain expression when cells were left unsorted (Table V.1).

These findings indicate that the KSHV-negative cells that overgrew the sorted dually infected, GFP-positive cells usually arose from pre-existing KSHV-negative, EBV-only infected cells which contaminated the FACS sorts. Therefore, both the KSHV+/EBV+ fast and the KSHV+/EBV+ slow cells were transformed to maintain KSHV and EBV stably

over time, but the KSHV+/EBV+ fast cells had a proliferative advantage over the EBV-only infected cells as opposed to the KSHV+/EBV+ slow cells.

KSHV gene expression is increased in the KSHV+/EBV+ fast transformed cells.

We analyzed the viral and cellular mRNAs expressed in the different types of dually infected cells. We analyzed enriched fractions of dually infected cells (≥ 60% GFP-positive) that spontaneously arose in the population or were obtained by FACS selection as shown in Figure V.5. We isolated RNA sequentially over a period of 3 to 5 months from seven samples of KSHV+/EBV+ fast cells and five samples of KSHV+/EBV+ slow cells. The viral RNAs were mapped to their respective genomes following the approach of Bruce et al. (108) to disentangle any overlapping transcripts (see CHAPTER II).

More than 6,000 cellular genes, some EBV genes (17 out of 78) and most KSHV genes (72 out of 98) were differentially expressed between the KSHV+/EBV+ fast and the KSHV+/EBV+ slow transformed cells (Figure V.6A). Differentially expressed EBV and KSHV genes were mainly upregulated in the KSHV+/EBV+ fast cells compared to the KSHV+/EBV+ slow cells and are represented in Figure V.6B and C. Among the 72 upregulated KSHV genes, most of the latency locus genes (30) were statistically upregulated in the KSHV+/EBV+ fast cells compared to the KSHV+/EBV+ slow cells, including v-FLIP (ORF71), v-cyclin (ORF72), LANA1 (ORF73), Kaposin A/C (ORF K12) and the miRNA cluster (miR region). In addition, expression of vIL-6 (ORF K2), which is thought to serve as a growth factor for PEL (48, 49), was increased in the KSHV+/EBV+ fast cells. Coverage plots of RNA-seq reads also showed the increased KSHV gene

expression in the KSHV+/EBV+ fast cells compared to the KSHV+/EBV+ slow cells which contrasted with the similar EBV gene expression in these two cell types (Figure V.6D).

KSHV+/EBV+ fast cells regulate the expression of some cellular genes as do PEL cells.

Principal Component Analysis (PCA) allows the identification of patterns within complex sets of data. We therefore used PCA to analyze the viral and cellular transcripts in the different types of dually infected, stably transformed cells. PCA confirmed the similar EBV gene expression and differential KSHV gene expression in KSHV+/EBV+ fast and KSHV+/EBV+ slow cells. A PCA of EBV gene expression did not distinguish the KSHV+/EBV+ fast and KSHV+/EBV+ slow cells (Figure V.7A) as opposed to a PCA of KSHV gene expression in which the seven samples of KSHV+/EBV+ fast cells clustered apart from the five samples of KSHV+/EBV+ slow cells (Figure V.7B). Cellular gene expression also distinguished the two types of dually infected cells (Figure V.7C) underscoring the correlation between the differential expression of KSHV genes and cellular genes in these cells. Cellular gene expression in nine cases of PEL has previously been compared to that in 53 cases of various non-PEL B-cell malignancies and a pattern of expression characteristic of PEL has been defined (113). Using Gene Set Enrichment Analysis (GSEA), we compared the sets of genes that were upregulated or downregulated in PEL and found that cellular genes characteristically inhibited in PEL were also inhibited in the KSHV+/EBV+ fast cells relative to the KSHV+/EBV+ slow cells ($p < 0.001$) (Figure V.7D).

In addition, using GSEA, we have identified cellular genes expressed at higher levels in the KSHV+/EBV+ fast relative to the KSHV+/EBV+ slow cells and found that genes in the pathway involving NF-κB were upregulated in the KSHV+/EBV+ fast cells ($p < 0.001$) (Figure V.7E). Among genes that were upregulated, we identified CCL20 as well as NFKB1. NF-κB was found to be constitutively activated in PEL cells and its activity was necessary for their survival (126). Increased expression of KSHV genes, in particular v-FLIP, likely contributes to increased NF-κB activity and CCL20 expression in the KSHV+/EBV+ fast cells (27, 127). This altered expression of viral and cellular genes in the KSHV+/EBV+ fast cells distinguishes their transformed properties from those of the KSHV+/EBV+ slow cells and associates them more closely with PEL cells.

Dually infected cells exhibit a range of phenotypes between those of the KSHV+/EBV+ slow and the KSHV+/EBV+ fast cells.

We analyzed the dually infected cells in one additional population (population 3). The percentage of dually infected cells in this population decreased over time as shown in Figure V.1 but a small number of GFP-positive cells then persisted in the population for several months. We termed these dually infected cells KSHV+/EBV+ intermediate cells. GFP-positive cells in population 3 were repeatedly sorted and the number of KSHV and EBV genomes was determined by qPCR directly following sorting. We found on average 5 EBV genomes and 9 KSHV genomes per cell in a single experiment (Figure V.8A). Analysis with MiXCR showed that the KSHV+/EBV+ intermediate cells were likely clonal because a clone predominated following FACS selection of the GFP-positive cells

(Figure V.8B). This clone also expressed IgM and λ light chain mRNA, similar to the KSHV+/EBV+ fast and the KSHV+/EBV+ slow cells (Table V.1).

Principal Component Analysis (PCA) showed that EBV gene expression was similar in the three types of dually infected cells (Figure V.8C). KSHV gene expression was increased in the KSHV+/EBV+ intermediate cells and was closer to that of the KSHV+/EBV+ fast cells (Figure V.8D). However, in a PCA of cellular gene expression, the KSHV+/EBV+ intermediate cells did not cluster with the KSHV+/EBV+ fast or the KSHV+/EBV+ slow cells (Figure V.8E). Their phenotype was intermediate between these two types of dually infected cells. Thus, it is likely that dually infected cells in populations of infected B cells exhibit a range of phenotypes between two extremes: the KSHV+/EBV+ slow cells and the KSHV+/EBV+ fast cells. Dually infected cells with a phenotype closer to the KSHV+/EBV+ fast cells have acquired additional proliferative and/or survival advantages that allow them to grow to predominate in a culture.

EBV's BART miRNAs provide selective advantages to the BC-1 PEL cell line.

We found that EBV fosters the infection of peripheral B cells with KSHV and both viruses are maintained in dually infected, transformed B cells as well as in PEL cells. Therefore, KSHV but also EBV contribute selective advantages to the transformed B cells. In order to understand the contributions of EBV to dually infected cells, we asked what EBV genes can complement the loss of EBV genomes from PEL cells. It should be noted that PEL cells have evolved both *in vivo* and in cell culture and their dependence on EBV is likely to be less than the newly transformed B cells. We introduced three EBNA1-OriP plasmids expressing different subsets of EBV genes known to be expressed

in PEL into the BC-1 PEL cell line (Figure V.9A). Cells carrying each individual plasmid were selected with hygromycin and the loss of the endogenous EBV genomes was measured by qPCR after 9 months of culture. Each plasmid was present in cells at 2 to 7 copies per cell, indicating that they were maintained as extrachromosomal plasmids (Figure V.9B). We found that introducing the plasmid p3829 that expresses EBNA1 and the BART miRNAs into BC-1 cells led to the complete loss of EBV genomes from these cells. The plasmids p3828, also expressing EBNA1, and p174, expressing EBNA1 and the EBV-encoded small RNAs (EBERs), did not lead to the loss of EBV genomes. Cells carrying these two plasmids had on average between 3 and 5 EBV genomes per cell, consistent with the number of EBV genomes found in the parental BC-1 cells (on average between 2 and 3 signals per cell by FISH). Therefore, ectopic expression of the EBV's BART miRNAs was sufficient to complement the loss of EBV genomes from BC-1 cells, indicating that they contribute to the survival and/or proliferation of these cells.

Figure V.1: The fraction of KSHV-positive cells decreases in some populations of infected peripheral B cells.

Isolated CD19+ B cells were exposed to KSHV 24 hours prior to or following EBV infection. KSHV infected GFP-positive cells were sorted 3 to 7 weeks post-infection.

(A) The number of GFP-positive cells was monitored over time by fluorescence microscopy. The percentage of GFP-positive cells was normalized to the number of GFP-positive cells at zero doublings (first day after sorting). Data from 3 independent biological experiments are shown for each population.

(B) The number of KSHV-infected cells was quantified by fluorescence *in situ* hybridization (FISH) and compared to the number of GFP-positive cells at 3 different time points in one experiment. The R-squared of the trendlines is indicated. N.S. $p > 0.05$ by Sen-Adichie test.

(C-F) The number of KSHV- and EBV-infected cells was quantified over time by FISH in both GFP-negative and GFP-positive cells. (C and E) Representative FISH images are shown when samples were incubated with hybridization probes for detection of KSHV (left) or EBV (right) plasmids; Bars, 10 μm. (D and F) The percentage of EBV- and KSHV-positive cells and the average number of signals per cell in positive cells were determined by FISH at different time points following sorting.

Figure V.1

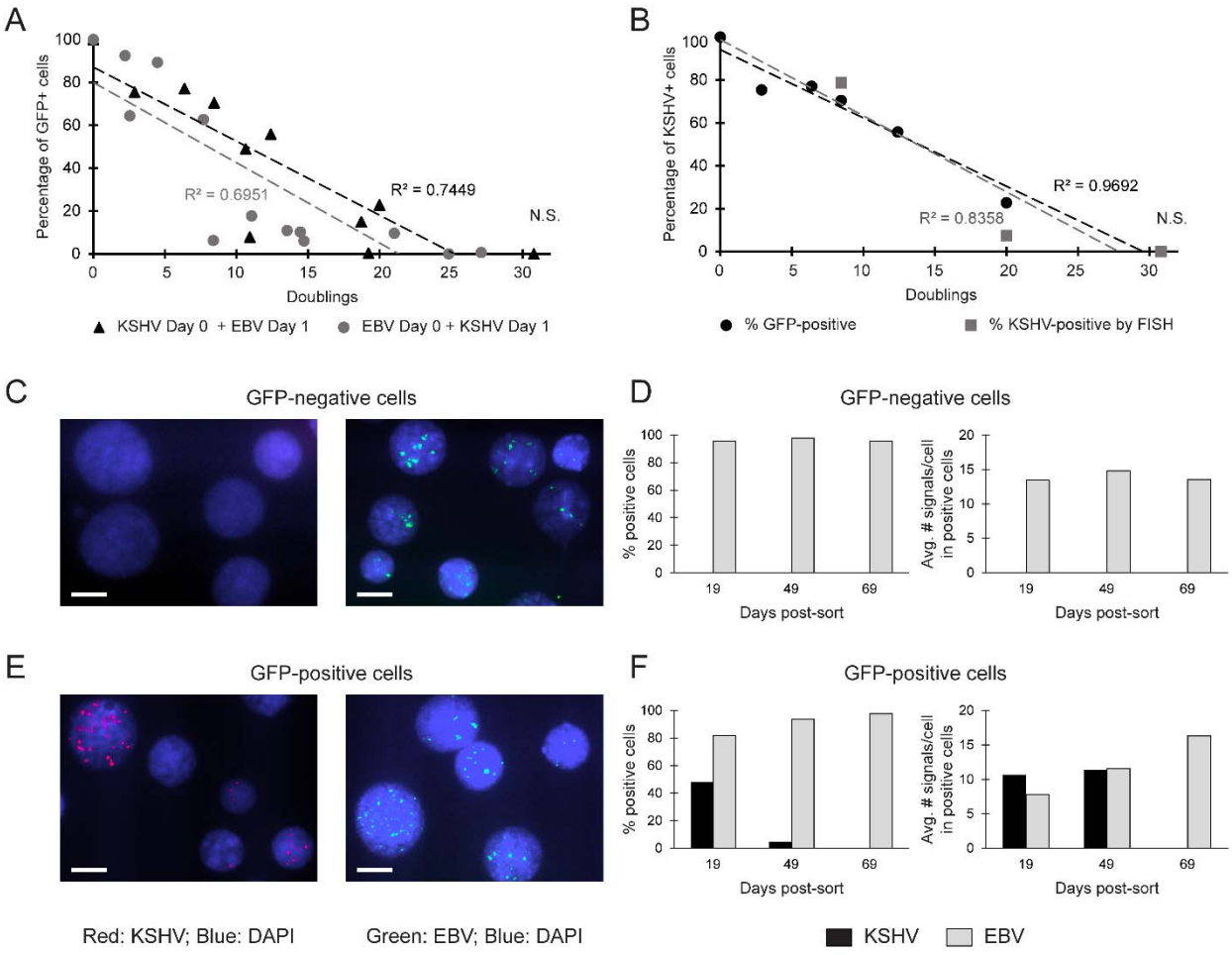
A
Percentage of GFP+ cells
Doublings
R² = 0.6951
R² = 0.7449
N.S.
KSHV Day 0 + EBV Day 1
EBV Day 0 + KSHV Day 1
B
Percentage of KSHV+ cells
Doublings
R² = 0.8358
R² = 0.9692
N.S.
% GFP-positive
% KSHV-positive by FISH
C
GFP-negative cells
D
GFP-negative cells
% positive cells
Avg. # signals/cell in positive cells
Days post-sort
E
GFP-positive cells
F
GFP-positive cells
Red: KSHV; Blue: DAPI
Green: EBV; Blue: DAPI
KSHV
EBV

Figure V.2: In populations of B cells analyzed in Figure V.1, the dually infected, GFP-positive cells grow at the same or slower rate than the GFP-negative cells.

KSHV infected GFP-positive cells were sorted 3 to 7 weeks post-infection. The growth of GFP-positive and GFP-negative cells was compared within (A) and between (B) each population of CD19+ B cells exposed to both EBV and KSHV. The first time point on the X-axis (Day 0) corresponds to the first day after sorting. Data from 3 independent biological experiments are shown for each population. The R-squared of the trendlines is indicated. * $p < 0.05$; ** $p < 0.01$; *** $p < 0.001$ by Sen-Adichie test.

Figure V.2

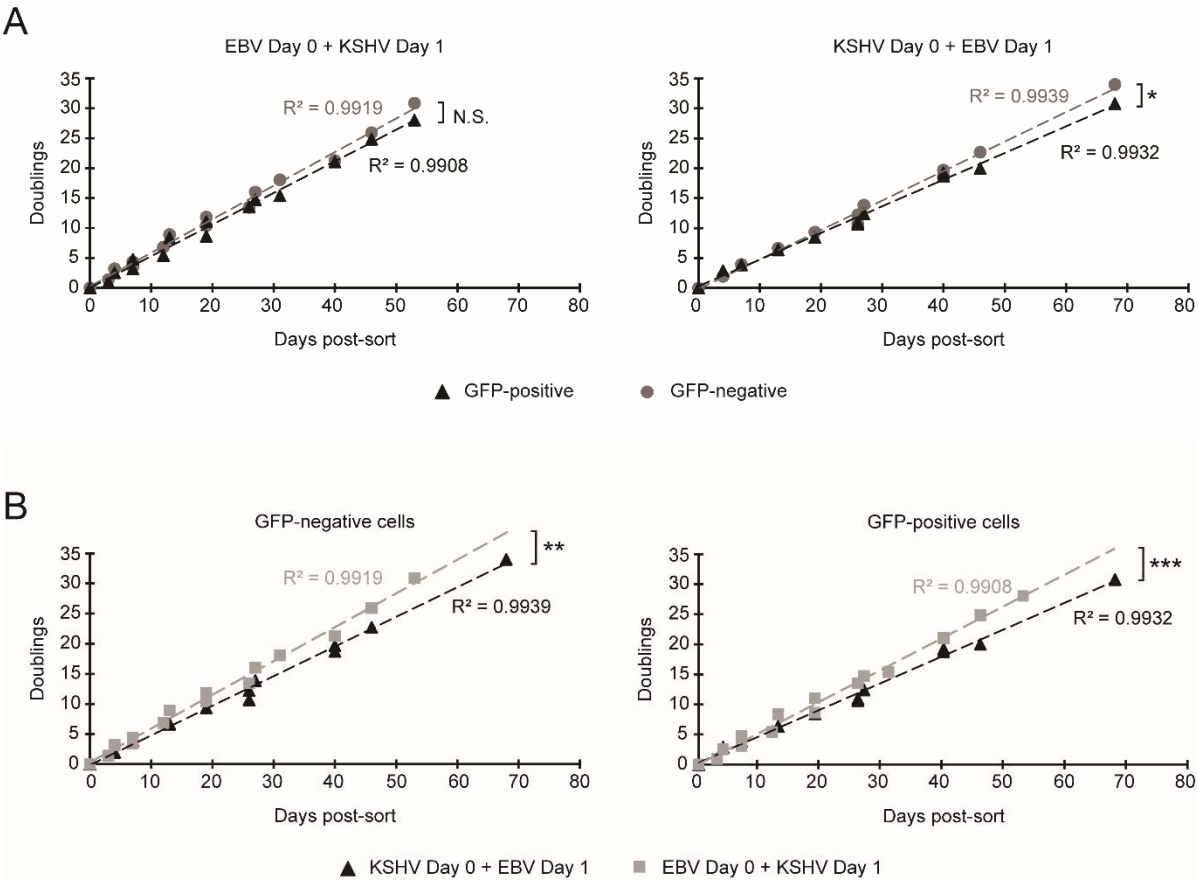
A
EBV Day 0 + KSHV Day 1
R² = 0.9919
N.S.
R² = 0.9908
Doublings
Days post-sort
KSHV Day 0 + EBV Day 1
R² = 0.9939
*
R² = 0.9932
Doublings
Days post-sort
GFP-positive
GFP-negative
B
GFP-negative cells
R² = 0.9919
**
R² = 0.9939
Doublings
Days post-sort
GFP-positive cells
R² = 0.9908
***
R² = 0.9932
Doublings
Days post-sort
KSHV Day 0 + EBV Day 1
EBV Day 0 + KSHV Day 1

Figure V.3: Some cells within populations of infected B cells maintain both viruses.

(A) Following KSHV infection, the percentage of GFP-positive cells was followed over time in the populations 1 and 2. Live cells were analyzed for GFP expression using a BD LSR Fortessa cytometer, and analysis was performed using FlowJo software.

(B) Populations shown in A were repeatedly sorted for GFP-positive cells (KSHV+/EBV+ fast and KSHV+/EBV+ slow cells respectively) (grey arrows) and harvested in Trizol at different time points. Following isolation of DNA, the average number of EBV and KSHV genomes per cell was quantified by qPCR.

Figure V.3

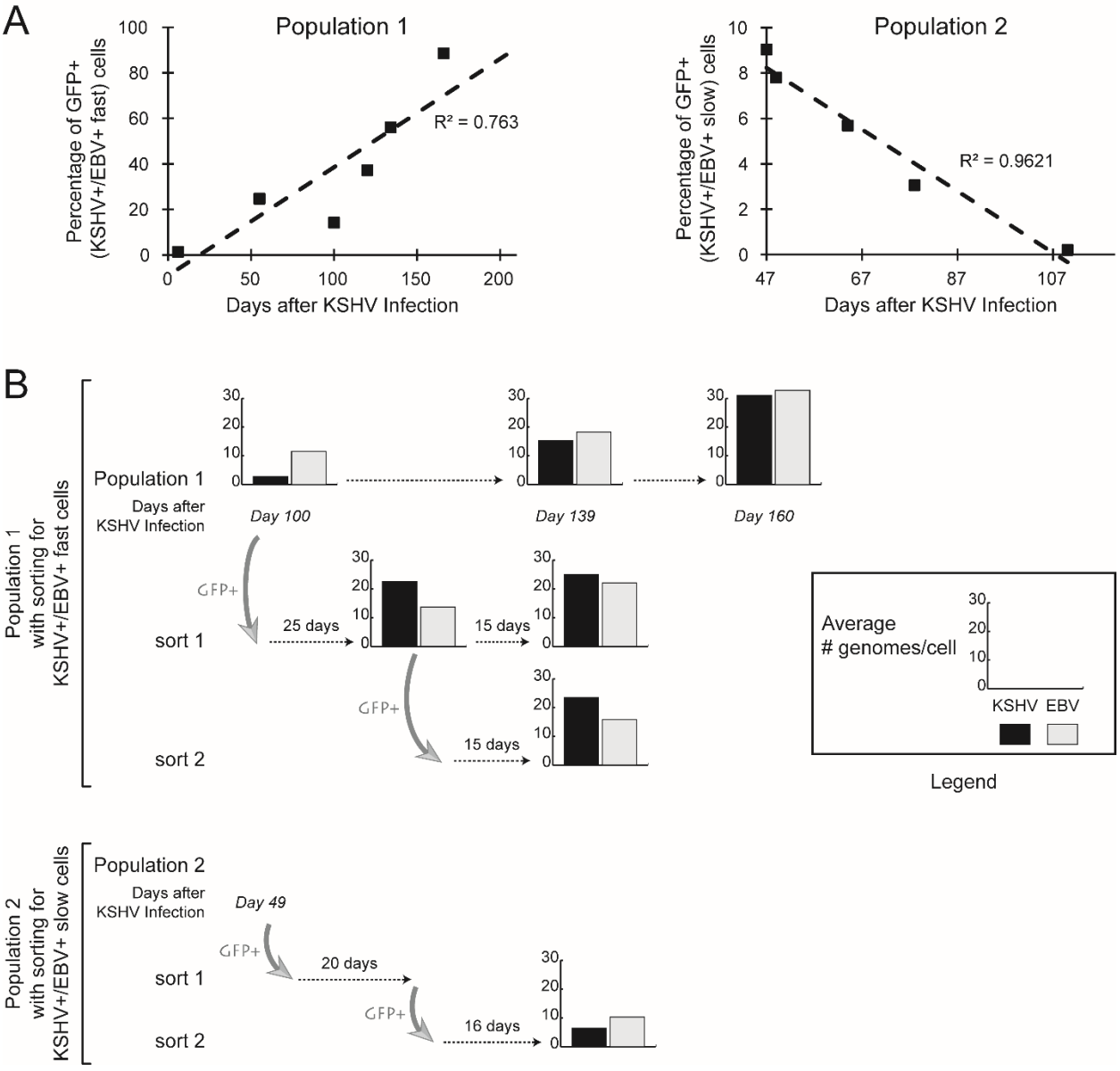
A
Population 1
Percentage of GFP+ (KSHV+/EBV+ fast) cells
R² = 0.763
Days after KSHV Infection
Population 2
Percentage of GFP+ (KSHV+/EBV+ slow) cells
R² = 0.9621
Days after KSHV Infection
B
Population 1 with sorting for KSHV+/EBV+ fast cells
Population 1
Days after KSHV Infection
Day 100
Day 139
Day 160
GFP+
sort 1
25 days
15 days
GFP+
sort 2
15 days
Average # genomes/cell
KSHV EBV
Legend
Population 2 with sorting for KSHV+/EBV+ slow cells
Population 2
Days after KSHV Infection
Day 49
GFP+
sort 1
20 days
GFP+
sort 2
16 days

Figure V.4: Some cells within populations of infected B cells maintain KSHV.

Populations of cells described in Figure V.3 were repeatedly sorted for GFP-positive cells (KSHV+/EBV+ fast and KSHV+/EBV+ slow cells respectively) (grey arrows) and fixed at different time points. The number of KSHV-infected cells and the average number of signals per cell in KSHV-positive cells were determined by fluorescence *in situ* hybridization (FISH).

Figure V.4

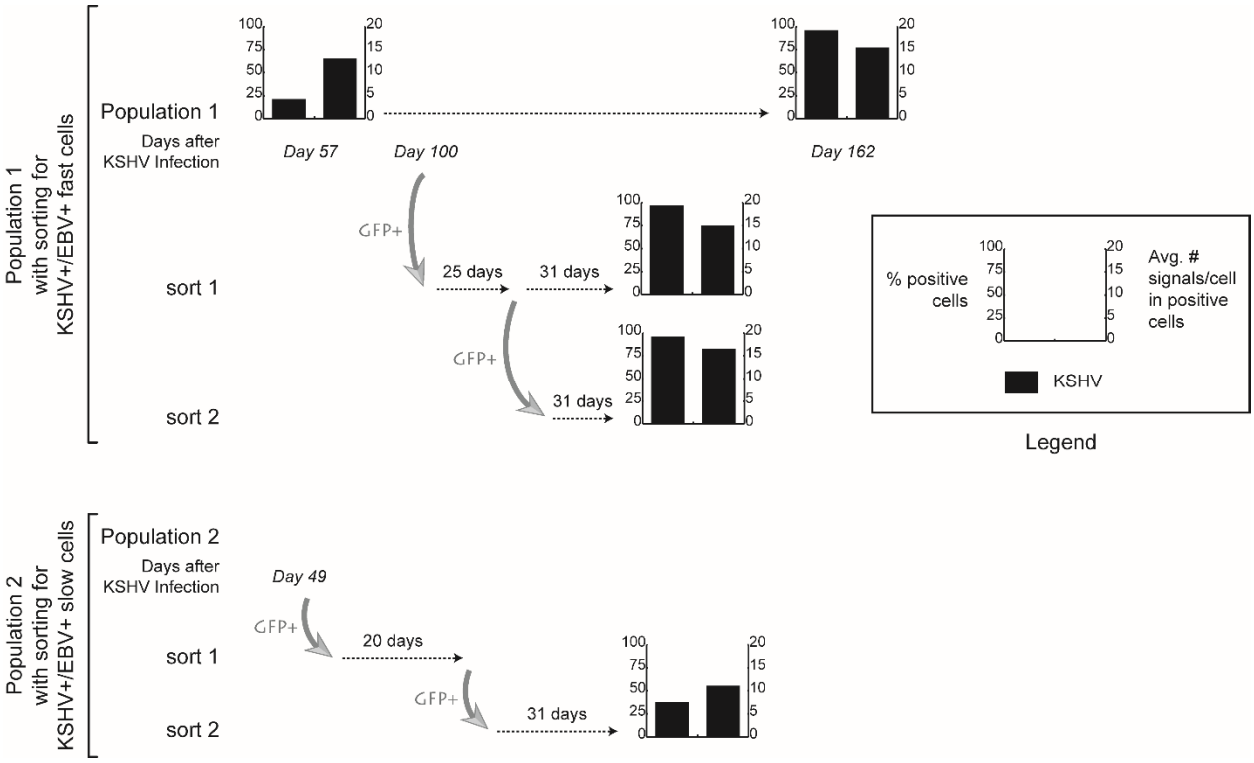
Population 1
with sorting for
KSHV+/EBV+ fast cells
Days after
KSHV Infection
Day 57
Day 100
Day 162
GFP+
25 days
31 days
sort 1
GFP+
31 days
sort 2
% positive
cells
Avg. #
signals/cell
in positive
cells
KSHV
Legend
Population 2
with sorting for
KSHV+/EBV+ slow cells
Population 2
Days after
KSHV Infection
Day 49
GFP+
20 days
sort 1
GFP+
31 days
sort 2

Figure V.5: KSHV-negative cells that overgrow the dually infected, GFP-positive cells arise from pre-existing KSHV-negative cells.

Populations of cells described in Figure 4 were repeatedly sorted for GFP-positive cells (KSHV+/EBV+ fast and KSHV+/EBV+ slow cells respectively) (grey arrows) and harvested in Trizol at different time points. RNA was isolated and analyzed with MiXCR to determine the percentage of each clone based on VDJ recombination in the immunoglobulin heavy chain (IGH) locus. Each clone with a percentage ≥ 0.5% in the population is represented with a single color. Clones with a percentage < 0.5% were combined and their total percentage is represented in grey. The percentage of GFP-positive cells at the time of harvest was determined when possible. Samples noted “ND” were directly sorted into Trizol and the number of GFP-positive cells could not be determined.

Figure V.5

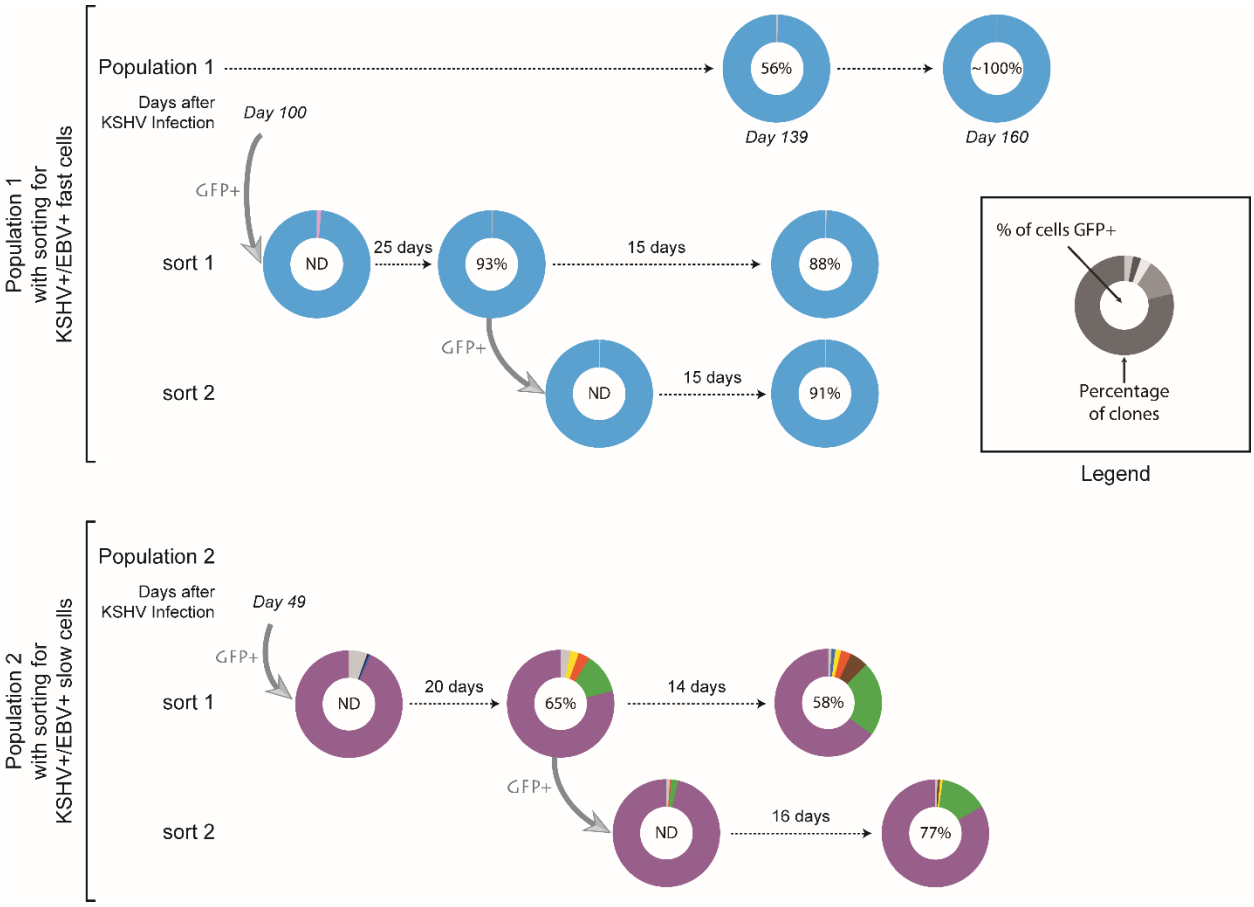
Population 1
with sorting for
KSHV+/EBV+ fast cells
Population 1
Days after
KSHV Infection
Day 100
GFP+
sort 1
ND
25 days
93%
15 days
88%
GFP+
sort 2
ND
15 days
91%
56%
Day 139
~100%
Day 160
% of cells GFP+
Percentage
of clones
Legend
Population 2
with sorting for
KSHV+/EBV+ slow cells
Population 2
Days after
KSHV Infection
Day 49
GFP+
sort 1
ND
20 days
65%
14 days
58%
GFP+
sort 2
ND
16 days
77%

Table V.1: Percentage of each immunoglobulin heavy and light chain in samples analyzed in Figure V.5 with sorting for KSHV-encoded GFP.

RNA from populations of cells repeatedly sorted for GFP-positive cells (KSHV+/EBV+ fast and KSHV+/EBV+ slow cells) was analyzed with MiXCR (see Figure V.5). The clonal composition of one additional population sorted for GFP-positive cells (KSHV+/EBV+ intermediate cells) (see Figure V.8) was also determined. The percentage of each type of immunoglobulin heavy and light chain in each sample is indicated.

Table V.1

Sample		*Days after KSHV infection*	*Days post-sort**	*Heavy Chain (in %)*					*Light Chain (in %)*	
				IgM	*IgG*	*IgA*	*IgD*	*IgE*	*κ*	*λ*
Population 1										
with sorting for KSHV+/EBV+ fast cells		*139*	-	**99.96**	0.04	0	0	0	0.13	**99.87**
		160	-	**99.98**	0.02	0	0	0	0.02	**99.98**
	sort 1	-	0	**99.98**	0.02	0	0	0	0.96	**99.04**
	sort 1	-	25	**99.99**	0.01	0	0	0	0.03	**99.97**
	sort 1	-	40	**99.97**	0.02	0	0	0	0.05	**99.95**
	sort 2	-	0	**99.96**	0.04	0	0	0	0.06	**99.94**
	sort 2	-	15	**99.96**	0.04	0	0	0	0.04	**99.96**
Population 2										
with sorting for KSHV+/EBV+ slow cells	*sort 1*	-	0	**97.22**	2.51	0.27	0	0	2.99	**97.01**
	sort 1	-	20	86.56	**13.33**	0.10	0	0	**16.23**	83.77
	sort 1	-	34	77.00	**22.98**	0.01	0.01	0	**34.10**	65.90
	sort 2	-	0	**97.74**	2.24	0.01	0	0	2.79	**97.21**
	sort 2	-	16	85.40	**14.58**	0.02	0	0	**34.31**	65.69
Population 3										
with sorting for KSHV+/EBV+ intermediate cells	*sort 3*	-	0	**95.51**	4.49	0	0	0	7.85	**92.15**

* At day 0, samples were directly sorted into Trizol.

Figure V.6: KSHV gene expression is increased in the KSHV+/EBV+ fast cells.

(A) Volcano plot of up- and downregulated cellular and viral genes in dually infected KSHV+/EBV+ fast cells relative to KSHV+/EBV+ slow cells.

(B and C) Heatmaps depicting the normalized expression values of the differentially expressed EBV (B) and KSHV (C) genes (adjusted p-value < 0.05 and fold change < -1.5 or > 1.5) between the KSHV+/EBV+ fast and KSHV+/EBV+ slow cells for each sample. Genes shown in heatmaps were ordered by p-value (the gene with the smallest p-value is on the left of the heatmap).

(D) Coverage plots of RNA-seq reads of the KSHV+/EBV+ fast and KSHV+/EBV+ slow cells mapped to the forward (blue) or reverse (red) strands of the EBV and KSHV genome. To allow visualization of transcription across the genome, the normalized expression of highly expressed genes was cropped.

Figure V.6

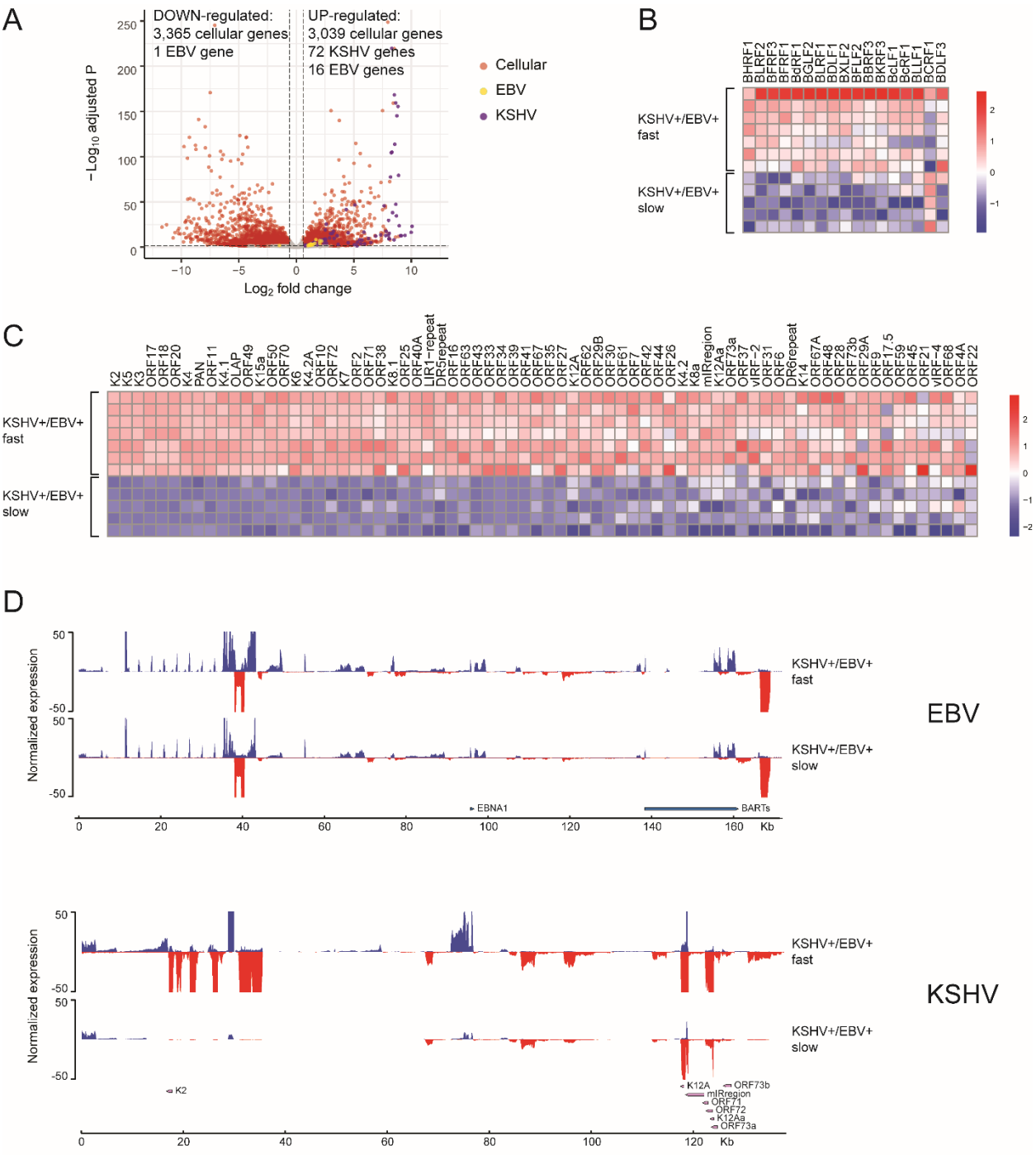
A
DOWN-regulated:
3,365 cellular genes
1 EBV gene
UP-regulated:
3,039 cellular genes
72 KSHV genes
16 EBV genes
Cellular
EBV
KSHV
−Log10 adjusted P
Log2 fold change
B
KSHV+/EBV+ fast
KSHV+/EBV+ slow
C
KSHV+/EBV+ fast
KSHV+/EBV+ slow
D
Normalized expression
KSHV+/EBV+ fast
KSHV+/EBV+ slow
EBV
KSHV
EBNA1
BARTs
Kb

Figure V.7: KSHV+/EBV+ fast cells regulate the expression of some cellular genes as do PEL cells.

(A, B and C) Principal Component Analysis based on EBV (A), KSHV (B) and cellular (C) transcript reads of seven samples of KSHV+/EBV+ fast and five samples of KSHV+/EBV+ slow cells.

(D) Heatmap depicting the normalized expression values for the core enriched genes in GSEA analysis of the seven samples of KSHV+/EBV+ fast cells compared to the five samples of KSHV+/EBV+ slow cells from the set of genes downregulated in PEL (113), $p < 0.001$, FDR q-value < 0.001.

(E) GSEA analysis of the seven samples of KSHV+/EBV+ fast cells compared to the five samples of KSHV+/EBV+ slow cells with the hallmark gene set “TNF-α signaling via NF-κB”, $p < 0.001$, FDR q-value < 0.001, Normalized Enrichment Score (NES) = 3.8.

Figure V.7

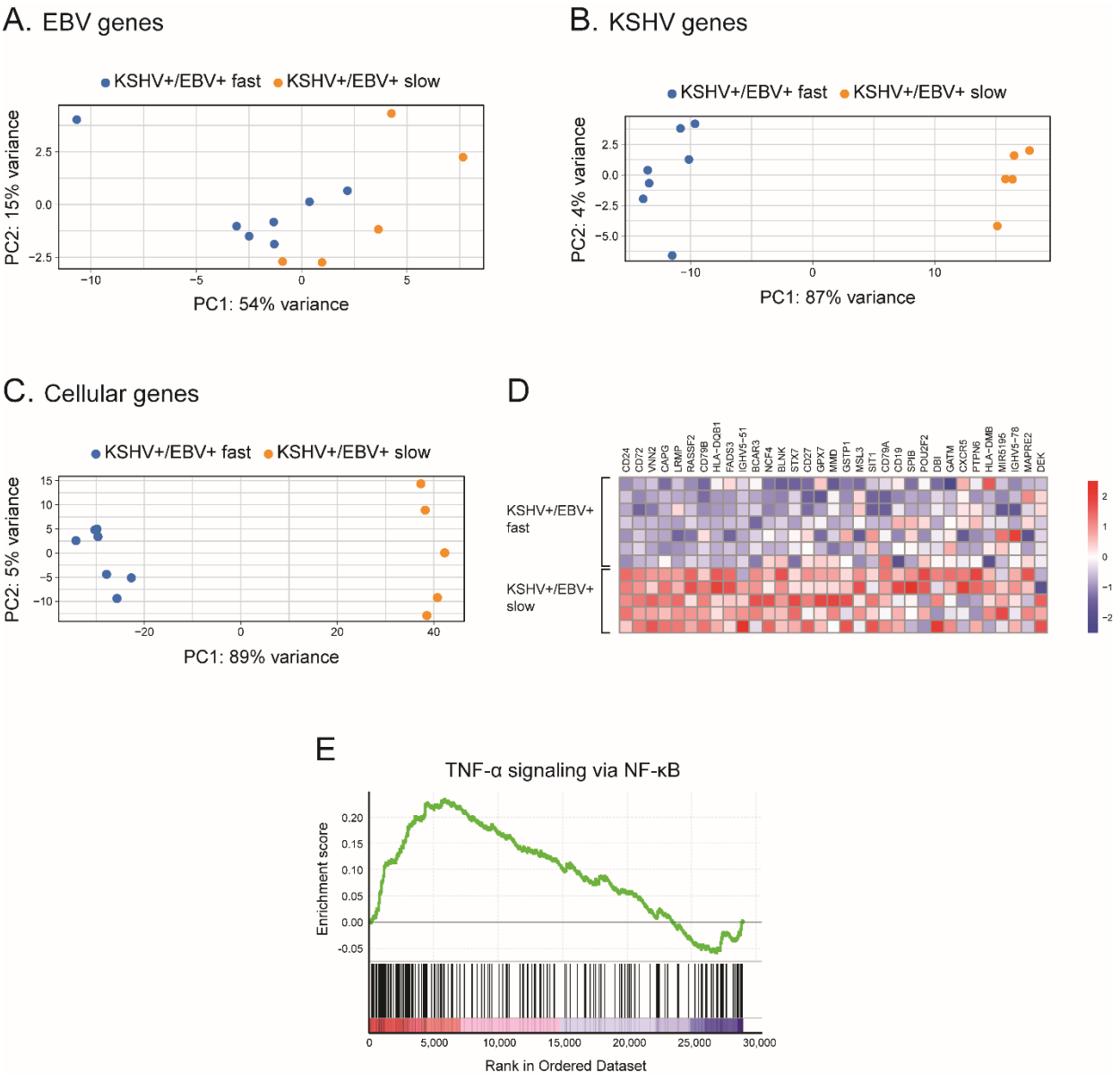
A. EBV genes
KSHV+/EBV+ fast
KSHV+/EBV+ slow
PC2: 15% variance
PC1: 54% variance
B. KSHV genes
KSHV+/EBV+ fast
KSHV+/EBV+ slow
PC2: 4% variance
PC1: 87% variance
C. Cellular genes
KSHV+/EBV+ fast
KSHV+/EBV+ slow
PC2: 5% variance
PC1: 89% variance
D
CD24
CD72
VNN2
CAPG
LRMP
RASSF2
CD79B
HLA-DQB1
FADS3
IGHV5-51
BCAR3
NCF4
BLNK
STX7
CD27
GPX7
MMD
GSTP1
MSL3
SIT1
CD79A
CD19
SPIB
POU2F2
DBI
GATM
CXCR5
PTPN6
HLA-DMB
MIR5196
IGHV5-78
MAPRE2
DEK
KSHV+/EBV+ fast
KSHV+/EBV+ slow
E
TNF-α signaling via NF-κB
Enrichment score
Rank in Ordered Dataset

Figure V.8: Dually infected cells exhibit a range of phenotypes between those of the KSHV+/EBV+ slow and the KSHV+/EBV+ fast cells.

Population 3 was repeatedly sorted for GFP-positive cells (KSHV+/EBV+ intermediate cells) (grey arrows) and harvested in Trizol at the indicated time point.

(A) Following isolation of DNA, the average number of EBV and KSHV genomes per cell was quantified by qPCR.

(B) RNA was isolated and analyzed with MiXCR to determine the percentage of each clone based on VDJ recombination in the immunoglobulin heavy chain (IGH) locus. Each clone with a percentage ≥ 0.5% in the population is represented with a single color. Clones with a percentage < 0.5% were combined and their total percentage is represented in grey. The percentage of GFP-positive cells at the time of harvest was determined when possible. Samples noted “ND” were directly sorted into Trizol and the number of GFP-positive cells could not be determined.

(C, D and E) Principal Component Analysis based on EBV (C), KSHV (D) and cellular (E) transcript reads of seven samples of KSHV+/EBV+ fast, five samples of KSHV+/EBV+ slow and one sample of KSHV+/EBV+ intermediate cells.

Figure V.8

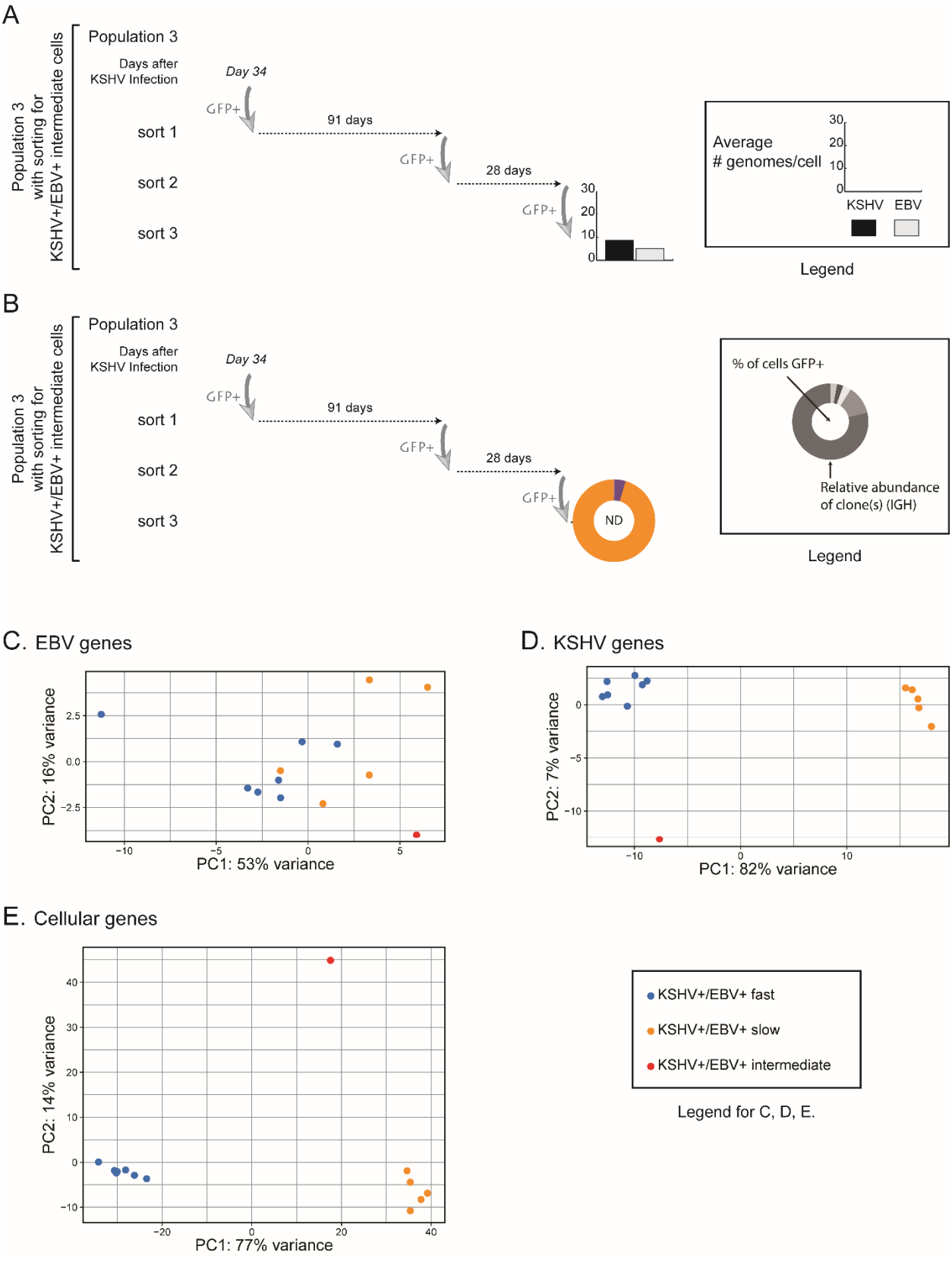
A
Population 3 with sorting for KSHV+/EBV+ intermediate cells
Population 3
Days after KSHV Infection
sort 1
sort 2
sort 3
Day 34
GFP+
91 days
28 days
Average # genomes/cell
KSHV
EBV
Legend
B
% of cells GFP+
Relative abundance of clone(s) (IGH)
ND
C. EBV genes
PC2: 16% variance
PC1: 53% variance
D. KSHV genes
PC2: 7% variance
PC1: 82% variance
E. Cellular genes
PC2: 14% variance
PC1: 77% variance
KSHV+/EBV+ fast
KSHV+/EBV+ slow
KSHV+/EBV+ intermediate
Legend for C, D, E.

Figure V.9: EBV's BART miRNAs provide selective advantages to the BC-1 PEL cell line.

(A) Schematic representation of the experimental method. Three EBNA1-OriP plasmids (p3828, p174 and p3829) encoding different subsets of EBV genes and a hygromycin resistance gene (HygR) were electroporated into the BC-1 PEL cell line. Cells carrying each individual plasmid were selected with hygromycin. The number of endogenous EBV genomes per cell was measured in them after 9 months of culture.

(B) Cells carrying each individual plasmid, p3828, p174 or p3829, were cultured for 9 months under hygromycin selection. The average number of endogenous EBV genomes (BALF5 molecules) and plasmids (hygromycin molecules) per cell was quantified by qPCR.

Figure V.9

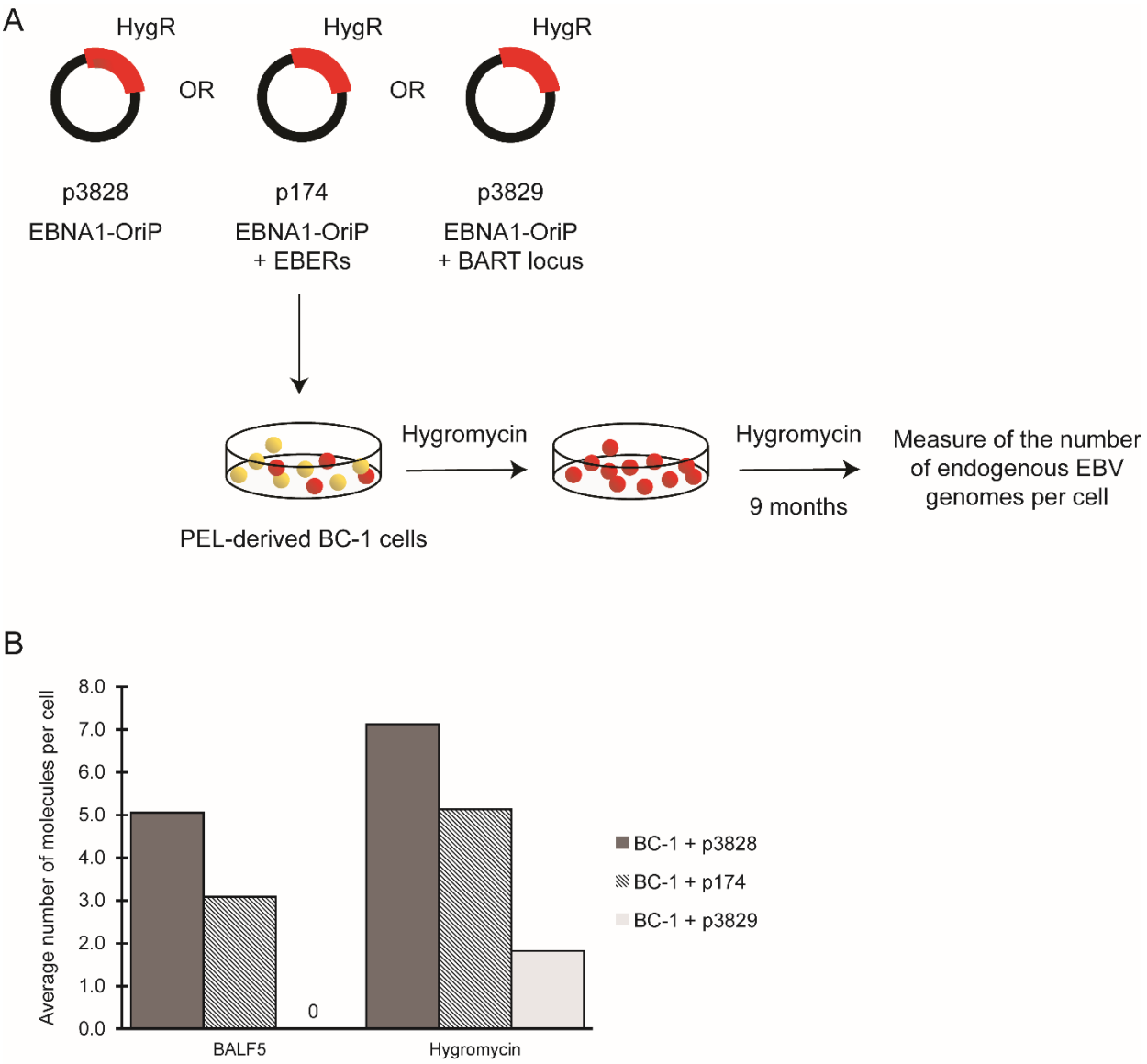
A
HygR
HygR
HygR
OR
OR
p3828
EBNA1-OriP
p174
EBNA1-OriP
+ EBERs
p3829
EBNA1-OriP
+ BART locus
Hygromycin
Hygromycin
9 months
Measure of the number of endogenous EBV genomes per cell
PEL-derived BC-1 cells
B
Average number of molecules per cell
8.0
7.0
6.0
5.0
4.0
3.0
2.0
1.0
0.0
0
BALF5
Hygromycin
BC-1 + p3828
BC-1 + p174
BC-1 + p3829

DISCUSSION

Most Primary Effusion Lymphomas (PELs) are dually infected with KSHV and EBV. We formerly lacked an *in vitro* model of PEL because of the difficulty in infecting B cells with KSHV *in vitro* and because KSHV has not been found to transform these cells. In CHAPTER IV, we have defined conditions to infect peripheral B cells with KSHV efficiently by co-infecting them with EBV. These conditions supported the long-term proliferation of dually infected cells. We have shown that the infecting EBV partner allowed activation of the B cells and expression of KSHV genes. It likely also supported proliferation of the dually infected cells given its ability to maintain proliferation of EBV-only infected cells. This likelihood is supported by the findings that forcing the loss of EBV genomes from PEL cells either by inhibiting EBNA1 with its dominant negative derivative or by targeting EBNA1 with CRISPR/Cas9 gRNAs inhibits both their proliferation and the maintenance of their KSHV genomes (60, 68).

We showed that the dually infected cells in populations of B cells exposed to both viruses varied in their proliferative capacities. Some were outgrown by B cells infected only with EBV and could be isolated by repeated rounds of FACS. These we refer to as KSHV+/EBV+ slow cells. Some dually infected cells outgrew the singly infected cells and are termed KSHV+/EBV+ fast cells. Importantly, both sets of cells maintained both viral genomes indicating that both KSHV and EBV contributed selective advantages to their proliferative and/or survival phenotypes and thus both were transformed by the dual infection. This understanding underscores the desirability of targeting not only KSHV but also EBV in developing new therapies for PEL. This is further supported by our finding

that EBV BART's miRNAs contribute to the survival and/or proliferation of the BC-1 PEL cells.

Both the KSHV+/EBV+ fast cells and the KSHV+/EBV+ slow cells expressed the λ light chain which is consistent with the work of Totonchy et al. (84) who showed that KSHV infection induces a B-cell receptor (BCR) revision resulting in expression of λ light chain. One study suggested that PELs often have lambda light chain genes productively rearranged (4). Even though heavy chain genes are expressed at the RNA level, PELs often do not express surface immunoglobulins detectably (1, 3, 4). We analyzed publicly available data from RNA sequencing of PEL cell lines with MiXCR and found a low expression of immunoglobulin heavy and light chain genes. This analysis confirmed the previously reported use of λ light chain in BCBL-1 cells and κ light chain in HBL-6 cells (4). In addition, we found BC-3 and AP3 cells to express λ light chain, too. The immunoglobulin light chain used in other analyzed PEL cell lines (AP5 and AP2) could not be determined due to its low or absent expression. Thus, 3 of 4 PEL cell lines express λ light chain mRNA as do both the KSHV+/EBV+ fast and the KSHV+/EBV+ slow transformed cells. Furthermore, we found that the KSHV+/EBV+ fast and the KSHV+/EBV+ slow cells were clonal, similar to PEL cells. On the contrary, EBV-only infected cells were polyclonal and expressed κ light chain mRNA.

The analysis of RNAs expressed in multiple samples of the KSHV+/EBV+ fast and the KSHV+/EBV+ slow cells revealed that the KSHV+/EBV+ fast cells have distinct, transformed properties. It showed that the KSHV+/EBV+ fast cells express higher levels of KSHV viral latent and lytic genes. KSHV latency locus and viral interleukin-6 genes, which are expressed in PEL, were among those genes upregulated in the KSHV+/EBV+

fast cells. Furthermore, GSEA analysis showed that cellular genes characteristically inhibited in PEL were also inhibited in the KSHV+/EBV+ fast cells relative to the KSHV+/EBV+ slow cells. In addition, NF-κB activity, which is essential for the survival of PEL cells (126), was increased in the KSHV+/EBV+ fast cells. These three characteristics define KSHV+/EBV+ fast cells' distinct, transformed properties, associating them with features of *bona fide* PEL cells.

The characteristic transformation of the KSHV+/EBV+ fast cells likely results from their increased expression of the KSHV transforming genes. The overexpression of KSHV vIL-6 in the KSHV+/EBV+ fast cells compared to the KSHV+/EBV+ slow cells was the most statistically significant. KSHV vIL-6 acts in an autocrine loop and PEL cells depend on this viral cytokine for proliferation and survival (48, 49). Increased expression of KSHV vIL-6 could therefore drive the transformation of the KSHV+/EBV+ fast cells. In addition, increased expression of KSHV v-FLIP likely contributes to the increased NF-κB activity and to the transformed phenotype of these cells (27, 127). Another insight into this transformation comes from the finding that it is not necessary for KSHV to express its lytic genes in order to infect B cells optimally along with EBV (see CHAPTER IV). This subset of viral genes therefore is not needed for the early events in transformation.

We found that dually infected cells in other populations of infected B cells can exhibit a phenotype between those of the KSHV+/EBV+ slow and the KSHV+/EBV+ fast cells: we called these cells KSHV+/EBV+ intermediate cells. The KSHV+/EBV+ intermediate cells did not overgrow the EBV-only infected cells but persisted for several months in the population. We found that the KSHV+/EBV+ intermediate cells upregulated the expression of KSHV genes, similar to the KSHV+/EBV+ fast cells, but their cellular

gene expression was intermediate between that of the KSHV+/EBV+ fast and the KSHV+/EBV+ slow cells. The KSHV+/EBV+ intermediate cells were also clonal and expressed λ light chain mRNA. It is thus likely that the KSHV+/EBV+ fast and KSHV+/EBV+ slow cells represent two extremes in the transformation of dually infected cells. These findings support the notion that multiple events need to occur for cells to evolve towards lymphomagenesis and that the upregulation of KSHV genes likely occurs prior to the differential expression of cellular genes.

The long-term dual infection and transformation of peripheral B cells by KSHV and EBV advances our ability to identify steps in a progression towards PEL. We can now identify the viral genes that regulate the expression of cellular genes in patterns shared with PEL. In a recent study, NSG mice that were reconstituted with human CD34-positive cells and subsequently infected with KSHV and EBV showed enhanced tumor formation compared to mice infected with EBV only (87). It is particularly revealing that the distinct, transformed properties of the KSHV+/EBV+ fast cells arose in the absence of any selective pressures in an animal or human host. Our model of dual infection *in vitro* therefore enables the genetic dissection of the viral and cellular genes that mediate the early stages of transformation towards PEL.

CHAPTER VI.

Discussion and Future Directions

Primary Effusion Lymphomas (PELs) are causally associated with Kaposi's sarcoma-associated herpesvirus (KSHV), and 90% of them are also co-infected with Epstein-Barr virus (EBV) (1, 2, 5, 6, 18, 19). KSHV and EBV are lost from proliferating cells if they do not provide their host cells selective advantages (24–26). Because both viruses are maintained as extrachromosomal plasmids in PELs, they both contribute to tumor phenotypes. PEL, therefore, is a unique tumor: it is the only human tumor to be known to depend on two oncogenic viruses. KSHV was found to express genes essential for the survival or proliferation of PEL cells (27–29). The role of EBV in PEL is still unclear, although several studies suggested that EBV plays a role in supporting proliferation of PEL cells and the maintenance of their KSHV genomes (60, 68). Even though KSHV is thought to be the genetic driver of PEL, B cells have notoriously been difficult to infect with KSHV *in vitro*, and when they can be infected, KSHV has not been found to transform them. We therefore formerly lacked a model which allows complete characterization *in vitro* of the early steps of development of PEL.

CONTRIBUTIONS DESCRIBED IN THIS DISSERTATION

I have established a protocol to produce and infect 293 cells with KSHV efficiently and reproducibly. I found that spinoculation increases KSHV binding to cells, which significantly enhances the efficiency of infection when cells are washed following exposure to the virus. Using this technique to expose cells to KSHV, I have defined a role for EBV in supporting co-infection of peripheral B cells by KSHV. I found that EBV plays a dual role in infection by KSHV and that optimal infection is achieved within 24 hours of EBV infection. My experiments underlined the role of B cell activation in KSHV infection

and suggested that EBV is allowing infection by KSHV in part by providing activation of the cells. These experiments further provided a possible explanation to why tonsillar B cells, which are often derived from activated tonsils, have been more susceptible to KSHV infection than peripheral B cells. I have then showed that the dually infected peripheral B cells are transformed and maintained both EBV and KSHV for months in culture. The dually infected cells were clonal and expressed lambda light chain mRNA similar to PEL cells. These dually infected cells varied in their proliferative capacities and showed distinct, transformed properties. Cells that grew to predominate in a culture showed enhanced KSHV gene expression, regulated the expression of some cellular genes as do PEL cells, and thus shared multiple properties with PEL cells. In this dissertation, I have therefore described a new model of dual infection *in vitro* that enables, for the first time, the genetic dissection of the viral and cellular genes that mediate the early stages of transformation towards PEL.

FUTURE DIRECTIONS

Future work will test for the mechanism by which EBV allows infection of peripheral B cells by KSHV. We found that EBV plays a dual role in infection of peripheral B cells by KSHV: early events of EBV infection promoted infection by KSHV while later events inhibited this co-infection. Our results suggested that KSHV can either bind irreversibly or enter non-activated peripheral B cells. If KSHV can enter resting B cells, EBV infection is therefore needed for KSHV gene expression. Later events of EBV infection could inhibit KSHV infection by decreasing its binding to cells or downregulating a receptor for entry. To test these hypotheses, we will monitor KSHV entry into non-activated B cells

compared to B cells exposed to KSHV prior to or following EBV infection. We will use fluorescence *in situ* hybridization (FISH) to measure the number of KSHV genomes in the nuclei of these cells. Preliminary experiments showed that KSHV binds to the surface of B cells and it can be difficult to distinguish the KSHV genomes bound to the surface from those in the nuclei. We therefore plan to treat cells with trypsin to remove the KSHV virions bound to the surface of the cells prior to analysis by FISH.

We have characterized and compared the phenotypes of two populations of dually infected cells: the KSHV+/EBV+ slow and the KSHV+/EBV+ fast cells. They were both transformed and maintained KSHV and EBV. Both populations were clonal and expressed lambda light chain mRNA, similar to PEL cells. The KSHV+/EBV+ slow cells were often overgrown by cells infected only with EBV while the KSHV+/EBV+ fast cells outgrew the singly infected cells. The KSHV+/EBV+ fast cells showed a higher level of KSHV gene expression compared to the KSHV+/EBV+ slow cells and regulated the expression of some cellular genes as do PEL cells.

By following the evolution of the dually infected, GFP-positive cells in populations of B cells, we have therefore identified different populations of dually infected cells based on their proliferative capacities compared to those of the EBV-only infected cells. We have then characterized their transformed properties and showed that the KSHV+/EBV+ fast cells have distinct, transformed properties that associate them more closely with features of PEL cells. In future experiments, the dually infected, GFP-positive cells will be cloned shortly following infection. By monitoring the number of GFP-positive cells over time, we will test whether all dually infected cells are transformed by EBV and KSHV or if some cells lose KSHV over time. Preliminary results suggest that a fraction of the dually infected

cells lose KSHV over time. We found that when the dually infected, GFP-positive cells were sorted and cloned at day 7 post-infection, only 40% of the wells that formed stably proliferating populations remained GFP-positive. We will measure the rate of growth and the expression of KSHV and cellular genes in each of these stably dually infected clones. Our results suggest that the clones of dually infected cells will differ in their rate of growth. These studies will determine the fraction of cells that acquire the phenotype of the KSHV+/EBV+ fast cells compared to that of the KSHV+/EBV+ slow cells. Our finding that some cells, the KSHV+/EBV+ intermediate cells, showed a phenotype between those of the KSHV+/EBV+ slow and the KSHV+/EBV+ fast cells suggests that the clones of dually infected cells will exhibit a range of phenotypes between those of the KSHV+/EBV+ slow and the KSHV+/EBV+ fast cells.

In preliminary experiments, we estimated the frequency at which KSHV+/EBV+ fast cells arise in populations of B cells exposed to both viruses. Dually infected, GFP-positive cells were sorted at day 7 post-infection and plated on human fibroblast feeders by limiting dilutions. We defined the KSHV+/EBV+ fast transformed cells as dually infected cells which overgrew mixed populations such that all cells grew to be GFP-positive. We looked at wells where multiple cells capable of proliferating were plated and counted those wells at 7 weeks in which all cells were GFP-positive. We found that the KSHV+/EBV+ fast transformed cells comprised approximately 1 cell per 10,000 B cells initially exposed to both KSHV and EBV.

We also plan to test what viral genes play a role in the transformation of the KSHV+/EBV+ fast cells. These cells upregulated KSHV genes found to be expressed in PEL such as the KSHV latency locus genes and vIL-6. The increased expression of these

genes, in particular v-FLIP and vIL-6, likely contribute to the characteristic cellular gene expression of the KSHV+/EBV+ fast cells. To ask if these genes are essential to the phenotype of the KSHV+/EBV+ fast cells, we will inhibit their expression using shRNAs and monitor the growth and survival of these cells. We will also use mutants of KSHV that lack expression of each KSHV latency locus gene or vIL-6 and infect primary B cells with each mutant in combination with EBV. Using the clonality assay described above, we will then compare the fraction of dually infected cells that acquire the phenotype of the KSHV+/EBV+ fast cells when cells were infected with a wild-type or a mutant strain of KSHV.

In addition, we plan to test for the role of EBV in supporting the growth or survival of the dually infected B cells. Based on our finding that EBV's BART miRNAs contribute to the survival and/or proliferation of the BC-1 PEL cells, these miRNAs could play a role in the transformation of the dually infected B cells. In future experiments, primary B cells will be infected with a mutated strain of EBV that does not express the BART miRNAs plus or minus KSHV. We will ask whether the absence of expression of EBV's BART miRNAs affects the efficiency of infection or the maintenance of KSHV in peripheral B cells. We will also compare the fraction of dually infected cells that acquire the phenotype of the KSHV+/EBV+ fast cells when cells were infected with the wild-type or the mutant strain of EBV. We will also test for the requirement of other EBV's genes. In preliminary experiments using ɣ-irradiation of the B95-8 strain of EBV, we found that EBV's nuclear antigens are required early for dual infection of peripheral B cells by KSHV. Using an EBNA2-null variant of EBV, HH514 clone 16, in dual infections, we found a 62% decrease in GFP-positive cells relative to B95-8 virus at day 5 post-infection. Our preliminary results

thus indicate that EBV must express one or more transforming genes, including EBNA2, in primary B cells for dual infection and transformation by KSHV.

Future work will also examine the role of EBV and KSHV lytic cycles in the transformation of the dually infected cells. We found that KSHV lytic genes and some EBV lytic genes were upregulated in the KHSV+/EBV+ fast cells compared to the KSHV+/EBV+ slow cells. Several of the differentially expressed lytic genes between the KSHV+/EBV+ fast and the KSHV+/EBV+ slow cells are thought to play a role in tumorigenesis (128). By using a strain of KSHV that does not express the viral protein RTA, we found that KSHV lytic gene expression is not required for infection of peripheral B cells by KSHV. This subset of viral genes therefore is not needed for the early events in transformation. We will extend this experiment by asking if the dually infected cells are transformed and maintain the mutated strain of KSHV. In preliminary experiments, I observed fluctuations in the percentage of GFP-positive cells over time that were similar in populations of cells exposed to the wild-type or to the mutant strain of KSHV. These results suggest that cells can be transformed by dual infection with the mutated strain of KSHV. We will ask whether a fraction of these dually infected cells shares the same characteristics in cellular gene expression with PEL cells than the KSHV+/EBV+ fast cells.

A recent study found that EBV lytic gene expression in dually infected mice lead to increase tumor formation (87). In future experiments, we will infect peripheral B cells with KSHV and a mutated strain of EBV that does not express BZLF1 and BRLF1 and therefore cannot undergo the lytic cycle. We will measure the efficiency of infection with KSHV and the maintenance of KSHV in these dually infected cells. If the cells are transformed by this dual infection, we will characterize the phenotypes of the dually

infected cells and test whether a smaller fraction of these cells acquire the phenotype of the KSHV+/EBV+ fast cells.

In preliminary experiments, we monitored the fraction of cells that undergo EBV's or KSHV's lytic cycle in the KSHV+/EBV+ fast compared to the KSHV+/EBV+ slow dually infected cells. We found that 1.2% of the KSHV+/EBV+ fast and 0.5% of the KSHV+/EBV+ slow cells display amplified, compartmentalized KSHV DNAs by FISH, which are characteristic of KSHV's lytic cycle. Using immunofluorescence, we found that 0.6% of the KSHV+/EBV+ fast cells and 0.8% of the KSHV+/EBV+ slow cells expressed the early antigen encoded by BHRF1, indicating that they support entry into EBV's lytic cycle similarly. These preliminary results indicate that the viral lytic phases are likely not determining the bulk properties of the KSHV+/EBV+ fast cells.

IN CONCLUSION

This new model of dual infection *in vitro* allows for the first time a mechanistic analysis of the contributions of EBV and KSHV to early steps in the development of PEL. Future work will identify the viral and cellular genes that mediate the transformation of the dually infected cells and their progression towards lymphomagenesis. This model also establishes a role for EBV in the development of PEL. EBV both promoted infection of peripheral B cells by KSHV and provided survival and/or proliferative advantages to the dually infected cells. Therefore, this work more generally underscores the desirability of targeting not only KSHV but also EBV in developing new therapies for PEL.

References

1. Nador RG, et al. (1996) Primary effusion lymphoma: a distinct clinicopathologic entity associated with the Kaposi's sarcoma-associated herpes virus. *Blood* 88(2):645–656.
2. Chen Y-B, Rahemtullah A, Hochberg E (2007) Primary effusion lymphoma. *Oncologist* 12(5):569–576.
3. Matolcsy A, Nádor RG, Cesarman E, Knowles DM (1998) Immunoglobulin V(H) gene mutational analysis suggests that primary effusion lymphomas derive from different stages of B cell maturation. *Am J Pathol* 153(5):1609–1614.
4. Fais F, et al. (1999) Immunoglobulin V region gene use and structure suggest antigen selection in AIDS-related primary effusion lymphomas. *Leukemia* 13(7):1093–1099.
5. Cesarman E, Chang Y, Moore PS, Said JW, Knowles DM (1995) Kaposi's sarcoma–associated herpesvirus-like DNA sequences in AIDS-related body-cavity–based lymphomas. *N Engl J Med* 332(18):1186–1191.
6. Cesarman E, et al. (1995) In vitro establishment and characterization of two acquired immunodeficiency syndrome-related lymphoma cell lines (BC-1 and BC-2) containing Kaposi's sarcoma-associated herpesvirus-like (KSHV) DNA sequences. *Blood* 86(7):2708–2714.
7. Rajewsky N (1996) Clonal selection and learning in the antibody system. *Nature* 381(6585):751–758.
8. Lam KP, Kühn R, Rajewsky K (1997) In vivo ablation of surface immunoglobulin on mature B cells by inducible gene targeting results in rapid cell death. *Cell*

90(6):1073–1083.

9. Lagunoff M, Ganem D (1997) The structure and coding organization of the genomic termini of Kaposi's sarcoma-associated herpesvirus. *Virology* 236(1):147–154.
10. Choi J-K, Lee B-S, Shim SN, Li M, Jung JU (2000) Identification of the novel K15 gene at the rightmost end of the Kaposi's sarcoma-associated herpesvirus genome. *J Virol* 74(1):436–446.
11. Lee B-S, Alvarez X, Ishido S, Lackner AA, Jung JU (2000) Inhibition of intracellular transport of B cell antigen receptor complexes by Kaposi's sarcoma–associated herpesvirus K1. *J Exp Med* 192(1):11–21.
12. Miller CL, et al. (1995) Integral membrane protein 2 of Epstein-Barr virus regulates reactivation from latency through dominant negative effects on protein-tyrosine kinases. *Immunity* 2(2):155–166.
13. Miller CL, Longnecker R, Kieff E (1993) Epstein-Barr virus latent membrane protein 2A blocks calcium mobilization in B lymphocytes. *J Virol* 67(6):3087–3094.
14. Miller CL, Lee JH, Kieff E, Longnecker R (1994) An integral membrane protein (LMP2) blocks reactivation of Epstein-Barr virus from latency following surface immunoglobulin crosslinking. *Proc Natl Acad Sci* 91(2):772–776.
15. Caldwell RG, Wilson JB, Anderson SJ, Longnecker R (1998) Epstein-Barr virus LMP2A drives B cell development and survival in the absence of normal B cell receptor signals. *Immunity* 9(3):405–411.
16. Mancao C, Hammerschmidt W (2007) Epstein-Barr virus latent membrane protein 2A is a B-cell receptor mimic and essential for B-cell survival. *Blood* 110(10):3715–3721.

17. Steinbrück L, et al. (2015) K1 and K15 of Kaposi's sarcoma-associated herpesvirus are partial functional homologues of latent membrane protein 2A of Epstein-Barr virus. *J Virol* 89(14):7248–7261.

18. Knowles DM, Inghirami G, Ubriaco A, Dalla-Favera R (1989) Molecular genetic analysis of three AIDS-associated neoplasms of uncertain lineage demonstrates their B-cell derivation and the possible pathogenetic role of the Epstein-Barr virus. *Blood* 73(3):792–799.

19. Cesarman E, Knowles DM (1999) The role of Kaposi's sarcoma-associated herpesvirus (KSHV/HHV-8) in lymphoproliferative diseases. *Semin Cancer Biol* 9(3):165–174.

20. Henle G, Henle W, Diehl V (1968) Relation of Burkitt's tumor-associated herpes-ytpe virus to infectious mononucleosis. *Proc Natl Acad Sci* 59(1):94–101.

21. Sugden B (2014) Epstein-Barr virus: the path from association to causality for a ubiquitous human pathogen. *PLoS Biol* 12(9):e1001939.

22. Chang Y, et al. (1994) Identification of herpesvirus-like DNA sequences in AIDS-associated Kaposi's sarcoma. *Science* 266(5192):1865–1869.

23. Soulier J, et al. (1995) Kaposi's sarcoma-associated herpesvirus-like DNA sequences in multicentric Castleman's disease. *Blood* 86(4):1276–1280.

24. Vereide D, Sugden B (2010) Insights into the evolution of lymphomas induced by Epstein-Barr virus. *Adv Cancer Res* 108:1–19.

25. Vereide DT, Sugden B (2011) Lymphomas differ in their dependence on Epstein-Barr virus. *Blood* 117(6):1977–1985.

26. Chiu YF, Sugden AU, Fox K, Hayes M, Sugden B (2017) Kaposi's sarcoma-

associated herpesvirus stably clusters its genomes across generations to maintain itself extrachromosomally. *J Cell Biol* 216(9):2745–2758.

27. Guasparri I, Keller SA, Cesarman E (2004) KSHV vFLIP is essential for the survival of infected lymphoma cells. *J Exp Med* 199(7):993–1003.
28. Wies E, et al. (2008) The viral interferon-regulatory factor-3 is required for the survival of KSHV-infected primary effusion lymphoma cells. *Blood* 111(1):320–327.
29. Godfrey A, Anderson J, Papanastasiou A, Takeuchi Y, Boshoff C (2005) Inhibiting primary effusion lymphoma by lentiviral vectors encoding short hairpin RNA. *Blood* 105(6):2510–2518.
30. Dittmer D, et al. (1998) A cluster of latently expressed genes in Kaposi's sarcoma-associated herpesvirus. *J Virol* 72(10):8309–8315.
31. Sadler R, et al. (1999) A complex translational program generates multiple novel proteins from the latently expressed kaposin (K12) locus of Kaposi's sarcoma-associated herpesvirus. *J Virol* 73(7):5722–5730.
32. Pearce M, Matsumura S, Wilson AC (2005) Transcripts encoding K12, v-FLIP, v-cyclin, and the microRNA cluster of Kaposi's sarcoma-associated herpesvirus originate from a common promoter. *J Virol* 79(22):14457–14464.
33. Samols MA, Hu J, Skalsky RL, Renne R (2005) Cloning and identification of a microRNA cluster within the latency-associated region of Kaposi's sarcoma-associated herpesvirus. *J Virol* 79(14):9301–9305.
34. Kedes DH, Lagunoff M, Renne R, Ganem D (1997) Identification of the gene encoding the major latency-associated nuclear antigen of the Kaposi's sarcoma-associated herpesvirus. *J Clin Invest* 100(10):2606–2610.

35. Ballestas ME, Chatis PA, Kaye KM (1999) Efficient persistence of extrachromosomal KSHV DNA mediated by latency-associated nuclear antigen. *Science* 284(5414):641–644.

36. Ballestas ME, Kaye KM (2001) Kaposi's sarcoma-sssociated herpesvirus latency-associated nuclear antigen 1 mediates episome persistence through cis-acting terminal repeat (TR) sequence and specifically binds TR DNA. *J Virol* 75(7):3250–3258.

37. Lim C, Sohn H, Lee D, Gwack Y, Choe J (2002) Functional dissection of latency-associated nuclear antigen 1 of Kaposi's sarcoma-associated herpesvirus involved in latent DNA replication and transcription of terminal repeats of the viral genome. *J Virol* 76(20):10320-10331.

38. Low W, et al. (2001) Internal ribosome entry site regulates translation of Kaposi's sarcoma-associated herpesvirus FLICE inhibitory protein. *J Virol* 75(6):2938–2945.

39. Pfeffer S, et al. (2005) Identification of microRNAs of the herpesvirus family. *Nat Methods* 2(4):269–276.

40. Ganem D (2010) KSHV and the pathogenesis of Kaposi sarcoma: listening to human biology and medicine. *J Clin Invest* 120(4):939–949.

41. Cai X, et al. (2005) Kaposi's sarcoma-associated herpesvirus expresses an array of viral microRNAs in latently infected cells. *Proc Natl Acad Sci* 102(15):5570–5575.

42. Cai X, Cullen BR (2006) Transcriptional origin of Kaposi's sarcoma-associated herpesvirus microRNAs. *J Virol* 80(5):2234–2242.

43. Lubyova B, Pitha PM (2000) Characterization of a novel human herpesvirus 8-encoded protein, vIRF-3, that shows homology to viral and cellular interferon

regulatory factors. *J Virol* 74(17):8194–8201.

44. Rivas C, Thlick A-E, Parravicini C, Moore PS, Chang Y (2001) Kaposi's sarcoma-associated herpesvirus LANA2 is a B-cell-specific latent viral protein that inhibits p53. *J Virol* 75(1):429–438.

45. Moore PS, Boshoff C, Weiss RA, Chang Y (1996) Molecular mimicry of human cytokine and cytokine response pathway genes by KSHV. *Science* 274(5293):1739–1744.

46. Neipel F, et al. (1997) Human herpesvirus 8 encodes a homolog of interleukin-6. *J Virol* 71(1):839–842.

47. Nicholas J, et al. (1997) Kaposi's sarcoma-associated human herpesvirus-8 encodes homologues of macrophage inflammatory protein-1 and interleukin-6. *Nat Med* 3(3):287–292.

48. Chatterjee M, Osborne J, Bestetti G, Chang Y, Moore PS (2002) Viral IL-6-induced cell proliferation and immune evasion of interferon activity. *Science* 298(5597):1432–1435.

49. Jones KD, et al. (1999) Involvement of interleukin-10 (IL-10) and viral IL-6 in the spontaneous growth of Kaposi's sarcoma herpesvirus-associated infected primary effusion lymphoma cells. *Blood* 94(8):2871–2879.

50. Belanger C, et al. (2001) Human herpesvirus 8 viral FLICE-inhibitory protein inhibits Fas-mediated apoptosis through binding and prevention of procaspase-8 maturation. *J Hum Virol* 4(2):62–73.

51. Djerbi M, et al. (1999) The inhibitor of death receptor signaling, FLICE-inhibitory protein defines a new class of tumor progression factors. *J Exp Med* 190(7):1025–

1032.

52. Zhi H, Zahoor MA, Shudofsky AMD, Giam CZ (2015) KSHV vCyclin counters the senescence/G1 arrest response triggered by NF-κB hyperactivation. *Oncogene* 34(4):496–505.

53. Jones T, et al. (2014) Viral cyclin promotes KSHV-induced cellular transformation and tumorigenesis by overriding contact inhibition. *Cell Cycle* 13(5):845–858.

54. Koopal S, et al. (2007) Viral oncogene-induced DNA damage response is activated in Kaposi sarcoma tumorigenesis. *PLoS Pathog* 3(9):1348–1360.

55. Leidal AM, Cyr DP, Hill RJ, Lee PWK, McCormick C (2012) Subversion of autophagy by Kaposi's sarcoma-associated herpesvirus impairs oncogene-induced senescence. *Cell Host Microbe* 11(2):167–180.

56. Baresova P, Musilova J, Pitha PM, Lubyova B (2014) p53 tumor suppressor protein stability and transcriptional activity are targeted by Kaposi's sarcoma-associated herpesvirus-encoded viral interferon regulatory factor 3. *Mol Cell Biol* 34(3):386–399.

57. Santag S, et al. (2013) Recruitment of the tumour suppressor protein p73 by Kaposi's sarcoma herpesvirus latent nuclear antigen contributes to the survival of primary effusion lymphoma cells. *Oncogene* 32(32):3676–3685.

58. Friborg J, Kong WP, Hottlger MO, Nabel GJ (1999) p53 inhibition by the LANA protein of KSHV protects against cell death. *Nature* 402(6764):889–894.

59. Abend JR, Uldrick T, Ziegelbauer JM (2010) Regulation of tumor necrosis factor-like weak inducer of apoptosis receptor protein (TWEAKR) expression by Kaposi's sarcoma-associated herpesvirus microRNA prevents TWEAK-induced apoptosis

and inflammatory cytokine expression. *J Virol* 84(23):12139–12151.

60. Mack AA, Sugden B (2008) EBV is necessary for proliferation of dually infected primary effusion lymphoma cells. *Cancer Res* 68(17):6963–6968.
61. Horenstein MG, et al. (1997) Epstein-Barr virus latent gene expression in primary effusion lymphomas containing Kaposi's sarcoma-associated herpesvirus/human herpesvirus-8. *Blood* 90(3):1186–1191.
62. Dresang LR, et al. (2011) Coupled transcriptome and proteome analysis of human lymphotropic tumor viruses: insights on the detection and discovery of viral genes. *BMC Genomics* 12:625.
63. Vereide DT, et al. (2014) Epstein-Barr virus maintains lymphomas via its miRNAs. *Oncogene* 33(10):1258–1264.
64. Yates JL, Warren N, Sugden B (1985) Stable replication of plasmids derived from Epstein-Barr virus in various mammalian cells. *Nature* 313(6005):812–815.
65. Krithivas A, Young DB, Liao G, Greene D, Hayward SD (2000) Human herpesvirus 8 LANA interacts with proteins of the mSin3 corepressor complex and negatively regulates Epstein-Barr virus gene expression in dually infected PEL cells. *J Virol* 74(20):9637–9645.
66. Chakravorty A, Sugden B (2015) The AT-hook DNA binding ability of the Epstein Barr virus EBNA1 protein is necessary for the maintenance of viral genomes in latently infected cells. *Virology* 484:251–258.
67. Mack AA (2007) Uncovering a mystery : what is the role of EBNA1 in primary effusion lymphomas? Dissertation (University of Wisconsin-Madison).
68. Bigi R, et al. (2018) Epstein–Barr virus enhances genome maintenance of Kaposi

sarcoma-associated herpesvirus. *Proc Natl Acad Sci* 115(48):E11379–E11387.

69. Dupin N, et al. (1995) Herpesvirus-like DNA sequences in patients with Mediterranean Kaposi's sarcoma. *Lancet* 345(8952):761–762.
70. Moore PS, Chang Y (1995) Detection of herpesvirus-like DNA sequences in Kaposi's sarcoma in patients with and those without HIV infection. *N Engl J Med* 332(18):1181–1185.
71. Boshoff C, et al. (1995) Kaposi's sarcoma-associated herpesvirus infects endothelial and spindle cells. *Nat Med* 1(12):1274–1278.
72. Ambroziak JA, et al. (1995) Herpes-like sequences in HIV-infected and uninfected Kaposi's sarcoma patients. *Science* 268(5210):582–583.
73. Blackbourn DJ, et al. (1997) Infectious human herpesvirus 8 in a healthy North American blood donor. *Lancet* 349(9052):609–611.
74. Decker LL, et al. (1996) The Kaposi sarcoma-associated herpesvirus (KSHV) is present as an intact latent genome in KS tissue but replicates in the peripheral blood mononuclear cells of KS patients. *J Exp Med* 184(1):283–288.
75. Myoung J, Ganem D (2011) Generation of a doxycycline-inducible KSHV producer cell line of endothelial origin: maintenance of tight latency with efficient reactivation upon induction. *J Virol Methods* 174(1–2):12–21.
76. Renne R, Blackbourn D, Whitby D, Levy J, Ganem D (1998) Limited transmission of Kaposi's sarcoma-associated herpesvirus in cultured cells. *J Virol* 72(6):5182–5188.
77. Bechtel JT, Liang Y, Hvidding J, Ganem D (2003) Host range of Kaposi's sarcoma-associated herpesvirus in cultured cells. *J Virol* 77(11):6474–6481.

78. Blackbourn DJ, et al. (2000) The restricted cellular host range of human herpesvirus 8. *AIDS* 14(9):1123–1133.

79. Mesri EA, et al. (1996) Human herpesvirus-8/Kaposi's sarcoma-associated herpesvirus is a new transmissible virus that infects B cells. *J Exp Med* 183(5):2385–2390.

80. Nicol SM, et al. (2016) Primary B lymphocytes infected with Kaposi's sarcoma-associated herpesvirus can be expanded in vitro and are recognized by LANA-specific CD4+ T cells. *J Virol* 90(8):3849–3859.

81. Hassman LM, Ellison TJ, Kedes DH (2011) KSHV infects a subset of human tonsillar B cells, driving proliferation and plasmablast differentiation. *J Clin Invest* 121(2):752–768.

82. Myoung J, Ganem D (2011) Active lytic infection of human primary tonsillar B cells by KSHV and its noncytolytic control by activated CD4+ T cells. *J Clin Invest* 121(3):1130–1140.

83. Myoung J, Ganem D (2011) Infection of primary human tonsillar lymphoid cells by KSHV reveals frequent but abortive infection of T cells. *Virology* 413(1):1–11.

84. Totonchy J, et al. (2018) KSHV induces immunoglobulin rearrangements in mature B lymphocytes. *PLOS Pathog* 14(4):e1006967.

85. Moss DJ, Pope JH (1972) Assay of the infectivity of Epstein-Barr virus by transformation of human leucocytes in vitro. *J Gen Virol* 17(2):233–236.

86. Sugden B, Mark W (1977) Clonal transformation of adult human leukocytes by Epstein-Barr virus. *J Virol* 23(3):503–508.

87. McHugh D, et al. (2017) Persistent KSHV infection increases EBV-associated

tumor formation in vivo via enhanced EBV lytic gene expression. *Cell Host Microbe* 22(1):61–73.

88. Mesri EA, Cesarman E, Boshoff C (2010) Kaposi's sarcoma and its associated herpesvirus. *Nat Rev Cancer* 10(10):707–719.
89. Chatlynne LG, Ablashi D V (1999) Seroepidemiology of Kaposi's sarcoma-associated herpesvirus (KSHV). *Semin Cancer Biol* 9(3):175–185.
90. Sarid R, Wiezorek JS, Moore PS, Chang Y (1999) Characterization and cell cycle regulation of the major Kaposi's sarcoma-associated herpesvirus (human herpesvirus 8) latent genes and their promoter. *J Virol* 73(2):1438–1446.
91. Talbot SJ, Weiss RA, Kellam P, Boshoff C (1999) Transcriptional analysis of human herpesvirus-8 open reading frames 71, 72, 73, K14, and 74 in a primary effusion lymphoma cell line. *Virology* 257(1):84–94.
92. Li H, Komatsu T, Dezube BJ, Kaye KM (2002) The Kaposi's sarcoma-associated herpesvirus K12 transcript from a primary effusion lymphoma contains complex repeat elements, is spliced, and initiates from a novel promoter. *J Virol* 76(23):11880–11888.
93. Grundhoff A, Sullivan CS, Ganem D (2006) A combined computational and microarray-based approach identifies novel microRNAs encoded by human gamma-herpesviruses. *RNA* 12(5):733–750.
94. Graham FL, Smiley J, Russell WC, Nairn R (1977) Characteristics of a human cell line transformed by DNA from human adenovirus type 5. *J Gen Virol* 36(1):59–72.
95. Nanbo A, Inoue K, Adachi-Takasawa K, Takada K (2002) Epstein-Barr virus RNA confers resistance to interferon-α-induced apoptosis in Burkitt's lymphoma. *EMBO*

J 21(5):954–965.

96. Garrone P, et al. (1995) Fas ligation induces apoptosis of CD40-activated human B lymphocytes. *J Exp Med* 182(5):1265–1273.
97. Wiesner M, et al. (2008) Conditional immortalization of human B cells by CD40 ligation. *PLoS One* 3(1):e1464.
98. Van Kuppeveld FJM, et al. (1992) Genus- and species-specific identification of mycoplasmas by 16S rRNA amplification. *Appl Environ Microbiol* 58(8):2606–2615.
99. Brulois KF, et al. (2012) Construction and manipulation of a new Kaposi's sarcoma-associated herpesvirus bacterial artificial chromosome clone. *J Virol* 86(18):9708–9720.
100. Toth Z, et al. (2012) Negative elongation factor-mediated suppression of RNA polymerase II elongation of Kaposi's sarcoma-associated herpesvirus lytic gene expression. *J Virol* 86(18):9696–9707.
101. Miller G, Robinson J, Heston L, Lipman M (1974) Differences between laboratory strains of Epstein-Barr virus based on immortalization, abortive infection, and interference. *Proc Natl Acad Sci U S A* 71(10):4006–4010.
102. Delecluse HJ, Hilsendegen T, Pich D, Zeidler R, Hammerschmidt W (1998) Propagation and recovery of intact, infectious Epstein-Barr virus from prokaryotic to human cells. *Proc Natl Acad Sci U S A* 95(14):8245–8250.
103. Yoo SM, et al. (2008) Centrifugal enhancement of Kaposi's sarcoma-associated virus infection of human endothelial cells in vitro. *J Virol Methods* 154(1–2):160–166.
104. Nanbo A, Sugden A, Sugden B (2007) The coupling of synthesis and partitioning

of EBV's plasmid replicon is revealed in live cells. *EMBO J* 26(19):4252–4262.

105. Russo JJ, et al. (1996) Nucleotide sequence of the Kaposi sarcoma-associated herpesvirus (HHV8). *Proc Natl Acad Sci* 93(25):14862–14867.
106. Dobin A, et al. (2013) STAR: ultrafast universal RNA-seq aligner. *Bioinformatics* 29(1):15–21.
107. Liao Y, Smyth GK, Shi W (2014) featureCounts: an efficient general purpose program for assigning sequence reads to genomic features. *Bioinformatics* 30(7):923–930.
108. Bruce AG, et al. (2017) Quantitative analysis of the KSHV transcriptome following primary infection of blood and lymphatic endothelial cells. *Pathogens* 6(1):E11.
109. Love MI, Huber W, Anders S (2014) Moderated estimation of fold change and dispersion for RNA-seq data with DESeq2. *Genome Biol* 15(12):550.
110. Zhu A, Ibrahim JG, Love MI (2019) Heavy-tailed prior distributions for sequence count data: removing the noise and preserving large differences. *Bioinformatics* 35(12):2084–2092.
111. Subramanian A, et al. (2005) Gene set enrichment analysis: a knowledge-based approach for interpreting genome-wide expression profiles. *Proc Natl Acad Sci* 102(43):15545–15550.
112. Mootha VK, et al. (2003) PGC-1α-responsive genes involved in oxidative phosphorylation are coordinately downregulated in human diabetes. *Nat Genet* 34(3):267–273.
113. Klein U, et al. (2003) Gene expression profile analysis of AIDS-related primary effusion lymphoma (PEL) suggests a plasmablastic derivation and identifies PEL-

specific transcripts. *Blood* 101(10):4115–4121.

114. Liberzon A, et al. (2015) The Molecular Signatures Database hallmark gene set collection. *Cell Syst* 1(6):417–425.
115. Bolotin DA, et al. (2015) MiXCR: software for comprehensive adaptive immunity profiling. *Nat Methods* 12(5):380–381.
116. Yakushko Y, et al. (2011) Kaposi's sarcoma-associated herpesvirus bacterial artificial chromosome contains a duplication of a long unique-region fragment within the terminal repeat region. *J Virol* 85(9):4612–4617.
117. Shin HJ, DeCotiis J, Giron M, Palmeri D, Lukac DM (2014) Histone deacetylase classes I and II regulate Kaposi's sarcoma-associated herpesvirus reactivation. *J Virol* 88(2):1281–1292.
118. Wang F-Z, Akula SM, Pramod NP, Zeng L, Chandran B (2001) Human herpesvirus 8 envelope glycoprotein K8.1A interaction with the target cells involves heparan sulfate. *J Virol* 75(16):7517–7527.
119. Birkmann A, et al. (2001) Cell surface heparan sulfate is a receptor for human herpesvirus 8 and interacts with envelope glycoprotein K8.1. *J Virol* 75(23):11583–11593.
120. Luna RE, et al. (2004) Kaposi's sarcoma-associated herpesvirus glycoprotein K8.1 is dispensable for virus entry. *J Virol* 78(12):6389–6398.
121. Rappocciolo G, et al. (2008) Human herpesvirus 8 infects and replicates in primary cultures of activated B lymphocytes through DC-SIGN. *J Virol* 82(10):4793–4806.
122. Chakraborty S, Veettil MV, Chandran B (2012) Kaposi's sarcoma associated herpesvirus entry into target cells. *Front Microbiol* 3(6):1–13.

123. Veettil MV, Bandyopadhyay C, Dutta D, Chandran B (2014) Interaction of KSHV with host cell surface receptors and cell entry. *Viruses* 6(10):4024–4046.

124. Jin C, et al. (2012) Multiple signaling pathways are involved in the interleukine-4 regulated expression of DC-SIGN in THP-1 cell line. *J Biomed Biotechnol* 2012(357060):1–10.

125. Kadowaki T, Inagawa H, Kohchi C, Hirashima M, Soma G (2011) Functional characterization of lipopolysaccharide derived from symbiotic bacteria in rice as a macrophage-activating substance. *Anticancer Res* 31(7):2467–2476.

126. Keller SA, Schattner EJ, Cesarman E (2000) Inhibition of NF-κB induces apoptosis of KSHV-infected primary effusion lymphoma cells. *Blood* 96(7):2537–2542.

127. Punj V, et al. (2009) Induction of CCL20 production by Kaposi sarcoma-associated herpesvirus: role of viral FLICE inhibitory protein K13-induced NF-κB activation. *Blood* 113(22):5660–5668.

128. Manners O, Murphy JC, Coleman A, Hughes DJ, Whitehouse A (2018) Contribution of the KSHV and EBV lytic cycles to tumourigenesis. *Curr Opin Virol* 32:60–70.

129. Shrestha P (2014) An analysis of the cis- and trans-acting elements of Kaposi's sarcoma- associated herpesvirus during latent infection. Dissertation (University of Wisconsin-Madison).

130. Kuzembayeva M (2013) MicroRNAs of Epstein - Barr virus and their contribution to the maintenance of EBV-associated lymphomas. Dissertation (University of Wisconsin-Madison).

APPENDIX.

A cautionary tale on integrants

APPENDIX 1. IDENTIFYING THE CONTRIBUTIONS OF KSHV TO PRIMARY EFFUSION LYMPHOMAS

INTRODUCTION

Previous work by Dr. Prabha Shrestha has shown that ectopic expression of genes from the KSHV latency locus in PEL cell lines leads to a partial but incomplete loss of endogenous KSHV genomes (129). My goal was to identify a limited set of KSHV genes that would be sufficient to complement the loss of KSHV genomes from PEL cells. In PEL, KSHV expresses an additional anti-apoptotic gene outside of the latency locus, called latent-nuclear antigen 2 (LANA2) or viral interferon regulatory factor 3 (vIRF3) (43, 44). First, I tested whether ectopic expression of LANA2 can complement the loss of KSHV genomes from PEL cells. Second, I wanted to ask whether ectopic expression of the KSHV latency locus genes along with LANA2 was sufficient to lead to a complete loss of KSHV genomes from PEL cells.

MATERIALS AND METHODS

Cloning of LANA2.

The DNA sequence of LANA2 was amplified from the genomic DNA of the JSC-1 PEL cell line using the forward primer: 5'-GCA GTG CGG CCG CAT TCT GAC AGG TCA CCA TGG CGG G-3' and the reverse primer: 5'-GCA GTA TGC ATA CTA TTA GTC ATC ACA TGT AAC TGA ACG C-3'. This sequence was then cloned into the retroviral vector p3051 and verified by sequencing. This construct was transfected into 293T cells to verify

the correct expression of LANA2 by Western Blotting. The LANA2 antibody CM-A807 from Novus Biologicals was used for detection of LANA2.

Introducing LANA2 into the BC-1 PEL cell line.

LANA2 was transduced into BC-1 cells using retroviral transduction by co-cultivation. Briefly, 293T cells were plated in 10 cm plates and transfected when they reached ~60% confluence with 10 μg of the retroviral vector expressing LANA2, 3 μg of Gag/Pol, 1 μg of NF-κB and 1 μg of VSVG using Lipofectamine 2000 (Invitrogen). 293T cells were then irradiated and co-cultivated with the BC-1 cells for 24 hours.

Quantitative reverse transcription PCR (RT-qPCR).

The plasmids p4170 and p4171 were transfected into 4 KSHV-negative cell lines using lipofectamine 2000 (Invitrogen). Cells were cultured under hygromycin selection for 5 days. Total RNA was isolated from 293 cells using Trizol reagent (Invitrogen) following the manufacturer's protocol. RNA was precipitated in presence of 5 μg/mL linear acrylamide (Ambion). RNA was then treated with Turbo DNAse (Ambion) and re-purified using Trizol. The reverse transcription was performed using AMV reverse transcriptase (Roche). The protocol used for real-time PCR and the primers used for detection of LANA1 are described in CHAPTER II. The primers used for detection of v-cyclin, v-FLIP and Kaposin A/C are as followed:

v-cyclin	Forward	5'-AGCTGCGCCACGAAGCAGTCA-3'
	Reverse	5'-CAGGTTCTCCCATCGACGA-3'
	Probe	5'-6-FAM-TAGCGTACTCTCGCGGCCCAGC-IABk-3'
v-FLIP	Forward	5'-CGTCTACGTGGAGAACAGTGAGCT-3'
	Reverse	5'-CTGGGCACGGATGACAGGGAAGTG-3'
	Probe	5'-6-FAM-TCTAAGTGAAGCAGGTCGCGCAA-IABk-3'
Kaposin A/C	Forward	5'-AACTCGTGTCCTGAATGCTAC-3'
	Reverse	5'-TTACTAAATGGGTGTCGCTGG-3'
	Probe	5'-6-FAM-ACCACTCGTTTGTCTGTTGGCGAT-IABk-3'

Real-time PCR (qPCR).

Total DNA was isolated using the DNeasy Blood and Tissue Kit (Qiagen). To measure the number of copies per cell of the plasmids p4170 and p294.8, the number of hygromycin and rhodopsin molecules was monitored by real-time PCR. The protocol and the primers used for real-time PCR are indicated in CHAPTER II.

Fluorescence *in situ* hybridization (FISH).

FISH to measure the number of KSHV genomes per cell was performed as previously described (see CHAPTER II). To monitor the number of copies of the plasmid p4170 by FISH, the plasmid p4170 was used as hybridization probe.

RESULTS

Ectopic expression of LANA2 leads to a partial loss of KSHV genomes from PEL cells.

Previous work by Dr. Prabha Shrestha showed that ectopic expression of the anti-apoptotic protein v-FLIP leads to a complete loss of KSHV genomes from a fraction a

PEL cells (129). Like v-FLIP, LANA2 was found to inhibit apoptosis (44, 56). Previous studies have shown that partial knock-down of LANA2 expression with siRNA reduces proliferation of PEL cells (28). We therefore asked whether ectopic expression of LANA2 can complement the loss of KSHV genomes from PEL cells. We used a retroviral vector to ectopically express LANA2 in the BC-1 PEL cell line. The number of KSHV genomes per cell was monitored by FISH after 2 months of culture. We found that the ectopic expression of LANA2 led to a decrease in the number of KSHV genomes per cell (Figure 1). These results indicate that LANA2 contributes to the survival and/or proliferation of the BC-1 cells. However. ectopic expression of LANA2 was not sufficient to lead to the complete loss of KSHV genomes from these cells.

The EBNA1-OriP plasmid p4170, and its backbone p294.8, integrate in 4 different cell lines.

We then wanted to ask whether ectopic expression of KSHV latency locus genes in combination with LANA2 was sufficient to complement the loss of KSHV genomes from PEL cells. Two EBNA1-OriP plasmids, p4170 and p4171, containing the DNA sequence of the KSHV latency locus have been generated (129). We first tested whether each gene of the KSHV latency locus was expressed from these plasmids by transfecting them into 293 cells.

The level of expression of KSHV genes from the plasmids p4170 and p4171 was measured by RT-qPCR in transient transfection of 293 cells. Expression of v-cyclin, v-FLIP, LANA1 and Kaposin A/C in 293 cells 5 days post-transfection was similar to their level of expression in PEL cell lines (Figure 2). Efficient expression of LANA1 from the

plasmids p4170 and p4171 was also confirmed by Western-Blotting. The protein LANA1 was expressed from both plasmids but the plasmid p4170 was found to express higher levels of LANA1 compared to the plasmid p4171.

We then performed qPCR experiments to monitor the number of copies per cell of the plasmid p4170 in 293 cells. We found that the plasmid p4170 was present at ~1 copy number per cell indicating that this plasmid was integrated in these cells. Furthermore, we showed that the plasmid p4170, but also its backbone p294.8, integrate in 4 different cell lines: 293, Saos2, AGS/EBNA1/CR2 and U2OS cells (Table 1). These results were confirmed by FISH. Our findings indicate that experiments using EBNA1-OriP vectors should always be performed with caution and the correct maintenance of these vectors as extrachromosomal plasmids in cells should be monitored.

Figure 1: Ectopic expression of LANA2 leads to a partial loss of KSHV genomes from PEL cells.

LANA2 was ectopically expressed in the BC-1 PEL cells for 2 months. (A) The average number of KSHV genomes per cell was measured by FISH. (B) The percentage of cells with the given number of KSHV genomes is indicated.

Figure 1

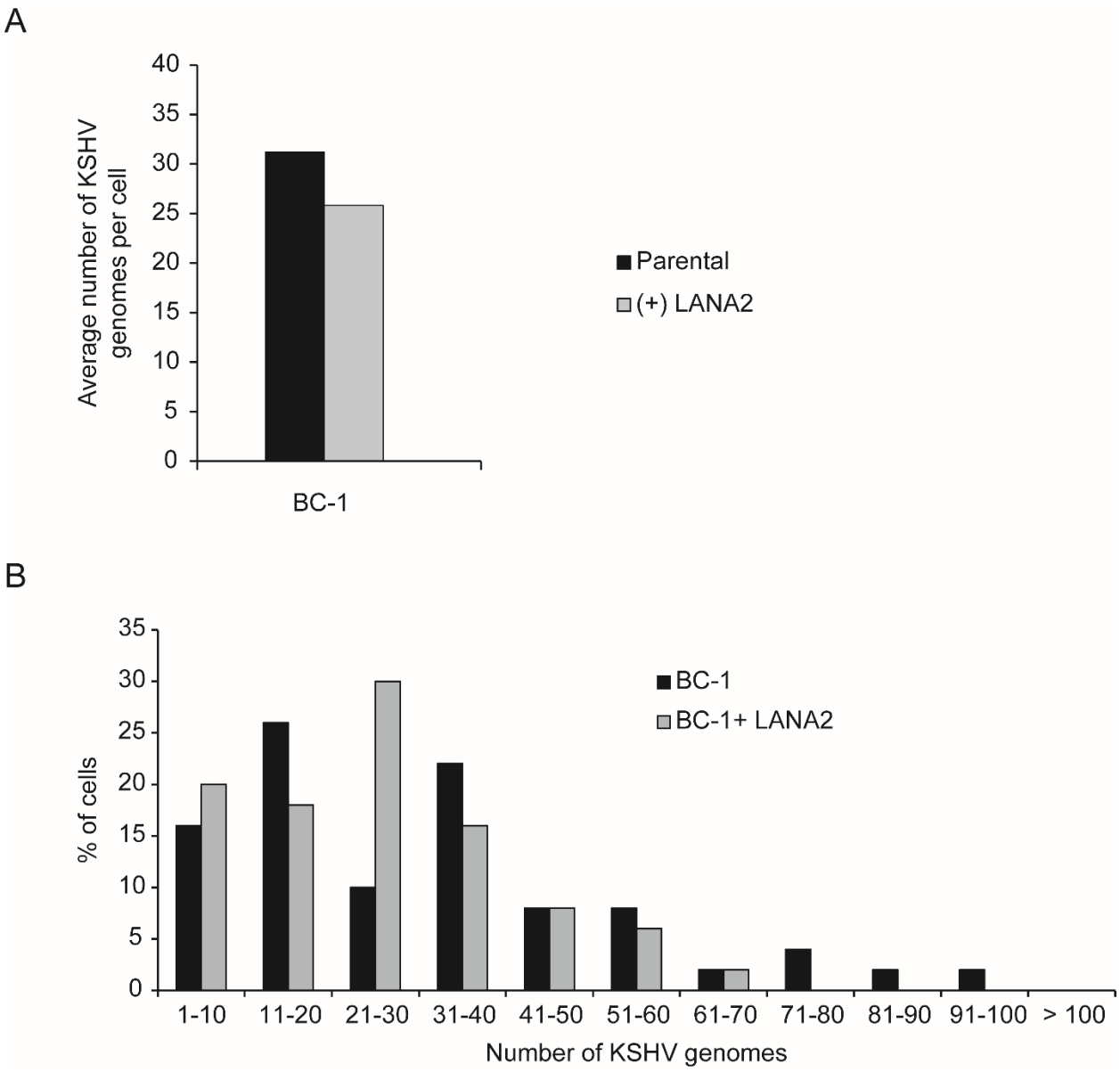
A
Average number of KSHV genomes per cell
40
35
30
25
20
15
10
5
0
BC-1
Parental
(+) LANA2
B
% of cells
35
30
25
20
15
10
5
0
1-10
11-20
21-30
31-40
41-50
51-60
61-70
71-80
81-90
91-100
> 100
Number of KSHV genomes
BC-1
BC-1+ LANA2

Figure 2: Expression of KSHV latency locus genes from the plasmids p4170 and p4171.

The expression of KSHV latency locus genes was measured by RT-qPCR in 293 cells 5 days following transfection of the plasmid p4170 or p4171 and in the JSC-1, BC-1 and BCBL-1 PEL cell lines. The expression of v-cyclin, v-FLIP, LANA1 and Kaposin A/C relative to the JSC-1 PEL cell line is indicated (expressed in fold change).

Figure 2

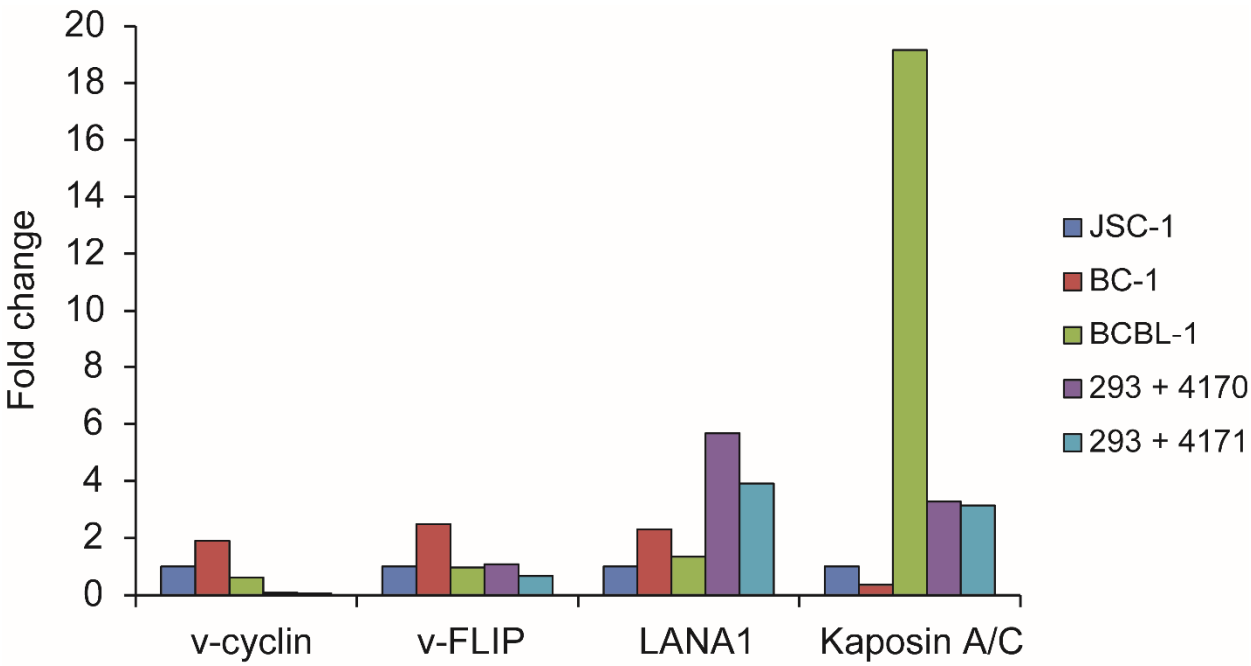
20
18
16
14
12
10
8
6
4
2
0
Fold change
v-cyclin
v-FLIP
LANA1
Kaposin A/C
JSC-1
BC-1
BCBL-1
293 + 4170
293 + 4171

Table 1: The EBNA1-OriP plasmids p4170 and p294.8 integrate in 4 different cell lines.

The number of plasmids p4170 or p294.8 per cell was monitored by real-time PCR in 4 different cell lines. The BJAB cell line was used as a negative control.

Table 1

Sample	# plasmids/cell
293 + 294.8	0.55
293 + 4170	0.62
Saos2 + 294.8	0.65
Saos2 + 4170	1.53
AGS/EBNA1/CR2 + 294.8	0.54
AGS/EBNA1/CR2 + 4170	0.61
U2OS + 4170 replicate #1	0.40
U2OS + 4170 replicate #2	0.93
BJAB	0.14

APPENDIX 2. IDENTIFYING THE CONTRIBUTIONS OF EBV'S BART miRNAS TO BURKITT'S LYMPHOMAS

INTRODUCTION

Previous work by Dr. Malika Kuzembayeva suggested that EBV's BART miRNAs foster the growth of Wp-restricted Burkitt's lymphoma cells (130). A retroviral vector encoding the cellular anti-apoptotic gene Bcl-xL was used to ectopically express Bcl-xL in the Oku‌I Burkitt's lymphoma cell line. The ectopic expression of Bcl-xL induced the loss of EBV from a fraction of these cells (130). An EBV-negative clone was generated, called Bcl-xL-positive EBV-negative Oku‌I clone 3.4. The Bcl-xL-positive EBV-negative Oku‌I cells grew significantly slower than the parental Oku‌I cells. Their rate of growth was restored by the ectopic expression of EBV's BART miRNAs. In order to identify the subset of EBV's BART miRNAs that provides selective advantages to the Oku‌I cells, several EBNA1-OriP plasmids expressing different subsets of these miRNAs were introduced into the Bcl-xL-positive EBV-negative Oku‌I cells.

MATERIALS AND METHODS

Real-time PCR.

Total DNA was isolated using the DNeasy Blood and Tissue Kit (Qiagen). To determine the number of endogenous EBV genomes per cell, the number of molecules of BALF5 and rhodopsin was measured by real-time PCR. The protocol and the primers used for real-time PCR are indicated in CHAPTER II.

Growth curves.

The rate of growth of the Bcl-xL-positive EBV-positive SalI cells and the Bcl-xL-positive EBV-negative SalI clone 3 cells was measured using a Coulter counter.

RESULTS

One copy of EBV is integrated in Bcl-xL-positive EBV-negative OkuI clone 3.4 cells.

Previous results showed that the Bcl-xL-positive EBV-negative OkuI cells grow significantly slower than the parental OkuI cells. Expression of different subsets of EBV's BART miRNAs restored the growth of these cells to the level of the parental OkuI cells. In particular, the Bcl-xL-positive EBV-negative OkuI cells transfected with the EBNA1-OriP plasmid p4046 encoding the cluster I of EBV's BART miRNAs grew significantly faster than those transfected with its backbone plasmid (p220.2).

I measured the number of endogenous EBV genomes per cell in the parental OkuI cells and the Bcl-xL-positive EBV-negative OkuI clone 3.4 by real-time PCR (Table 1). The number of EBV genomes was also measured in the population of OkuI cells transduced with the retroviral vector expressing Bcl-xL, called the Bcl-xL-positive EBV-positive OkuI cells. Only a fraction of these cells loses EBV and the majority of cells in this population remain EBV-positive. I found on average between 5 and 7 EBV genomes per cell in the parental OkuI cells and the Bcl-xL-positive EBV-positive OkuI cells. However, the Bcl-xL-positive EBV-negative OkuI clone 3.4 cells contained 1 EBV genome per cell. The same results were obtained with the Bcl-xL-positive EBV-negative OkuI clone 3.4 cells that were transfected with the EBNA1-OriP plasmid p4046 or its backbone p220.2. These results indicate that one copy of the endogenous EBV genome is

integrated in Bcl-xL-positive EBV-negative OkuI clone 3.4 cells. These results were confirmed by FISH (FISH was performed by Ya-Fang Chiu and Bill Sugden).

EBV does not provide a proliferative advantage to Bcl-XL-positive EBV-negative SalI cells.

Bcl-xL was ectopically expressed in another Wp-restricted Burkitt's lymphoma cell line, named SalI. The ectopic expression of Bcl-xL also induced the spontaneous loss of EBV from a fraction of these cells. An EBV-negative clone, named Bcl-xL-positive EBV-negative SalI clone 3 cells, was generated. I measured the number of endogenous EBV genomes in these cells compared to the Bcl-xL-positive EBV-positive SalI cells (Table 1). I found no evidence of integration of the EBV genome in the Bcl-xL-positive EBV-negative SalI clone 3 cells.

I then asked whether I could reproduce the results observed with the OkuI cell line: the OkuI cells that lost EBV upon expression of Bcl-xL showed a reduced rate of growth compared to the parental OkuI cells. I measured the rate of growth of the Bcl-xL-positive EBV-positive SalI cells compared to the Bcl-XL-positive EBV-negative SalI clone 3 cells and found no difference in cell growth between these two cell types (Figure 1).

Table 1: One copy of EBV is integrated in Bcl-xL-positive EBV-negative OkuI clone 3.4 cells.

The number of endogenous EBV genomes per cell was measured by real-time PCR in OkuI and SalI cells. BJAB cells were used as a negative control. *repl.*: replicate.

Table 1

Sample	# EBV genomes/cell
OkuI	4.70
Bcl-xL+/EBV+ OkuI	7.20
Bcl-xL+/EBV- OkuI clone 3.4 *repl. #1*	0.55
Bcl-xL+/EBV- OkuI clone 3.4 *repl. #2*	0.38
Bcl-xL+/EBV- OkuI clone 3.4 *repl. #3*	0.80
Bcl-xL+/EBV- OkuI clone 3.4 *repl. #4*	0.63
Bcl-xL+/EBV- OkuI clone 3.4 + p220.2	0.63
Bcl-xL+/EBV- OkuI clone 3.4 + p4046	0.86
Bcl-xL+/EBV+ SalI	7.22
Bcl-xL+/EBV- SalI clone 3	0.00
BJAB	0.00

Figure 1: EBV does not provide a proliferative advantage to Bcl-XL-positive EBV-negative SalI cells.

The rate of growth of the Bcl-xL-positive EBV-positive SalI cells and the Bcl-xL-positive EBV-negative SalI clone 3 cells was monitored in 3 independent biological replicates for each population. Error bars show the standard deviation.

Figure 1

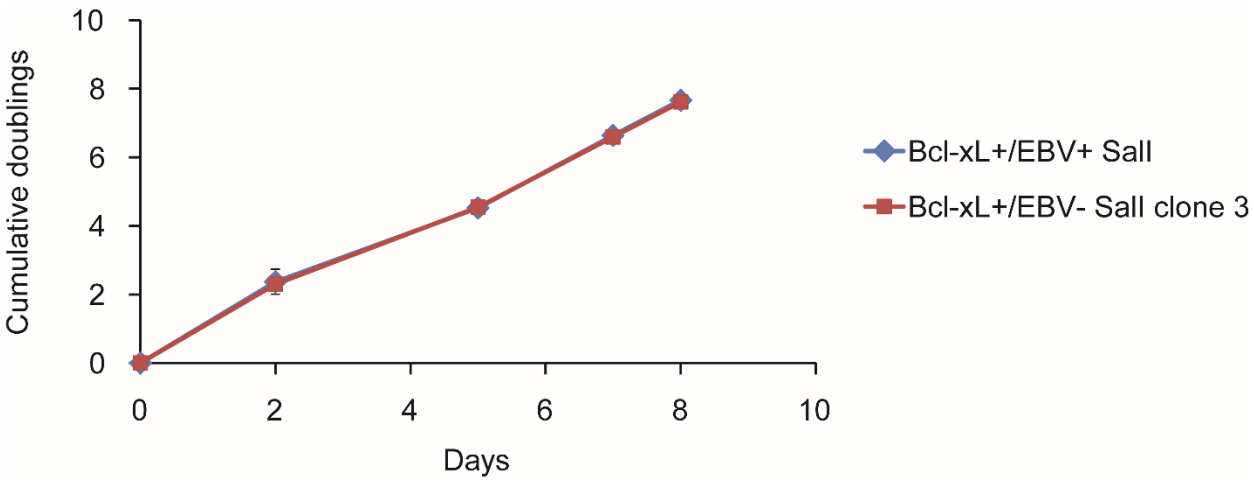
Cumulative doublings
10
8
6
4
2
0
0
2
4
6
8
10
Days
Bcl-xL+/EBV+ SalI
Bcl-xL+/EBV- SalI clone 3

The transcripts of the DNA-binding inhibitor *ID3* are targeted by EBV's BART miRNAs in Okul cells.

The following work was carried out by an undergraduate student, Dalton Banh, under my mentorship as part of the Integrated Biological Sciences Summer Research Program at the University of Wisconsin-Madison.

Do Epstein-Barr virus microRNAs target the transcripts of the DNA-binding inhibitor *ID3*?

Dalton V. Banh
University of Southern California

Aurélia Faure & Bill Sugden
McArdle Laboratory for Cancer Research
(Department of Oncology)
School of Medicine and Public Health
University of Wisconsin-Madison

Abstract

Epstein-Barr virus (EBV) is able to sustain Burkitt's lymphoma (BL) cells using its BART locus of microRNAs (miRNAs). Mature miRNAs repress translation of a transcript by incorporating themselves into an RNA-induced silencing complex (RISC) and binding to a complementary sequence in the 3'-untranslated region (3'-UTR) of the transcript. Here, we test whether EBV's BART miRNAs are able to target the transcripts of *ID3*, which encodes a DNA-binding inhibitor that has important roles in T- and B-cell development. *ID3* is commonly mutated in Burkitt's lymphomas and we propose that the BART miRNAs silence the expression of ID3 in order to sustain lymphomas. We have obtained preliminary evidence for *ID3* as an authentic target for regulation by EBV's BART miRNAs expressed at physiological levels.

Introduction

Epstein-Barr virus (EBV) preferentially infects human B-lymphocytes, residing primarily in quiescent memory B-cells. EBV is a γ-herpesvirus, a family of DNA viruses known for their latent, recurrent mode of infection. It is estimated that over 90% of the human population is infected by EBV, which often persists asymptomatically for the lifetime of the individual. However, EBV can cause infectious mononucleosis, which is a self-limiting proliferation of EBV-infected B-cells. It has also been shown that EBV is causally associated with

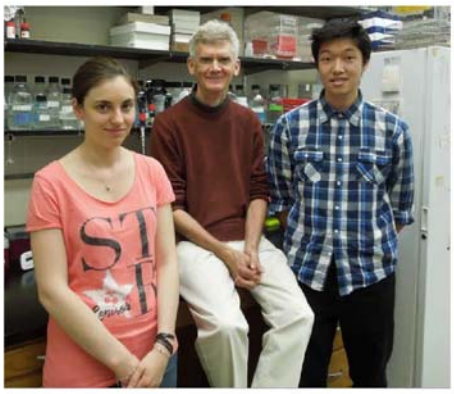

the development of several tumors, including Burkitt's lymphoma (BL), Hodgkin's lymphoma (HL), post-transplant lymphoproliferative-disorder (PTLD), gastric carcinoma, and nasopharyngeal carcinoma. In this study, we have focused on African Burkitt's lymphomas, in which EBV is present nearly 100% of the time. BLs are characterized by a translocation of the *MYC* locus to an immunoglobulin locus, resulting in a constitutively active *MYC* oncogene.

How do we know that EBV affects its host? During latency, EBV maintains its genome as a plasmid replicon in the host cell. Since not all copies of the viral genome are replicated each cell cycle, EBV is lost from infected cells at a rate of 8% per cell each generation. Only if it affords cells a selective advantage will EBV be retained in a proliferating population of cells.[1] There are several mechanisms by which EBV contributes advantages to its host. One is to drive or promote cell proliferation by efficiently inducing the cell's exit from G_1/G_0.[2] This is done usually by the expression of viral proteins with transforming capabilities, such as LMP1 and EBNA2. A second mechanism is to inhibit apoptosis (programmed cell death) in the host cell, allowing it to survive. Viral proteins such as BHRF1, EBNA3A, EBNA3C, and most recently the BART miRNAs have been shown to protect cells from apoptosis.[3] Both of these viral strategies provide a selective advantage for cells infected with EBV and allows for both the host cell and the virus to persist through many generations.

EBV expresses multiple genes in newly infected cells (Fig. 1). However, in canonical BLs, it expresses only the BART miRNAs, the EBERs, and EBNA1, and none of the viral proteins known

to transform B-cells are expressed in these tumor cells. EBER1 and EBER2 are both small nuclear RNAs (snRNAs) that are not required for host cell transformation. EBNA1 is a viral protein present in all EBV-infected cells and plays an important role in both the maintenance, as well as the partitioning of EBV's plasmid replicon. However, the full capabilities of EBNA1 are not yet fully understood and continue to be an active topic of research. EBV's microRNAs (miRNAs), specifically those encoded by the BamHI A Rightward transcript (BART) locus of miRNAs, have been shown to play a role in sustaining lymphomas by targeting host mRNA transcripts and preventing their translation.[3] Identifying tumor suppressors or pro-apoptotic proteins that are targeted by EBV's miRNAs will help to elucidate the mechanisms by which EBV sustains BLs.

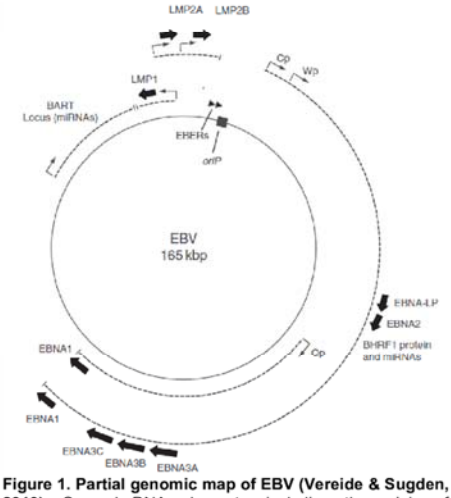

Figure 1. Partial genomic map of EBV (Vereide & Sugden, 2010). Several DNA elements, including the origin of replication *oriP* and the promoters Cp, Wp, and Qp, are shown. Transcripts, including the BART locus which encodes for a set of EBV's miRNAs, are represented by dotted lines. Protein-coding open reading frames (ORFs) are represented by solid black arrows.

miRNAs are small (~22-nucleotide long) noncoding RNA molecules that can regulate gene expression post-transcriptionally. To become functionally mature miRNAs, they must undergo various cleavage and transport steps after their transcription[4,5] (Fig. 2). Genes encoding miRNAs are transcribed to yield "a primary miRNA" (pri-miRNA) molecule, which undergoes cleavage in the nucleus by Drosha to

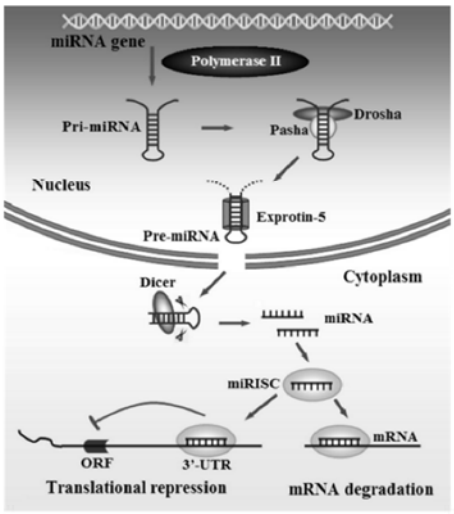

Figure 2. Overview of miRNA biogenesis and function (Shi and Guo, 2009). The transcript encoding for miRNA must undergo multiple cleavage and transport steps before finally becoming mature miRNA to be incorporated into RISC.

form a 60-70 nt-long "precursor miRNA" (pre-miRNA), which is transported into the cytoplasm by Exportin-5. There, pre-miRNA undergoes cleavage by Dicer to create a miRNA duplex—one strand becomes the active mature miRNA, while the other "passenger strand" is thought to be degraded. The mature miRNA incorporates itself into the RNA-induced silencing complex (RISC) and base-pairs with a 6-8 nucleotide-long complementary sequence within the transcript, leading to the repression of translation.

It has been shown that the BART miRNAs target *IPO7* and *CASP3* transcripts.[3] CASP3 is a protease with a central role in the apoptotic cascade, while the role of IPO7 is not currently understood. By repressing the expression of CASP3, EBV inhibits the host cell's ability to undergo apoptosis. EBV's miRNAs are particularly insidious because they are not immunogenic. It has been hypothesized that canonical BLs express a minimal number of viral genes due to a selective pressure—if EBV expresses immunogenic products, its host cell will be detected by the host immune system.[6] The BART miRNAs avoid this detection, allowing them to sustain lymphomas.

Through computational programs such as PITAbash[7], as well as RISC immunoprecipitation

and other proteomic methods[8], we have identified likely targets for regulation by EBV's miRNAs. Two of the candidates we are currently interested in are PTEN and ID3. *PTEN*, which encodes phosphatase and tensin homolog, is an intriguing candidate since it is a well-known tumor-suppressor. *ID3*, which encodes inhibitor of DNA-binding 3, is also an attractive candidate, since inappropriate regulation and mutation of the ID-family of proteins have been associated with tumorigenesis.

Recent studies have proposed ID3 as a novel tumor suppressor and have shown that *ID3* is mutated in at least one-third, and up to about two-thirds of all BLs.[9,10] Furthermore, Love et al. experimentally showed that silencing mutations in *ID3* promotes proliferation and cell cycle progression.[9] Furthermore, Richter et al. proposed that cooperation between *ID3* inactivation and the IG-MYC translocation found in all BLs is a hallmark of Burkitt's lymphomagenesis.[10] These findings support the hypothesis that EBV uses its miRNAs to inhibit the expression of ID3 to promote proliferation of infected cells. In this study, we test whether *ID3* transcripts are targets for regulation by EBV's miRNAs.

Methods

We used computational tools, molecular cloning techniques, and a luciferase reporter assay to characterize the binding of EBV's BART miRNAs to the 3'-UTR of human *ID3* transcripts.

PITAbash

PITAbash is a computational program that rapidly identifies miRNA targets and computes the difference between the free energy gained from the formation of the miRNA-target duplex and the energetic cost of unpairing the target. We used PITAbash to analyze the binding favorability of all the BART miRNAs to the 3'-UTR sequences of *ID3*. The sequences for the BART miRNAs were obtained from miRBase: the microRNA database. The 3'-UTR sequence for *ID3* was obtained from the UCSC Genome database. Both databases are accessible online.

Molecular Cloning

Polymerase Chain Reaction: to amplify the sequence of interest (i.e. the 3'-UTR of *ID3*) from ID3 cDNA (obtained by RT-PCR on mRNA obtained from the lymphoblastoid cell line (LCL) 721), we constructed primers containing restriction sites (see Table 1 below) and performed PCR with Herculase HotStart DNA Polymerase (Agilent) for 35 cycles using the following optimal parameters: denaturation (95 ºC, 30s), annealing (49 ºC, 30s), extension (72 ºC, 4min). PCR purification was conducted using the QIAquick PCR Purification Kit (QIAGEN). Gel electrophoresis using 0.7% agarose was performed to confirm that our PCR-amplification product was of the appropriate size.

Table 1. PCR primer sequences used for amplification of the *ID3* 3'-UTR. *Note: GTTTAAAC is the restriction site for PmeI; CTCGAG is the restriction site for XhoI.*

Forward Primer	5'-GCAGT GTTTAAAC CTCGGCCGTGTCCT-3'
Reverse Primer	5'-GCAGT CTCGAG TATGCAAAATGTTAAC-3'

Restriction enzyme digestion: restriction-digestion was performed using the enzymes PmeI and XhoI. The empty expression vector p4063 (based on the pmirGLO vector from Promega) was digested in a 37 ºC water-bath for 1 hr. and then treated with calf-intestinal alkaline phosphatase (CIP). CIP catalyzes the removal of 5'-phosphate group and prevents re-circularization of the empty vector at the cut ends. The mix was then placed back at 37 ºC for another hour. The PCR-amplified 3'-UTR was digested at 37 ºC for 2 hrs. without treatment by CIP. The digestion products were then purified using QIAGEN's purification kit, as described above.

Ligation: the digested p4063 vector and 3'-UTR insert were ligated together in a 3:1 insert to vector ratio using T4 DNA Ligase. The reaction was performed overnight at room temperature.

Transformation using Electroporation: electro-competent DH10B *E. coli* at -80 ºC were thawed on ice and mixed with the desired construct. Cells were electroporated at 200Ω, 1.5 kV, and 25μF. Cells were incubated in Super Optimal Broth with catabolite repression (SOC) in a 37 ºC shaker for 1 hr. Cells were then plated on selective plates containing LB + ampicillin (or carbenicillin) and incubated overnight at 37 ºC. Colonies were then picked the next day and incubated in overnight cultures containing LB + ampicillin.

Diagnostic restriction digest: the transformed clones were then mini-prepped using the

QIAprep Spin Miniprep Kit (QIAGEN) and a diagnostic digest was performed at 37 ºC for 2 hrs. We performed two restriction digests using PvuII and SmaI + SpeI. Gel analysis was performed to confirm that we obtained the correct construct containing the *ID3* 3'-UTR insert.

Plasmid Maxiprep: transformed *E. coli* were grown overnight in 500ml LB supplemented with 100 µg/ml ampicillin and were then alkaline-lysed. DNA was extracted using CsCl-gradient centrifugation.

Transfection and Luciferase Reporter Assay

As described above, the 3'-UTR of *ID3* was cloned downstream of firefly luciferase (FLuc) in the vector p4063, based on the expression plasmid pmirGLO (Promega). p4063 contains a separate expression cassette encoding renilla luciferase (RLuc) as an internal control. Cells at a density of 1 x 10^7 per cuvette were electroporated under standard conditions (1100 V, 3 capacitor banks) to take up the desired plasmids. Transformed cells were harvested at a density of 2.5 x 10^6, washed with PBS, and then lysed in Passive Lysis Buffer. The lysate was then assayed using the Dual-Luciferase Reporter Assay Kit (Promega). Expression values were calculated by dividing the FLuc measurement with the RLuc measurement. These values were then further normalized by dividing the expression values of the constructs containing the 3'-UTR with the expression values of the empty carrier vectors.

Cell Lines and Culture

The following lymphoma cell lines were used in the reporter assay: Oku1 is a Burkitt's lymphoma-derived, EBV-positive cell line; 721 is an EBV-transformed, lymphoblastoid cell line (LCL); BJAB is a Burkitt's lymphoma-derived, EBV-negative cell line. All cell cultures were grown in RPMI 1640 (Gibco, Grand Island, NY, USA) supplemented with 10% fetal bovine serum (R10F). All cell culture media were supplemented with 200 U/ml penicillin and 200 µg/ml streptomycin. All cells were grown at 37 ºC in a 5% CO_2 humidified atmosphere.

Sequencing of construct containing *ID3* 3'-UTR

We used BigDye thermal cycling sequencing for 25 cycles using optimal parameters (96 ºC for 30s; 50 ºC for 15s; 60 ºC for 2 min) using two independent pmirGLO sequencing primers: PMIR156R (UTR R) and PMIR374R (UTR R2) (see Table 2 below). Clean-up was performed using CleanSeq magnetic beads.

Table 2. pmirGLO primers used for sequencing of our vector construct containing the *ID3* 3'-UTR.

PMIR 156R	5'-GCATTCTAGTTGTGGTTTGTCC-3'
PMIR 374R	5'-CCGCATCAGGAAATTGTAAGC-3'

Results

Predicted target sites and corresponding miRNA seed sequences

Using PITAbash, we predicted possible sites in the 3'-UTR where the BART miRNA seed sequences could bind and the energetic favorability (measured by ΔΔG) of each interaction (Table 3). Our threshold (based on previous work with CASP3 and IPO7) for a favorable target was ΔΔG ~ -10.00. Thus, we predict using computational methods that BART3 is most likely able to bind to the 3'-UTR.

Table 3. Sequences in the *ID3* 3'-UTR that are predicted binding sites for the BART miRNAs. ΔΔG is equal to $\Delta G_{Duplex} - \Delta G_{Open}$, the difference between the free energy gained from the formation of the miRNA-target duplex and the free energy lost from unpairing of the duplex. Data was computed using PITAbash.

EBV miRNA	Target Site (bp)	Target Seq.	ΔΔG
BART3	**157-163**	**UGGUGC**	**-12.02**
BART1-3'	32-38	GGUGCU	0.16
BART1-3'	158-164	GGUGCU	0.75

Construction of vector containing the *ID3* 3'-UTR

PCR amplification was successful: we amplified the 3'-UTR from *ID3* cDNA. Gel analysis is shown below (Fig. 3). We observed a band approximately 500 bp long. The expected size of the *ID3* 3'-UTR is 511 bp.

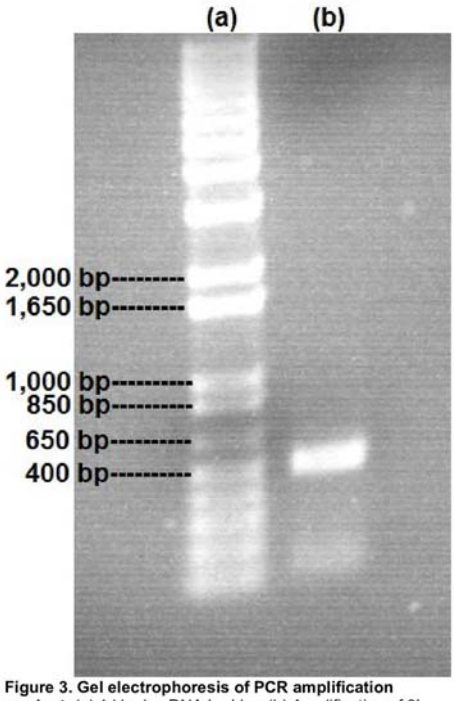

Figure 3. Gel electrophoresis of PCR amplification product. (a) 1 kb plus DNA Ladder; (b) Amplification of 3'-UTR using Herculase HotStart DNA Polymerase

Ligation of 3'-UTR into p4063 and Transformation were successful: we ligated the 3'-UTR into the p4063 vector and transformed the construct into *E. coli*. To confirm that we harvested the desired plasmid, we performed two diagnostic restriction enzyme digests. Gel analysis is shown below (Fig. 4). In the first digest, PvuII was used. If our ligation product consisted only of empty p4063 (i.e. unsuccessful ligation), we expected to observe only three bands, of size 1,605 bp, 2,029 bp, and 3,615 bp (from Serial Cloner, ver. 2.5). If our p4063 contained the 3'-UTR insert, we expected to observe four bands, of size 690 bp, 1,605 bp, 1,816 bp, and 3,615 bp. Our product of restriction-digest and ligation displayed four bands of the expected size (lane c), providing evidence that our ligation and transformation were successful. In the second digest, we performed a double digest using SmaI and SpeI. If our product consisted of empty p4063, we expected only one band of size 7,249 bp. If our product contained the desired 3'-UTR insert, we expected two bands, of size 2,028 bp and 5,698 bp. Our product displayed two bands of the appropriate size (lane e), confirming that our ligation and transformation were successful.

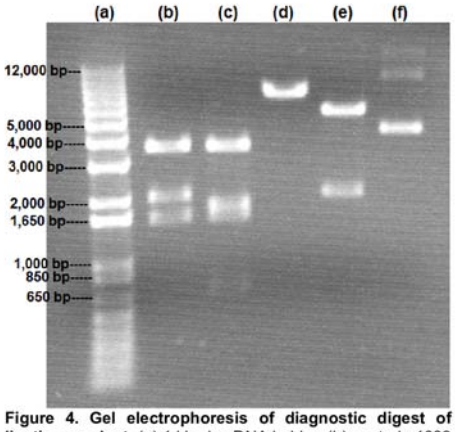

Figure 4. Gel electrophoresis of diagnostic digest of ligation product. (a) 1 kb plus DNA ladder; (b) control p4063 w/PvuII; (c) ligation product w/PvuII; (d) control p4063 w/SmaI+SpeI; (e) ligation product w/SmaI+SpeI; (f) control ligation product w/o digestion.

Sequencing of construct containing ID3 3'-UTR: We found that our 3'-UTR was 99.8% identical to the reference sequence on the NCBI database. The one difference was a C→T single nucleotide polymorphism (SNP) at position 271 of the 3'-UTR. Further analysis revealed that the presence of a T was actually more common (~80%) in the human population than the presence of a C (~20%). Sequencing revealed that our construct contained the full 3'-UTR and that there were no mutations in the 6-nt target site that could interfere with our experiment.

Luciferase Reporter Assay

EBV-positive Oku1 cells transfected with the construct containing the ID3 3'-UTR displayed reduced luciferase activity: there was a significant difference between our negative control, the EBV-negative cell line BJAB, and the EBV-positive cell line Oku1 transfected with our positive control vector containing the IPO7 3'-UTR (Fig. 5), as well as with our experimental vector containing the *ID3* 3'-UTR (Fig. 6). With the IPO7 3'-UTR, we detected a 38% decrease in normalized luciferase activity in Oku1 compared to BJAB. In comparison, with the *ID3* 3'-UTR, we detected a 55% decrease in luciferase activity. However, the difference

between the normalized luciferase activity detected in the EBV-positive cell line 721 and the activity detected in BJAB was not significant in either transfection with the IPO7 3'-UTR and the *ID3* 3'-UTR. Finally, we found that there was no significant difference between the normalized luciferase activities detected in Oku1 and in 721, which was what we expected.

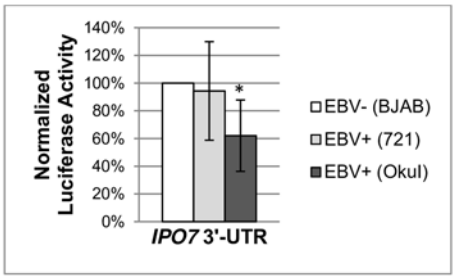

Figure 5. We introduced the vector p4024 into EBV-positive (i.e. Oku1 and 721) or EBV-negative cells (i.e. BJAB). p4024, which contained the IPO7 3'UTR, was used as a positive control. The normalized luciferase activity in the EBV-negative BJAB cell line was set to 100%. Data are the average of four independent experiments ± s.d. (*P = 0.034, Wilcoxon rank sum test).

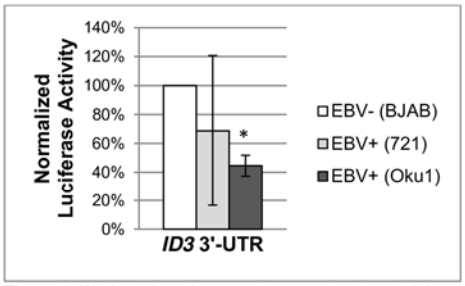

Figure 6. We introduced our vector construct containing the ID3 3'-UTR into EBV-positive (i.e. Oku1 and 721) or EBV-negative cells (i.e. BJAB). The normalized luciferase activity in the EBV-negative BJAB cell line was set to 100%. Data are the average of four independent experiments ± s.d. (*P = 0.021, Wilcoxon rank sum test).

Discussion

We have obtained some evidence supporting *ID3* being a target for binding by EBV's miRNAs. This evidence, however, is limited due to the few biological replicates of the assay we performed in our experiment (n=4), variations in transfection efficiency between cell lines, and differences inherent to the cell lines used: Oku1, 721, and BJAB. For example, different cell lines undoubtedly respond to transfection with varying efficiencies. In addition, the EBV present in Oku1 expresses different levels of BART3 than the EBV present in 721 LCL. In some instances, EBV expresses completely different sets of BART miRNAs in different cell lines, as previously shown by Pratt et al. in 2009.[11] For example, 721 does not express BART16, which is known to target IPO7 transcripts. As a result, we shall need to account for the levels of expression of the BART miRNAs in each cell line when comparing them.

We recognize the limitations in our preliminary findings and plan to improve upon them in future experiments. In addition to simply repeating the assay for a larger number of biological replicates, we should introduce vectors encoding different sets of BART miRNAs into Oku1's engineered Bcl-xL-complemented, EBV-negative counterpart (Oku1 3.4 cell line) and perform the reporter assay. We expect that 3.4 cells transfected with the vectors encoding the BART3 miRNA would display decreased luciferase activity. In contrast, if the cells were transfected with a vector that does not encode BART3, but instead other combinations of miRNAs, we expect there to be no significant decrease in luciferase activity. In addition, a second approach in further characterizing ID3 as a target would be to induce mutations in the predicted 6-nt binding site in the 3'-UTR and then perform the reporter assay. If the *ID3* 3'-UTR is indeed a binding site for EBV's miRNAs, then we should observe increased luciferase activity to normal, unrepressed levels when the sequence of the binding site in the 3'-UTR is changed with mutations.

Burkitt's lymphoma is endemic in sub-Saharan Africa, primarily affecting children whose immune systems are compromised by concurrent infection with malaria (or HIV) and EBV. Thus, it is important to understand the molecular mechanisms utilized by EBV to promote proliferation of its host cell and sustain BLs. Our study suggesting that *ID3* is a potential target for EBV's BART miRNAs is a step forward in characterizing both the role of EBV's miRNAs in Burkitt's lymphoma, as well as the importance of the expression of certain genes in the host in preventing (or causing) tumor formation. In addition to expanding our study to further characterize *ID3* as a target, we hope to investigate other candidate targets for EBV's miRNAs, such as the tumor suppressor PTEN, using the methods and approaches described in this study. Perhaps in the near future when we

are able to identify BART miRNA targets crucial for EBV to sustain BLs, we will be able to prevent EBV's miRNAs from binding, or implement gene therapies to engineer and artificially express an untargeted variant of the transcript in the host cell to restore the normal cell life cycle and effectively treat the cancer.

Acknowledgements

I would like to thank my mentor Aurélia Faure for guiding me through my project. I would also like to acknowledge Mitch Hayes for showing me various techniques and experimental troubleshooting, Rup Chakravorty for helping me with statistical analysis, and all the other members of the Sugden Lab for their hospitality and support. Lastly, I would like to thank Bill Sugden for his compassion and for giving me the opportunity this summer to learn from him and the rest of the lab.

In addition, I wish to thank my Virology subgroup mentors Paul Ahlquist and Johan den Boon for their helpful feedback and advice.

I would also like to acknowledge Lucas Moyer-Horner and Janet Branchaw at the Institute for Biology Education for a chance to undertake this research project as part of the IBS-SRP program.

Finally, I would like to acknowledge my research advisor at USC, Steve Finkel, for his unwavering support of my academic endeavors.

This research is supported by the:

- National Science Foundation (DBI-1063085)
- UW-Madison Graduate School

References

1. Nanbo, A., Sugden, A., Sugden, B. The coupling of synthesis and partitioning of EBV's plasmid replicon is revealed in live cells. *EMBO J*, 2007; 26: 4252-4262.

2. Vereide. D., Sugden, B. Insights into the evolution of lymphomas induced by Epstein-Barr virus. *Advances in cancer research*, 2010; 108: 1-19.

3. Vereide, D.T., Seto, E., Chiu, Y.-F., Hayes, M., Tagawa, T., Grundhoff, A., Hammerschmidt, W., and Sugden, B. Epstein-Barr Virus Maintains Lymphomas Via Its miRNAs. *Oncogene*, in press, 2013 [Epub ahead of print Mar 18 2013].

4. Kim, V.N. MicroRNA Biogenesis: Coordinated Cropping and Dicing. *Nat Rev Mol Cell Biol*, 2005; 6: 376-385.

5. Shi, M., Guo, N. MicroRNA expression and its implications for the diagnosis and therapeutic strategies of breast cancer. *Cancer Treat Rev*, 2009; 35: 328-334.

6. Vereide, D.T., and Sugden, B. Lymphomas Differ in Their Dependence on Epstein-Barr Virus. *Blood*, 2011; 117: 1977-1985.

7. Kertesz, M., Iovino, N., Unnerstall, U., Gaul, U., Segal, E. The role of site accessibility in microRNA target recognition. *Nat Genet*, 2007; 39: 1278-1284.

8. Kuzembayeva, M., Chiu, Y-F., Sugden, B. Comparing proteomics and RISC immunoprecipitations to identify targets of Epstein-Barr viral miRNAs. *PLoS One*, 2012; 7: e47409.

9. Love, C. et al. The genetic landscape of mutations in Burkitt lymphoma. *Nat Genet*, 2012; 44: 1321-1325.

10. Richter, J. et al. Recurrent mutation of the *ID3* gene in Burkitt lymphoma identified by integrated genome, exome, and transcriptome sequencing. *Nat Genet*, 2012; 44: 1316-1320.

11. Pratt, Z. L., Kuzembayeva, M., Sengupta, S., Sugden, B. The microRNAs of Epstein-Barr Virus are expressed at dramatically differing levels among cell lines. *Virology*, 2009; 386: 387-397.